LUMBAR MECHANICS FROM ULTRASOUND IMAGING

by

Geoffrey Thor Desmoulin
Bachelor of Science (Hons), Simon Fraser University 2002

THESIS SUBMITTED IN PARTIAL FULFILMENT OF
THE REQUIREMENTS FOR THE DEGREE OF

MASTER OF SCIENCE

In the
School of Kinesiology

SIMON FRASER UNIVERSITY

Fall 2005

APPROVAL

Name: **Geoffrey Thor Desmoulin**

Degree: **MASTER OF SCIENCE (KINESIOLOGY)**

Title of Thesis: **LUMBAR MECHANICS FROM ULTRASOUND IMAGING**

Examining Committee:

Chair: **Title and Name**

Professor Ted Milner
Senior Supervisor
School of Kinesiology

Associate Professor Steve Robinovitch
Co-Supervisor
School of Kinesiology

Professor Thomas Oxland
External Examiner
University of British Columbia

Date Defended/Approved: Nov. 29/05

DECLARATION OF PARTIAL COPYRIGHT LICENCE

STATEMENT OF ETHICS APPROVAL

The author, whose name appears on the title page of this work, has obtained, for the research described in this work, either:

(a) Human research ethics approval from the Simon Fraser University Office of Research Ethics,

or

(b) Advance approval of the animal care protocol from the University Animal Care Committee of Simon Fraser University;

or has conducted the research

(c) as a co-investigator, in a research project approved in advance,

or

(d) as a member of a course approved in advance for minimal risk human research, by the Office of Research Ethics.

A copy of the approval letter has been filed at the Theses Office of the University Library at the time of submission of this thesis or project.

The original application for approval and letter of approval are filed with the relevant offices. Inquiries may be directed to those authorities.

Simon Fraser University Library
Burnaby, BC, Canada

ABSTRACT

Using ultrasound, the feasibility of estimating lumbar mechanics in-vivo was evaluated. In Experiment 1, images were obtained while subjects were seated with the pelvis fixed and pulled on an anchored cable by isometrically contracting trunk muscles at different force levels. Linear regression identified ultrasound measurements which were correlated with trunk force. In Experiment 2, the cable was released and the trunk was rapidly displaced by shortening springs during the isometric contraction. Ultrasound images of the transverse processes of the L1-L2 vertebrae were acquired during this displacement for the purposes of estimating L1-L2 joint stiffness.

Results suggest that ultrasound is more suitable for estimating lumbar mechanics in the coronal plane than the sagittal plane. A linear trend was found between changes in thickness of some muscles and trunk force and with changes in muscle activity. Displacement of the vertebrae during perturbation occurred too quickly to be tracked by conventional ultrasound.

KEYWORDS

Mechanics, Ultrasound, In-vivo, Spine, Pain

DEDICATION

To my family... thank you for your patience.

ACKNOWLEDGEMENTS

Workers Compensation Board of British Columbia. A government body dedicated to the safety and health of worker's in British Columbia located in Richmond, British Columbia, Canada supplied an abundance of resources for this project including development funding for specialized ultrasound image analysis software, scholarship support to offset my cost of living, equipment specific money to help purchase required electronic equipment and provided reimbursement for much of my travel expenses to international symposiums to disseminate the results of this research. Thank you for believing in and funding this project. I hope you see the benefits of continued support of this work by the Neuromuscular Control Laboratory at Simon Fraser University as clearly as I do.

Dr. Ted Milner (Professor, School of Kinesiology, Simon Fraser University). Provided me prompt scientific responses to all of my questions within and outside the scope of this work. I have met many motivated and bright individuals but Dr. Milner is by far the hardest working and most creative. It was an easy choice to work with him on such a worthy project.

Ms. Vickie Lessoway (Professional Sonographer, BC Women's Health Centre). Without Vickie's tenacious attitude and sonography expertise this project would not have moved forward as it did.

Mr. Mike McFarland (Electronics Engineer, McKesson Medical Imaging). Mike is a charismatic engineer who helped me with the electromyography and force data collection equipment set-up at the Robotics and Control Laboratory at the University of British Columbia.

Dr. Robert Rohling (Professor, Electrical and Computer Engineering, University of British Columbia). Dr. Rohling provided the GE Medical Systems Voluson 730 ultrasound machine and space to conduct the experiments.

TABLE OF CONTENTS

Approval ii

Abstract iii

Dedication iv

Acknowledgements v

Table of Contents vii

List of Figures ix

List of Tables xiii

1 Scientific Summary and Review of Existing Literature 1

1.1 Scope of the Problem 1
1.2 Low Back Mechanics and Injury Mechanisms 2
1.3 Utilizing Medical Imaging to Study Muscle Mechanics 4
1.3.1 Ultrasound vs Other Imaging Technologies 5
1.3.2 Basics of Diagnostic Ultrasound Physics 5
1.3.3 Diagnostic Ultrasound Wave Properties – Image Effects 6
1.3.3.1 Sound Definition 6
1.3.3.2 Transducer Frequency Effects – Spatial Resolution 6
1.3.3.3 Transducer Frequency Effects – Axial Resolution 7
1.3.3.4 Transducer Frequency Effects – Lateral Resolution 7
1.3.3.5 Reflection and Transmission at Interfaces 8
1.3.3.6 Reflection 8
1.3.3.7 Refraction 9
1.3.3.8 Attenuation of Ultrasound Waves in Tissue 9
1.3.3.9 Ultrasound Instrumentation – Image Features 10
1.3.3.10 Image Quality and Artifacts 11
1.3.4 Ultrasound Imaging of Muscle 12
1.3.5 Ultrasound and Muscle Mechanics 13
1.3.6 Ultrasound and Tendon Mechanics 15
1.3.7 Ultrasound and Muscle-Tendon Unit Mechanics 15
1.3.8 Ultrasound, Electromyography and Muscle Mechanics 17
1.3.9 Ultrasound and Muscle Dynamics 17

2 Introduction 19

2.1 Objectives and Hypotheses 19

3 Methodology 21

3.1 Ethics Approval 21
3.2 Subjects 21
3.3 Apparatus 21

3.4 Data Acquisition 24
3.5 Protocol 25
3.6 Data Analysis 39
3.7 Statistical Analysis 42

4 Results 44

4.1 Ultrasound Images – Preliminary Testing 44
4.1.1 Resolution 44
4.1.2 Phantom Calibration 46
4.1.3 Pilot Tests of Ultrasound Imaging 54
4.2 Ultrasound Images - Descriptive Statistics 60
4.3 Linear Regression Analysis 64
4.3.1 Individual Subject Data 64
4.3.2 Data Averaged over all Subjects 69
4.4 Ultrasound Images – Dependence on Trunk Orientation 73
4.5 Lumbar Stiffness Estimation 77
4.6 EMG, Force and Ultrasound 80

5 Discussion 85

6 Conclusions 98

7 Future Research 99

References 100

Appendix A - Diagnostic Ultrasound Safety 108

Appendix B – Research Design 110

Appendix C – Recruitment Poster 111

Appendix D – Data Acquisition Form 112

Appendix E – Torque Impulse Calculation 119

Appendix F – Vertebrae Angle Calculation 121

Appendix G – Technical Problems 125

LIST OF FIGURES

Figure 3.1 Subject in apparatus pulling in extension.....22

Figure 3.2 Subject in apparatus pulling in lateral flexion.....22

Figure 3.3 First scan region: A sagittal plane scan of the longisimus thoracis and associated vertebral transverse processes at lumbar segments L1 and L2.....26

Figure 3.4 Example of caliper placement #1 (Region #1; Experiment #1) (D2) and caliper placement #2 (Region#1; Experiment 1) (D1). Measuring the thickness of the longissimus muscle. 28

Figure 3.5 Example of caliper placement #3 (Region #1; Experiment 1). Measuring the pennation angle of the erector spinae.....28

Figure 3.6 Transverse plane of second, third and fourth scan region.....29

Figure 3.7 Example of structures imaged during second scan region. 29

Figure 3.8 Example of caliper placement #1 (Region #2; Experiment 1) (D1) and caliper placement #2 (Region #2; Experiment 1) (D2). Measuring the thickness of the erector spinae in the transverse plane.....31

Figure 3.9 Example of structures imaged during third scan region.....32

Figure 3.10 Example of caliper placement #1 (Region #3; Experiment 1) (D1), caliper placement #2 (Region #3; Experiment 1) (D2) and caliper placement #3 (Region #3; Experiment 1) (D3). Measure the distance from the skin, the A-P diameter and the M-L diameter of the quadratus lumborum.....33

Figure 3.11 Example of structures imaged in the fourth scan region.....34

Figure 3.12 Example of caliper placement #1 (Region #4; Experiment 1) (D2), caliper placement #2 (Region #4; Experiment 1) (D3) and caliper placement #3 (Region #4; Experiment 1) (D4). Measuring the M-L thickness of the external oblique, internal oblique and transversus abdominis muscles 35

Figure 3.13 Example of caliper placement #1 (Region #1; Experiment 2). Distance between the L1-L2 transverse processes before perturbation. 38

Figure 3.14 Example of caliper placement #2 (Region #1; Experiment 2). Distance between the L1-L2 transverse processes at maximum displacement during the perturbation.....39

Figure 4.1 Mechanical effects of diagnostic ultrasound on human soft tissues. Rarefraction measures are used in the calculation of "Mechanical Index" 48

Figure 4.2 Image from phantom calibration testing. Vertical plane target group. (9 x 0.1 mm diameter wires separated by 1 cm). Caliper measurement is displayed in bottom right corner. 49

Figure 4.3 Near field resolution image from phantom testing of 0.1 mm diameter wire located 1mm from the surface of the phantom (arrow)..... 50

Figure 4.4 Axial (horizontal) resolution image from phantom testing of 6 x 0.1 mm diameter wires separated by 2 cm; 2 x 0.1 mm wires separated by 0.5 mm (arrow). Caliper measurement is displayed in bottom right corner. 51

Figure 4.5 Lateral resolution image from phantom testing with 3 groups of 6 x 0.1 mm wire placed at 3 different depths and lateral orientation. 53

Figure 4.6 Quadratus lumborum (right side) relaxed (A) and during exertion of 50% of maximal right lateral flexion force (B). Both images show the distance from the muscle to the skin (D1) A-P thickness (D2) and M-L thickness (D3). 56

Figure 4.7 Longissimus thoracis relaxed (A) and during exertion of 50% of maximal trunk extension force (B). Both images give the pennation angle (a) in the bottom right corner. 57

Figure 4.8 Tips of the transverse processes of L1-L2 (right side) when torso is oriented vertically (A) and laterally flexed to the left (B). Both images give the distance between the tips of the transverse processes (D1) in the bottom right corner. 58

Figure 4.9 Tips of the transverse processes of L1-L2 (right side) when torso is oriented vertically and subject is contracting in lateral flexion to the right at 25% MVC (A) and at the point where the direction of motion changes during perturbation as previously described (B). Both images give the distance between the tips of the transverse processes (D1) in the bottom right corner. 59

Figure 4.10 Scatter plot of the ultrasound variable with the lowest correlation with trunk force in extension (longissimus thoracis – pennation angle) from 1 subject. (Normalized to 10% MVC)..... 66

Figure 4.11 Scatter plot of the ultrasound variable with the highest correlation with trunk force in extension (erector spinae - lateral) from 1 subject. (Normalized to 10% MVC)..... 66

Figure 4.12 Scatter plot of the ultrasound variable with the lowest correlation with trunk force in lateral flexion (longissimus thoracis – L1) from 1 subject. (Normalized to 10% MVC)..... 67

Figure 4.13 Scatter plot of the ultrasound variable with the highest correlation with trunk force in lateral flexion (internal oblique diameter) from 1 subject. (Normalized to 10% MVC) 67

Figure 4.14 Mean (diamond), ±1 standard error (solid bar) and ±1 standard deviation (broken bar) for scatter plot of the ultrasound variable with the lowest correlation with trunk force in extension (longissimus thoracis – pennation angle) averaged over 10 subjects. (Normalized to 10% MVC) 70

Figure 4.15 Mean (diamond), ±1 standard error (solid bar) and ±1 standard deviation (broken bar) for scatter plot of the ultrasound variable with the highest correlation with trunk force in extension (erector spinae - medial) averaged over 10 subjects. (Normalized to 10% MVC) 70

Figure 4.16 Mean (diamond), ±1 standard error (solid bar) and ±1 standard deviation (broken bar) for scatter plot of the ultrasound variable with the lowest correlation with trunk force in lateral flexion (longissimus thoracis – L1) averaged over 10 subjects. (Normalized to 10% MVC) 71

Figure 4.17 Mean (diamond), ±1 standard error (solid bar) and ±1 standard deviation (broken bar) for scatter plot of the ultrasound variable with the highest correlation with trunk force in lateral flexion (internal oblique diameter) averaged over 10 subjects. (Normalized to 10% MVC) 71

Figure 4.18 Scatter plot of the ultrasound variable with the lowest correlation with trunk orientation (longissimus-thoracis – L2) from 1 subject. 75

Figure 4.19 Scatter plot of the ultrasound variable with the highest correlation with trunk orientation (external oblique) from 1 subject. 75

Figure 4.20 Distance between the L1-L2 transverse processes vs %MVC at the time just prior to torso perturbation 78

Figure 4.21 Distance between the L1-L2 transverse processes vs %MVC at the time of maximum displacement during torso perturbation. 79

Figure 4.22 Change in distance between the L1-L2 transverse processes vs %MVC at the time of maximum displacement compared to pre-perturbation. 80

Figure E.1 Typical force trace during a perturbation trial 119

Figure E.2 Integral calculation of torque impulse 120

Figure F.1 Examples of vertebral parameters required for angle calculations. 123

Figure G.1 Force during isometric torso extension at 50% MVC with infiltrating 60 Hz noise 125

Figure G.2 Erector Spinae (longissimus thoracis) EMG during dynamic torso flexion/extension with 60 Hz noise. 126
Figure G.3 Erector Spinae (longissimus thoracis) EMG during isometric torso extension tests at 50% MVC when acquiring force simultaneously. 127
Figure G.4 Force during isometric torso extension at 50% MVC after changing data acquisition system. 128
Figure G.5 Erector Spinae (longissimus thoracis) EMG during isometric torso extension at 10% MVC after changing data acquisition system. 128
Figure G.6 Erector Spinae (longissimus thoracis) EMG during isometric torso extension at 25% MVC after changing data acquisition system. 129
Figure G.7 Erector Spinae (longissimus thoracis) EMG during isometric torso extension at 50% MVC after changing data acquisition system. 129

LIST OF TABLES

Table 1.1 Advantages and disadvantages of muscle imaging technologies. 5

Table 4.1 Pilot test results of ultrasound imaging. 55

Table 4.2 Summary of measurements made from ultrasound images. 60

Table 4.3 Coefficients of Variation for raw data of each ultrasound variable measured at each contraction level for lateral flexion averaged from individual values for 10 subjects. 60

Table 4.4 Coefficients of Variation for raw data of each ultrasound variable measured at each contraction level for extension averaged from individual values for 10 subjects. 61

Table 4.5 Means, Standard Deviations and Coefficients of Variation for raw data of each ultrasound variable measured at each contraction level for lateral flexion computed for 10 subjects 62

Table 4.6 Means, Standard Deviations and Coefficients of Variation for raw data of each ultrasound variable measured at each contraction level for extension computed for 10 subjects 63

Table 4.7 Average linear regression parameters for individual subject data. 68

Table 4.8 Summary of linear regressions on averaged data. 72

Table 4.9 Summary of linear regression analysis with the subject of post-hoc test #1Trunk Orientation) 76

Table 4.10 Linear regression parameters for the subject of post-hoc test #2 (Ultrasound Measurement vs. Trunk Force). 82

Table 4.11 Linear regression parameters for the subject of post-hoc test #3 (Ultrasound Measurement vs. EMG) 84

Table B.1 Research Design for Static Measurements (Experiment 1) 110

Table B.2 Research Design for Dynamic Measurements (Experiment 2) 110

Table F.1 Geometrical measurement survey of lumbar vertebrae 124

1 SCIENTIFIC SUMMARY AND REVIEW OF EXISTING LITERATURE

1.1 Scope of the Problem

Low Back Pain (LBP) is a common condition affecting a large percentage of the population. It is estimated that between 70 to 85 % of the population will experience LBP at some point in their lives (Andersson, 1997; Biering-Sorensen, 1983; Waddell, 1987). The majority of these cases resolve without medical intervention within the first six weeks (Waddell, 1987); however, the small minority of cases that progress to become chronic bears a significant cost burden (Abenhaim and Suissa, 1987; Spengler et al., 1986). Not surprisingly, LBP is one of the most prevalent and costly health problems in Western Society (Andersson, 1999). Within British Columbia, LBP claims account for 25% of all workplace injuries and approximately 40% of compensation costs (Worker's Compensation Board of British Columbia, 2001). Injury trends have shown that disability from LBP dramatically increased between 1950 and 1980 (Frymoyer and Cats-Baril, 1987; Waddell, 1987) with disability rates increasing by 14 times the rate of population growth over this time period (Frymoyer and Cats-Baril, 1987). Improper medical management is believed to be one of the primary causes of this rise in number and associated cost (Waddell, 1987). The need for further understanding of these conditions is required to develop evidence-based approaches to minimize the impact of LBP in society.

1.2 Low Back Mechanics and Injury Mechanisms

McGill (1998) describes the mechanical properties of the spine by comparing it to a flexible rod that has muscles attached much like guidewires attached to a ship's mast. Crisco et al., (1992) showed that a lumbar spine devoid of muscles (ligaments only) will buckle under compressive loading at about 90 N (19.8 lbs.). Activation of muscles attached to the spine is necessary to prevent this buckling by acting as guidewires. Even though these guidewires ultimately increase the compressive forces on the spine, the spine's tolerance to buckling is significantly increased as the spine stiffens. Injury to the spine and subsequent LBP may occur if these muscles are not capable of stiffening the spine because of a lack of strength, compromised passive structures, abnormal muscle coordination or impaired control.

Risk of developing LBP is multi-factorial with exposure to physical loading being one of the most significant risk factors (Marras et al., 2001). Occupations where manual material handling is required, in particular lifting, have been strongly correlated with LBP, accounting for 50-70% of all back disorders (Bigos et al., 1986). Unexpected loading when muscle activity is low, as may occur during slips and trips is associated with the most serious low back injuries (Troup et al., 1981; Bigos et al., 1986). However, spinal loading is not always as indicative of high risk as one might expect. Evidence suggests that occupations with high incidence of LBP are not necessarily associated with levels of spinal loading beyond the recommended limit of 6400 N set by NIOSH (Herrin et al., 1986). Furthermore, employees in high spinal loading occupations continue working without ever developing LBP (Granata et al., 1996). These observations suggest that although spinal loading is considered a factor in developing LBP, it is not necessarily

the degree of loading that is important. How people cope with these spinal loads plays a key role in determining injury and subsequent LBP.

How does spine injury occur? Panjabi (1992) proposed a novel injury model based on spine stability. He has defined the term instability: "...as a significant decrease in the capacity of the stabilizing system of the spine to maintain the intervertebral neutral zones within the physiological limits so that there is no neurological dysfunction, no major deformity, and no incapacitating pain". They identified three subsystems contributing to this spine stability: 1) the passive subsystem consisting of the vertebrae and facet joints, ligaments, and intervertebral disks; 2) the active subsystem consisting of the muscles and tendons surrounding the spinal column; 3) the neural and feedback subsystem consisting mainly of the control centres that excite and coordinate the active subsystem. A dysfunction in any one of these three subsystems can contribute to instability of the spine and, therefore, lead to subsequent injury.

In the literature there is strong evidence to suggest that individuals with LBP have altered muscle recruitment patterns which may affect internal spine loads (Lariviere et al., 2000; Marras et al., 2001) and delayed reflex responses which may reduce lumbar stability under sudden loading (Radebold et al., 2000; Radebold et al., 2001; Reeves et al., 2005). However, it is not known if these changes in muscle activation are significant enough to produce lumbar instability under dynamic loading or whether their destabilizing effects can be compensated by increased coactivation, which is observed in LBP patients (Lariviere et al., 2000; Marras et al., 2001). One method of investigating the effects of muscle activation on spine mechanics is to develop a model of the lumbar spine that is capable of quantifying stability under dynamic loading.

Currently, only a few models exist which are capable of quantifying lumbar stability (Bergmark, 1989; Cholewicki and McGill, 1996; Gardner-Morse et al., 1995; Granata and Marras, 2000).The model developed by Cholewicki is capable of assessing the mechanical effect of different muscle recruitment strategies (i.e. spinal loading coping mechanisms) by converting electromyographic signals recorded from trunk muscles into mechanical outputs (Cholewicki et al., 1996; Gardner-Morse et al., 1995; Granata et al., 1996). There are several limitations however, to this and other current models: 1) they are static in nature – meaning the predicted results from these models can only be applied or generalized to situations of static loading of the spine; 2) they assume that the activation of non-superficial muscles is similar to the activation recorded from superficial muscles. For example, the activation of the psoas muscle and the quadratus lumborum are predicted from synergistic surrogate muscles (Lafortune et al., 1988) and deep spinal muscles such as the intertransversarii and rotators, are lumped with the passive properties of the vertebrae and facet joints, ligaments, and intervertebral disks (Cholewicki et al., 1996). This may limit the accuracy of these models. There is a need to extend these models to encompass dynamic loading conditions and to assess the validity of assuming that surface EMG is representative of deep muscle activation.

1.3 Utilizing Medical Imaging to Study Muscle Mechanics

Medical imaging technologies offer the possibility of non-invasive observation of the dynamic behavior of the lumbar spine. Quantification of mechanical properties from temporal and spatial changes in the images in response to changes in muscle activation or perturbations of the lumbar spine could provide parameter estimates needed for a model of dynamic spine loading. Currently, there are three major technologies for imaging

internal body structures: computed tomography, magnetic resonance imaging and ultrasound.

1.3.1 Ultrasound vs Other Imaging Technologies

Although, ultrasound has poor spatial resolution in comparison to computed tomography and magnetic resonance imaging, the examination can be quickly repeated and there is no exposure to ionizing radiation (Clague et al., 1995). Furthermore, it is better suited for examining temporal changes in internal body structures. Table 1.1 highlights differences between these three imaging technologies.

Table 1.1 Advantages and disadvantages of muscle imaging technologies.

Variables of Imaging Technologies	Ultrasonography	Computed Tomography	Magnetic Resonance Imaging
Availability	Readily available	Readily available	Increasing
Cost	Inexpensive	Expensive	Very expensive
Portability	Portable	Fixed	Fixed
Soft tissue contrast	Fair	Good	Excellent
Muscle detail	Fair	Good	Very good
Safety	Excellent	Ionizing Radiation	Excellent
Time to acquire image	Real time (ms)	Long (seconds to minutes)	Long (minutes to hours)
Spatial resolution	1-2 mm	<1 mm	<1 mm
Temporal resolution	Tens of ms	Hundreds of ms	Seconds

Source: Adapted from Clague et al., 1995

1.3.2 Basics of Diagnostic Ultrasound Physics

The fundamental mechanism that creates the ultrasound image is the strength of the reflected sound waves (echoes). Ultrasound involves sending an array of sound wave pulses into tissues and analyzing the temporal and acoustic properties of their echoes in order to reconstruct an image (Riley, 1996a, b; Kremkau, 2002). The probe or ultrasound transducer that is placed on the subject both emits sound wave pulses and records its echoes. When an electric current passes through the component material of the transducer

(quartz crystal) it causes a slight conformational change that induces vibration and hence a sound wave pulse. However, this same material also generates an electric current when the returning sound waves reflected from structures inside the body cause it to vibrate. Newer materials used in ultrasound transducers (synthetic ceramics) are also capable of bidirectional transduction of electrical and acoustic energy (Riley, 1996a, b; Kremkau, 2002).

1.3.3 Diagnostic Ultrasound Wave Properties – Image Effects

1.3.3.1 Sound Definition

The physical definition of sound is *mechanical energy transmitted by pressure waves in a material medium* (Webster's ninth new collegiate dictionary, 1986). The sound waves emitted from diagnostic ultrasound probes are longitudinal waves that travel through human tissue (Zagzebski, 1996).

1.3.3.2 Transducer Frequency Effects – Spatial Resolution

As previously mentioned sound requires a vibrating source that acts on molecules of the surrounding medium, in this case tissue, and transmits this wave through it. The frequency of this vibration determines the wave frequency travelling through the medium. In diagnostic ultrasound these frequencies fall in the range of 1 to 20 MHz (Zagzebski, 1996). The speed of sound is independent of frequency and is solely determined by the root of the ratio between the *bulk modulus* (stiffness of the medium) and the *density of the medium*. Although speeds differ in every tissue of the body the speed of sound in muscle is 1600 m/s and the average speed in soft tissue averages 1540 m/s (Zagzebski, 1996). Wavelength of the transmitted sound wave then, is dependent on

the relation of both speed of sound and its frequency. So as the frequency increases the wavelength decreases. The wavelength is important in diagnostic ultrasound because it is related to several imaging features such as spatial resolution. Spatial resolution refers to how closely positioned two reflectors (objects of higher density than the main medium) can be to one another and still be identified as separate on the reconstructed image. The spatial resolution of the ultrasound image is directly proportional to the frequency of the incident sound. However, the depth of penetration is inversely related to this frequency (Riley 1996a, b; Kremkau, 2002). Hence, it is necessary to compromise between depth of penetration and resolution, with the choice of frequency depending on the object being scanned. It follows that with high frequency ultrasound transducers superficial structures can be studied in greater detail than deeper layers.

1.3.3.3 Transducer Frequency Effects – Axial Resolution

Axial resolution refers to the minimum reflector spacing along the axis of the ultrasound beam that results in separate, distinguishable echoes in the image. Axial resolution is determined by the pulse duration, which is the duration of the ultrasonic pulses transmitted into the medium by the transducer. The pulse duration is equal to the ratio between the number of cycles and the frequency of the transducer. Reducing the pulse duration will increase the axial resolution of the ultrasound image (Zagzebsk, 1996).

1.3.3.4 Transducer Frequency Effects – Lateral Resolution

Lateral resolution refers to the ability to distinguish two closely spaced reflectors that are positioned perpendicular to the axis of the ultrasound beam. Lateral resolution is

dependent on the near field length (NFL). NFL is characterized by fluctuations in the amplitude and intensity from one point in the beam to another and runs parallel to the beam. NFL is determined by the square of the diameter of the transducer divided by four times the wave length. Since, wave length is inversely proportional to transducer frequency as we increase frequency we increase NFL. This may be counter intuitive since we have already learned that as we increase frequency we decrease beam penetration (Wells, 1977).

1.3.3.5 Reflection and Transmission at Interfaces

Reflection or refraction of sound waves occurs whenever a boundary is encountered between materials that transmit sound at different speeds. This difference is called acoustic impedance. The acoustic impedance is equal to the product of the density of the medium and its speed of sound (Robinson et al., 1981).

1.3.3.6 Reflection

The amount of energy that is reflected and refracted depends on the angle of incidence and acoustic impedances of the interface between the two materials. Some reflection will occur whenever the sound wave encounters an interface between two materials having different acoustic impedances. The acoustic impedance differences could be due to the change in speeds of sound or a change in densities or both. The larger the difference, the greater the proportion of the energy of the incident sound wave that will be reflected and the less that will be refracted and transmitted through the object. According to Snell's law, the greater the angle of incidence, the greater the angle of

reflection which makes structures with large angles of reflection hard to see since the intensity of the image is dependent on the amplitude of the reflected sound waves.

1.3.3.7 Refraction

Refraction refers to the "bending" of the sound wave, that is, a change in the direction of the transmitted sound wave, at the interface. This is also dictated by Snell's law. Typical values of the refraction angle when the incident angle is 30 degrees are 27.1 degrees for muscle-fat interface and 28.8 degrees for muscle-fluid interface (Robinson et al., 1981). Refracted sound energy penetrates deeper into the body and can undergo further reflections. Thus, ultrasound is suitable for mapping not only superficial structures but may also be suitable for imaging deeper structures as well.

1.3.3.8 Attenuation of Ultrasound Waves in Tissue

As a sound wave traverses tissue, its amplitude and intensity are reduced as a function of distance from the transducer. This is called attenuation. Reflection and absorption are the two main sources of attenuation. The degree of sound wave attenuation in a tissue is usually given in decibels per centimeter (dB/cm). The attenuation coefficient for muscle at 1 MHz is 1.2 (Zagzebski, 1996). For perspective, a drop of 3 dB results in half of the original intensity. As previously mentioned, frequency of the sound wave and attenuation are strongly related. In fact, in most cases attenuation is proportional to the frequency (Zagzebski, 1996). This increased attenuation with increasing frequency results in poorer "penetration" into tissues with higher frequency sound waves. This is one of the limitations of diagnostic ultrasound.

1.3.3.9 Ultrasound Instrumentation – Image Features

The intensity of the echo is converted into a brightness level to create a visible image. Contrasts in the image arise from differences in the intensity of the echoes which are determined primarily by the difference in the speed of sound in a material compared to its speed in water, the principal constituent of internal body structures. However, the energy carried by echoes from deeper structures will be lower than that carried by the more superficial echoes. Therefore, the deeper the penetration the greater the need for amplification of the echoes (Riley, 1996a, b; Kremkau, 2002). Structures that do not have high water content such as bone or air pockets do not refract sound, i.e, they only reflect it so their internal structure cannot be probed using ultrasound nor can ultrasound penetrate beyond them. Therefore, ultrasound is restricted to structures superficial to these types of low water content tissues.

As well, frame rate or scanning speed is an important performance characteristic of real-time scanners such as the one used in this study. This aspect of imaging performance is tightly related to temporal resolution. The higher the frame rate, the better the ability to image rapidly moving objects. The principle behind this is quite simple. We are limited by the time it takes a series of sound wave pulses to be sent and reflected back. Between each pulse the sound wave direction is shifted and until the entire region of interest has been swept out. Hence, as we increase the size of the sweep angle or depth of the scan region we increase the duration required for one sweep and reduce the temporal resolution.

1.3.3.10 Image Quality and Artifacts

A B-mode or 'brightness' mode ultrasound image appears granular rather than uniformly gray. This is referred to as image texture. The understanding of why the image appears this way leads to more accurate interpretation of the imaged structures. Texture on an ultrasound image is a result of refracted and reflected waves from sites distributed throughout an organ. For muscle, many of these sites represent fascicle boundaries (Fischer et al., 1988). However, there are also many other features that act to refract sound and they are the topic of many research projects (Zagzebski, 1996). Depending on their arrangement these refracting features can either cause constructive or destructive interference between reflected waves. Hence, the mottled dot appearance or speckle.

According to Zagzebski (1996) there are three assumptions made by diagnostic ultrasound. 1) Reflectors give rise to echoes lying along the transmission axis of the sound wave. Each dot on a B-mode image is positioned along a line corresponding to this axis when the echo is picked up. 2) The speed of sound is assumed to be 1540 m/s. This number is required to compute the distance each reflector lies away from the transducer. 3) The echo strength displayed as a shade of grey on a B-mode image, only indicates organ echogenicity.

These assumptions are never entirely met. For example, sound speed changes depending on the stiffness and density of the tissue. As well, reflections may be picked up from areas slightly off the transmission axis or the sound wave may be refracted and therefore any reflections subsequent to this path change will be inaccurate. As well, attenuation can cause shadowing of deep structures.

Despite these errors it is possible to make relatively accurate measurements. This is because the errors mentioned above are usually create not more than 1-2% of the true dimensions of the structure being imaged. Distance measurements are usually more reliable if they are taken along the path of the ultrasound wave (Goldstein et al., 1987).

1.3.4 Ultrasound Imaging of Muscle

The simplest application of ultrasound to imaging of muscle involves the anatomic study of healthy muscle. Muscle can be examined using B-mode (Brightness-mode) or real-time ultrasound scanning techniques. Normal muscle parenchyma appears as a homogeneous echogenic matrix separated internally by hyperechogenic fascial planes (Fischer et al., 1988; Cady et al., 1983). Muscle cells themselves generate few echoes because of their highly regular internal structure of repeating proteins called sarcomeres (Heckmatt and Dubowitz, 1988; Ferrel et al., 1989; Walker et al., 1990). This arrangement provides minimal interfaces for sound reflection. Muscle tissue also exhibits anisotropy in that the degree of echogenicity varies with the direction of the sound wave.

For routine imaging of muscle, it has been suggested to include sections of the images that contain other tissues. These provide an objective reference for evaluating the relative echogenicity of the muscle (Walker, 1996, 1998). Bone on the other hand typically generates bright echoes that defines its outer edge as almost all sound is reflected from its surface. As a result, it casts a shadow below its surface as sound cannot penetrate to create echoes of deeper lying structures (Walker et al., 2004). Including identifiable bony landmarks in an image is also helpful for comparative studies identifying the equivalent structure located on opposite sides of the body or for serial studies (Walker et al., 2004). Typically, it has been difficult to image muscles that lie

over one another. As technology has evolved, this difficulty has become less problematic but still remains a challenge in deeper structures, such as the psoas or paraspinal complexes (Walker et al., 2004).

Different muscles have differing amounts of fibrous tissue and therefore, may have varying levels of echogenicity. For example the triceps are typically less echogenic than the biceps (Walker, 1996). As well, trained muscles that have undergone hypertrophy may be somewhat hypoechoic due to a volume effect; similarly deconditioned muscle may be hyperechoic (Walker and Jackson, 1997). Adipose tissue can also reduce the echogenicity of muscle images since, it absorbs a great amount of the penetrating sound energy leaving less to be reflected by muscle perimysium (Reimers et al., 1993a, b).

Because most architectural parameters change with muscle contraction, ultrasonography may be used as a non-invasive method to detect or measure activity of specific muscles during isometric contractions. Ultrasound has been routinely used to estimate the cross-sectional area of muscles for clinical purposes such as the identification of dystrophic muscle (Heckmatt et al., 1988), the wasting of lumbar muscle in patients with low back pain (Hide et al., 1994) and the function of respiratory muscles during dynamic pulmonary changes (McKenzie et al., 1994), but only recently has it been applied to investigating muscle mechanics (See section 1.3.5).

1.3.5 Ultrasound and Muscle Mechanics

The first published study using ultrasound to quantify muscle mechanical parameters appeared in 1995 (Herbert and Gandevia, 1995) and examined changes in the

angle of pennation of the brachialis muscle during isometric contraction and changes in elbow joint angle. Additional studies looking specifically at in-vivo muscle parameters relating to mechanics were carried out by Fukunaga et al. (1997), who measured fascicle length and pennation angle in contracting human muscle in-vivo. They found that the fascicle length decreased and pennation angle increased as muscle contraction strength increased. Kawakami et al. (1998) studied the triceps surae muscles to determine how muscle architecture (fascicle length and pennation) changed with different ankle angles, passively and during contraction. As ankle extension increased, fascicle angle increased and fascicle length decreased over both conditions. However, fascicle length was shorter and pennation angle steeper across all ankle angles in the active condition. Other researchers investigated how pennation angle increases with joint torque at the knee (Rutherford et al., 1992) and ankle (Maganaris et al., 1999), as well as how fascicle length and pennation angle change with isometric muscle contraction (Narici et al., 1996; Maganaris et al., 1998). A more recent study of muscle architechture in-vivo found that muscle thickness decreased and pennation angle increased along the length of the medial gastrocnemius from proximal to distal, under the same fixed condition, although the fascicle length did not change (Muramatsu et al., 2002). Muramatsu et al. (2002) also determined how fascicle curvature, previously assumed to be straight, underestimated the true fascicle length by over 6%. This knowledge is crucial in the understanding of the mechanical functions of human skeletal muscle in-vivo. Richardson et al. (2002) studied how increases in the transversus abdominis muscle thickness detected by ultrasound (indicating muscle activity) was related to the sacroiliac joint stiffness.

1.3.6 Ultrasound and Tendon Mechanics

Other fundamental studies utilized ultrasound measurements to investigate tendon mechanics. Maganaris et al. (1999) measured tibialis anterior tendon displacement and cross sectional area changes during maximum contractions. As well, Young's modulus, creep and hysteresis were calculated from the elongation of the gastrocnemius tendon during isometric planterflexion and estimates of tendon force from joint torque measurements (Maganaris and Paul, 2002; Maganaris, 2002; Maganaris et al., 2004). Other studies suggest plasticity of tendon mechanical properties such as decreasing hysteresis and stiffness under pre-stretched conditions (Kubo et al., 2001) and decreasing hysteresis but no decrease in stiffness as a result of a three week stretching regime (Kubo et al., 2002).

1.3.7 Ultrasound and Muscle-Tendon Unit Mechanics

Further advances in this field have come from researchers incorporating the evolving muscle and tendon information into studies of dynamic muscle-tendon interactions. For example, Fukunaga et al. (1997) showed that although pennation angle and fascicle length changed with contraction levels of the tibialis anterior and vastus lateralis muscles, the tendon elongated during isometric contractions when compared to moving the limb freely without a load. Similarly, Ichinose et al. (1997) measured the same variables when the subject increased joint torque from zero to maximum with changes in knee angle. At each knee angle, fascicle length decreased and pennation angle increased with increasing torque indicating the compliance of the muscle-tendon unit (MTU). The compliance of the MTU increased as the knee was extended. In-vivo dynamics was the next step investigated first by Kubo et al. (2000). This research group

measured fascicle length in the medial gastrocnemius muscle during plantar flexion/dorsiflexion cycles (1 Hz). They showed that during the switching phase from dorsiflexion to plantar flexion the fascicle length did not change while the tendon underwent rapid shortening. They calculated that the observed tendon behaviour contributed up to 42.5% of the total amount of work required for the plantar flexion phase. Kawakami et al. (2002) compared gastrocnemius fascicle length during strict plantar flexion contractions and plantar flexion contractions preceded by dorsiflexion. They found that the fascicle length shortened throughout the movement during the strict plantar flexion motion but remained relatively isometric when the movement was preceded by dorsiflexion, leaving the task of storing and releasing elastic energy to the tendon. Muramatsu et al. (2001) and Muraoka et al. (2002) determined that the amount of strain along the Achilles tendon and gastrocnemius aponerosus is uniform. Kawakami et al. (2002) discovered that shifts in the torque-angle relationship of the knee were due to elongations of the tendinous tissues of the vastus lateralis and intermedius as a function of the force applied to them. Investigators have also used ultrasound to investigate electromechanical delay (EMD). Muraoka et al. (2004) discovered that EMD of the ankle joint is affected by tendon slack. However, for ankle angles where there was no tendon slack EMD was not significantly different. Recently, Muraoka et al. (2005) discovered that Achilles tendon stiffness and ability to store elastic energy were both increased in subjects with larger plantar flexion strength. These findings suggest that the Achilles tendon of a stronger gastrocnemius muscle allows for more efficient transfer of force.

1.3.8 Ultrasound, Electromyography and Muscle Mechanics

Recently, several research groups have investigated how electromyography (EMG) and ultrasound measurements relate. Regression equations were used to predict activation (EMG) levels from ultrasound variables. Hodges et al. (2003) investigated the ability to estimate muscle activity using parameters such as pennation angles, fascicle lengths, and muscle thickness. They examined the tibialis anterior, biceps brachii, brachialis, transversus abdominis, internal oblique and external oblique. The results of this study indicated that there are limitations to what can be inferred about muscle contraction levels from ultrasound measurements. Most muscle architectural parameters changed markedly with contractions up to 30% maximum voluntary contraction (%MVC) but changed little at higher levels of contraction. Similarly, McKeenen et al. (2004) found that as transversus abdominis EMG activity increased so too did its thickness as observed with either B-mode or M-mode (Motion-mode) ultrasonography.

1.3.9 Ultrasound and Muscle Dynamics

Recording dynamic changes in muscle using ultrasound presents a challenge. Although, many of the studies referred to above have recorded from muscle contracting dynamically, the ultrasound probe remained stationary and secured to the stationary segment of the moving joint. This is to avoid unnecessary movement between the skin and the ultrasound transducer which would affect the quality of images. However, a research group in Japan (Fukunaga et al., 2001) recorded from the medial gastrocnemius using an ultrasound probe during walking on a treadmill. In particular, fixation of the ultrasound probe is key. Using non-elastic tape to secure not only the probe but also the skin on which it lies seems to allow for motion involving moderate accelerations without

losing image quality due to motion artifact or echogenicity of the tape. Ultrasound has also been used in the place of EMG to detect muscle fasciculations as it has the ability to sample larger areas of muscle in a 2D cross section than the small sphere of detection of a single EMG needle (Walker et al., 1990). Dynamic muscle imaging has also been used to measure tremor frequency and temporal aspects of other involuntary movement disorders using the M-mode of ultrasonography (Walker, 1998). With this technique, the image of a single line of ultrasound data is displayed over time, showing temporal effects of perturbations along a single dimension (Walker, 1996, 1998).

2 INTRODUCTION

The overall goal of the study is to determine whether ultrasound could be used to obtain estimates of muscle specific parameters for development of a dynamic model of lumbar stability. With such a model, further insight into low back dysfunction could be obtained that might help explain how people are injured during slips and trips, and load shifts. The model could be used to assess spinal function in relation to predisposition to injury or re-injury, and to evaluate various treatment options to enhance stability of the spine under dynamic loading. Examples of questions that the model could answer are "Does the abnormal activation patterns seen with LBP subjects and sometimes non injured subjects predispose them to re/injury?" and "Is the co-contraction seen with LBP subjects sufficient enough to stiffen the spine column against unexpected loads such as a slip or trip." Answering such questions could help to prevent low back injury and reduce the incidence of LBP.

2.1 Objectives and Hypotheses

The first objective of this project was to test whether changes in the shape of lumbar muscles that can be measured with ultrasound are a valid and reliable estimate of muscle force. Our hypothesis was that the pennation angle and thickness of contracting muscles would increase with trunk force.

The second objective of this project was to determine whether stiffness of the L1-L2 joint could be estimated from changes in joint torque and movement of the transverse

processes recorded in ultrasound images during trunk perturbation. Our hypothesis was that the maximum change in distance between the tips of the transverse processes during perturbation of the trunk would be reduced as isometric trunk force increased.

3 METHODOLOGY

3.1 Ethics Approval

Ethics approval has been obtained from both the University of British Columbia and Simon Fraser University's Research Ethics Review Committee for the research procedures outlined in this proposal. The procedures were clearly explained to all subjects prior to participation and subjects were asked to sign a consent form agreeing to participate in the research project. They were informed that they could withdraw from the study at any time without repercussions. All information regarding the subjects has been kept confidential.

3.2 Subjects

This was a feasibility study that looked at the ability of the methods to detect and accurately estimate lumbar stiffness and the ability to relate ultrasound parameters to force. Therefore, power calculations were not relevant; only 10 subjects, 6 female and 4 male, were recruited so that the project could be completed within an acceptable time frame and at a reasonable cost, given that a professional sonographer had to be hired to conduct all of the ultrasound scans. These subjects were all in good physical condition between the ages of 18 and 45 and had no history of disabling LBP in the past two years.

3.3 Apparatus

Subjects sat in an apparatus during all experiments (See Figures 3.1 and 3.2). The apparatus consisted of an octagonal frame constructed from sections of 2 inch aluminium

Figure 3.1 Subject in apparatus pulling in extension.

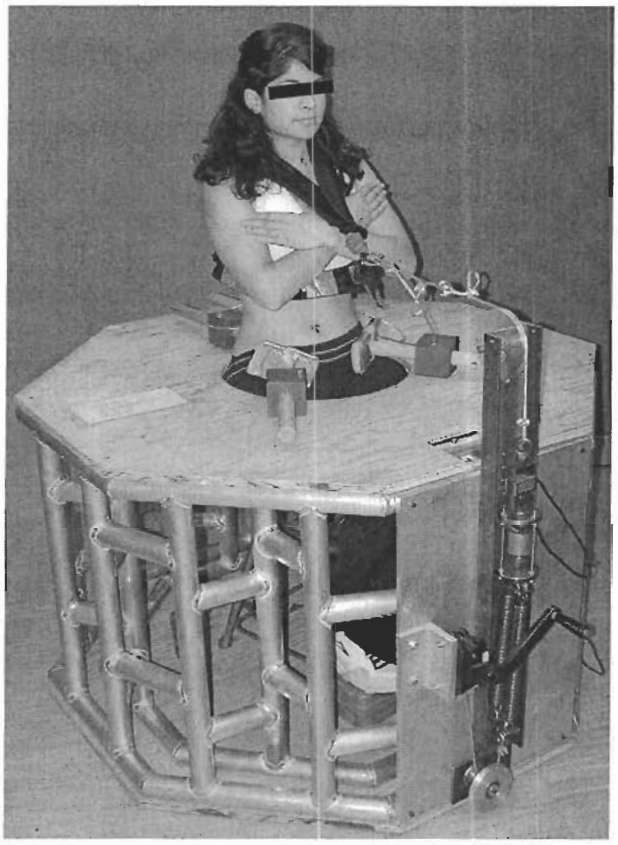

Figure 3.2 Subject in apparatus pulling in lateral flexion

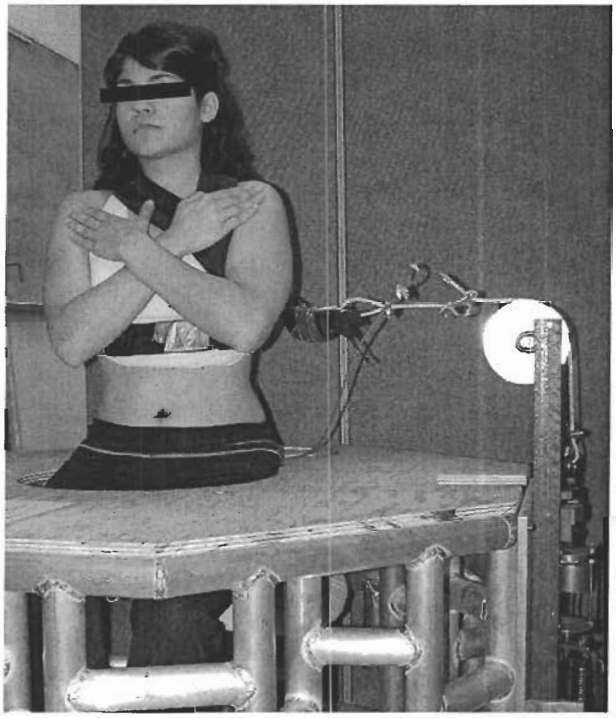

pipe, cross-braced to form an enclosure 4 ft wide by 3 ft tall. Sheets of ¾ inch plywood were affixed to the top and bottom of this frame for two reasons. First, the wood acted to electrically isolate the subject sitting inside from the aluminum enclosure and second, the wood acted to reinforce the mechanical structure. A circular hole was cut in the center of the top sheet of plywood. The subject entered the enclosure through the hole and sat on a stool. The stool's height was adjustable so that the pelvis of every subject was raised to the same height above the plywood sheet which had several holes that were used to position mechanical stops that restrained the pelvis. With the pelvis restrained only the torso was free to move. Since the pelvis was above the plywood the ultrasound probe was able to scan muscles of both the lumbar and iliac crest regions. A chest harness was worn by the subject. A force transducer was placed in series with a cable that rounded a pulley mounted on the apparatus and attached to the chest harness. The cable pulley height was adjustable so that the cable pulled at 90 degrees to the vertical when attached to the harness.

In the first experiment, the subject pulled isometrically against the cable, which was anchored to the frame. A computer screen displayed a target bar that corresponded to the force goal. A second bar displayed the corresponding force transducer output. The subject was instructed to match the height of the target bar.

In the second experiment, the cable was attached to preloaded springs that were disengaged by means of an electromagnet to permit the subject to contract isometrically until the electromagnet was released. Two springs were used each with a stiffness of 2500 N/m. The springs were attached in parallel to double the stiffness. The springs were loaded by shortening the cable with a winch that had a ratchet mechanism. The cable

could be shortened in 2.5 cm increments to a maximum of 12.5 cm, which produced a force of (0.125 m)(5000 N/m) = 625 N. However, it was found that 375 N was sufficient for most subjects. Once released, the springs were free to displace the subject's torso.

3.4 Data Acquisition

In the first experiment, ultrasound images of the key lumbar muscles were recorded unilaterally (right side) using a GE Medical Systems Voluson 730 ultrasound machine equipped with a 4 – 8 MHz software adjustable transducer with 2D or 3D capabilities. All measurements from ultrasound images were made with software calipers by the professional sonographer under single blinded conditions. The values of the measured angles and distances displayed on the ultrasound monitor were hidden from the sonographers view in order to avoid measurement bias. Tension in the cable attached to the chest harness was measured with the force transducer and recorded at 2000 Hz for 5 seconds, using a 12 bit data acquisition card (National Instruments Model No. 6014) when a command button in the Visual C program being used for data collection was depressed.

In the second experiment, ultrasound images of the transverse processes at the L1-L2 vertebral level were recorded unilaterally (right side) during the displacement to estimate the amount of joint rotation. EMG and tension in the cable were also recorded. Surface EMG electrodes were used to record unilaterally (right side) from the external oblique muscle and the longissimus muscle of the erector spinae group. Activity from these superficial muscles could be recorded with surface electrodes without risk of cross talk from neighbouring muscles. The surface electrodes used, were active electrodes with variable gain differential amplification (25X to 2000X) and band pass filtering from 30

Hz to 500 Hz. The stainless steel electrode contacts were 3 mm in diameter with a separation distance of 13 mm. The EMG was sampled at 2000 Hz, using a 12 bit data acquisition card (National Instruments Model No. 6014). The skin over the desired recording area was shaved and then cleaned using medical grade alcohol swabs. A small amount of conducting gel was placed on each electrode contact and the electrodes were attached to the skin with double sided adhesive. One electrode was placed in line with the fibers of the longissimus muscle and the second was placed in line with the fibers of the external oblique muscle close to the ultrasound transducer positions used in scanning these muscles (described below).

3.5 Protocol

In the first experiment, data was acquired for 2 different force directions, 4 different force levels and 4 different scanning regions. The subject sat on the stool with the torso in a neutral erect posture. The subject's feet were supported on a raised platform or on the bottom of the enclosure whichever was most comfortable. However, the subjects were instructed not to push on the frame with their feet while performing torso extension or lateral flexion pulls. The subject first performed isometric contractions for the 4 force levels in extension (Fig. 3.1). This was then repeated for lateral flexion towards the right side (Fig. 3.2).

The subject's torso was kept in the vertical orientation for the different force levels by adjusting the chest harness and length of the cable attached to the harness. The subject's posture was monitored by both the sonographer who sat behind the subject and the researcher who was in front of the subject during the experiments. The 4 different contraction levels consisted of the relaxed state, 10%, 25% and 50% of the subject's

maximum voluntary contraction (MVC). The 100% MVC force was determined from 3 trials in which the subject was instructed to produce maximum force. Each trial was separated by a rest period and the subject was not asked to progress to the next trial until ready.

All scans were 2D planar scans. The 3D capabilities of the probe were not used because they were not needed in Experiment 1 . Images were obtained from four different regions. The first region was a sagittal scan of the erector spinae at lumbar segments L1 and L2 (Fig. 3.3).

Figure 3.3 First scan region: A sagittal plane scan of the longisimus thoracis and associated vertebral transverse processes at lumbar segments L1 and L2.

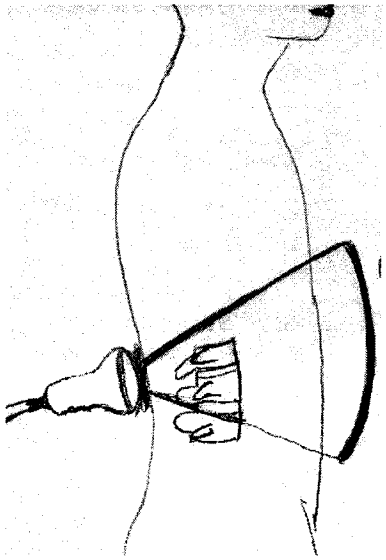

The transducer was oriented to obtain an image in the sagittal plane to the right of the midline, at the tips of the L1 and L2 transverse processes. Three caliper measurements were made from the image of the first region by using the caliper function of the GE Voluson 730. The calipers are a set of cross hairs that can be positioned

anywhere on the image. Once the positions are set, various parameters, such as the distance between caliper locations, are automatically computed. Caliper Placement #1 (Region #1; Experiment 1): Erector spinae diameter was obtained from the middle of the surface echo of the Right L1 transverse process, in a straight line posteriorly to the inside margin of the posterior border of the erector spinae muscles (inside to inside). See Figure 3.4.

Caliper placement #2 (Region #1; Experiment 1): Erector spinae diameter was obtained from the middle of the surface echo of the Right L2 transverse process, in a straight line to the inside margin of the posterior border of the erector spinae muscles (inside to inside). See figure 3.4.

Figure 3.5 shows caliper placement #3 (Region #1; Experiment 1): Pennation angle of a longissimus (middle of the 3 erector spinae muscles) fascicle was obtained using the "Hip Angle" function of the ultrasound machine, by placing one set of calipers along the plane formed by leading edge echoes from the surface of L1 and L2, and the second set of calipers parallel to the plane formed by the echoes from the fascicles located directly posterior to L1-L2.

Figure 3.4 **Example of caliper placement #1 (Region #1; Experiment #1) (D2) and caliper placement #2 (Region#1; Experiment 1) (D1). Measuring the thickness of the longissimus muscle.**

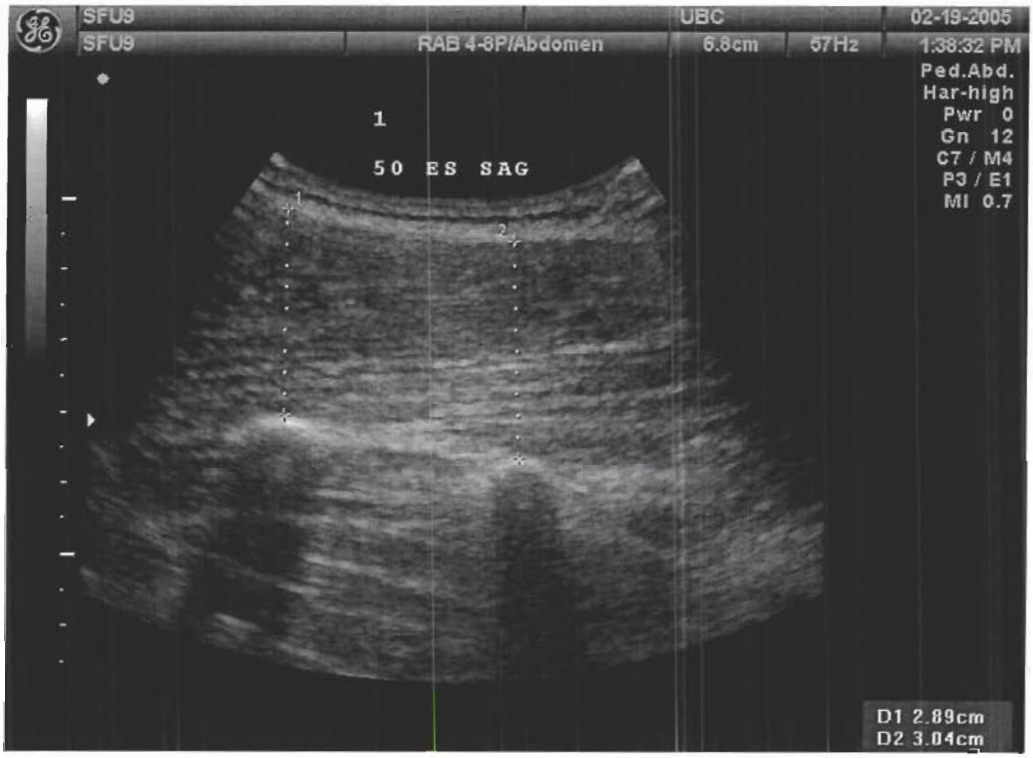

Figure 3.5 **Example of caliper placement #3 (Region #1; Experiment 1). Measuring the pennation angle of the erector spinae.**

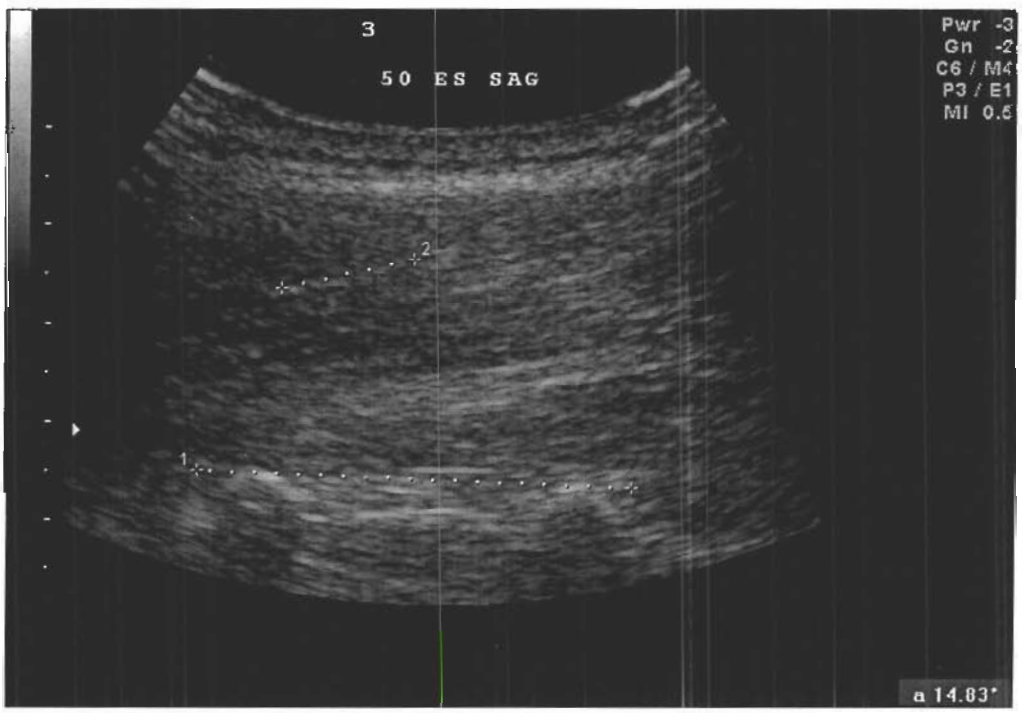

The second scan region again included the erector spinae muscle group. However, the ultrasound transducer was rotated so that the muscles could be scanned primarily in a transverse plane at the level of L2 (Figure 3.6 and 3.7).

Figure 3.6 Transverse plane of second, third and fourth scan region.

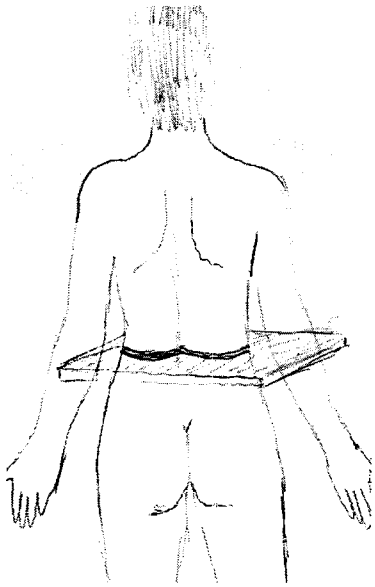

Figure 3.7 Example of structures imaged during second scan region.

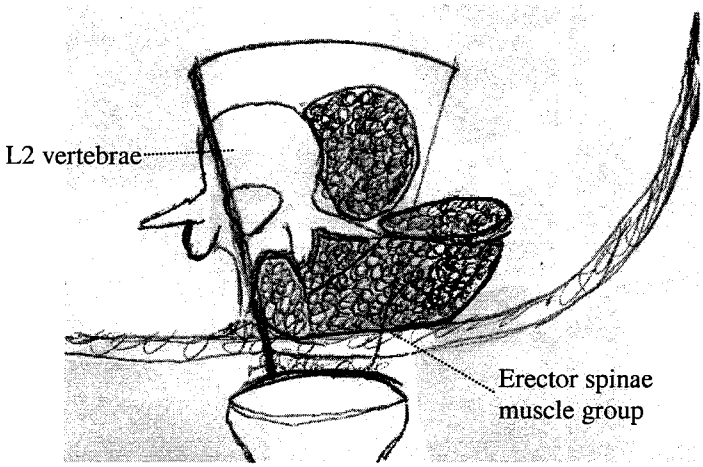

This plane was slightly oblique to a true transverse plane with the medial border of the transducer angled slightly rostral to include the L1-L2 echo complex formed from

the surface of the superior and inferior articular processes medially, and the surface echoes from the full length of the L2 transverse process laterally. Two caliper measurements were made from the image of the second region. Figure 3.8 shows caliper placement #1 (Region #2; Experiment 1): Diameter of the erector spinae muscle group was obtained by placing one caliper on the leading edge, at the mid point of the echoes arising from the surface of the articular processes and in a straight line moving posteriorly to the inside margin of the posterior border of the muscle (inside to inside). Caliper placement #2 (Region #2; Experiment 1): Diameter of the erector spinae muscle was obtained by placing one caliper on the leading edge, at the mid point of the echoes arising from the surface of the transverse process and the second caliper in a straight line posteriorly to the inside margin of the posterior border of the muscle (inside to inside). See figure 3.8.

Figure 3.8 **Example of caliper placement #1 (Region #2; Experiment 1) (D1) and caliper placement #2 (Region #2; Experiment 1) (D2). Measuring the thickness of the erector spinae in the transverse plane.**

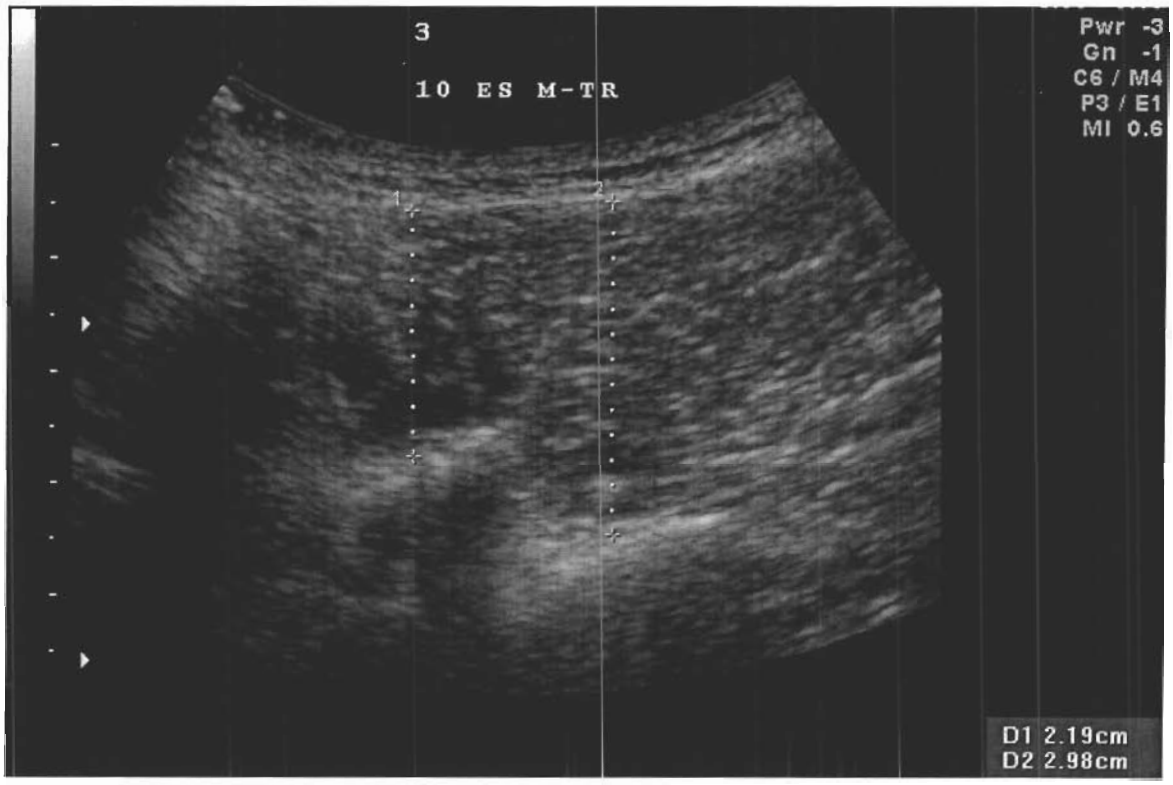

For the third region the transducer was placed more laterally than the previous scans so that the quadratus lumborum echo could be seen. The transducer was oriented to obtain an image of the quadratus lumborum in the transverse plane at the level of the L3 transverse process, to include as much of the length of the transverse process as possible (Fig. 3.6 and 3.9).

Figure 3.9 Example of structures imaged during third scan region.

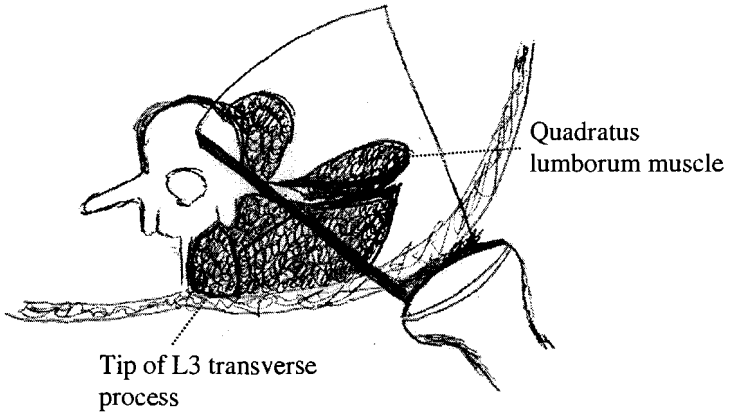

The image included the lateral tip of the L3 transverse process. The portion of the transverse process included in the image varied according to subject size with images from larger subjects containing only a short portion of the length of the process. Figure 3.10 shows the three caliper measurements that were made from the image of the third region. Caliper placement #1 (Region #3; Experiment 1): The distance from the surface of the quadratus lumborum to the skin surface was obtained by placing one caliper on the leading edge at the middle of the echoes arising from the posterior surface of the muscle, and the second caliper was placed in a straight line posteriorly to the skin surface (leading edge to leading edge). Caliper placement #2 (Region #3; Experiment 1): Anterior-posterior (A-P) diameter of the quadratus lumborum muscle at the widest point (inside to inside). Caliper placement #3 (Region #3; Experiment 1): Medial-lateral (M-L) diameter of the quadratus lumborum muscle at the widest point (inside to inside). See Figure 3.10.

Figure 3.10 **Example of caliper placement #1 (Region #3; Experiment 1) (D1), caliper placement #2 (Region #3; Experiment 1) (D2) and caliper placement #3 (Region #3; Experiment 1) (D3). Measure the distance from the skin, the A-P diameter and the M-L diameter of the quadratus lumborum**

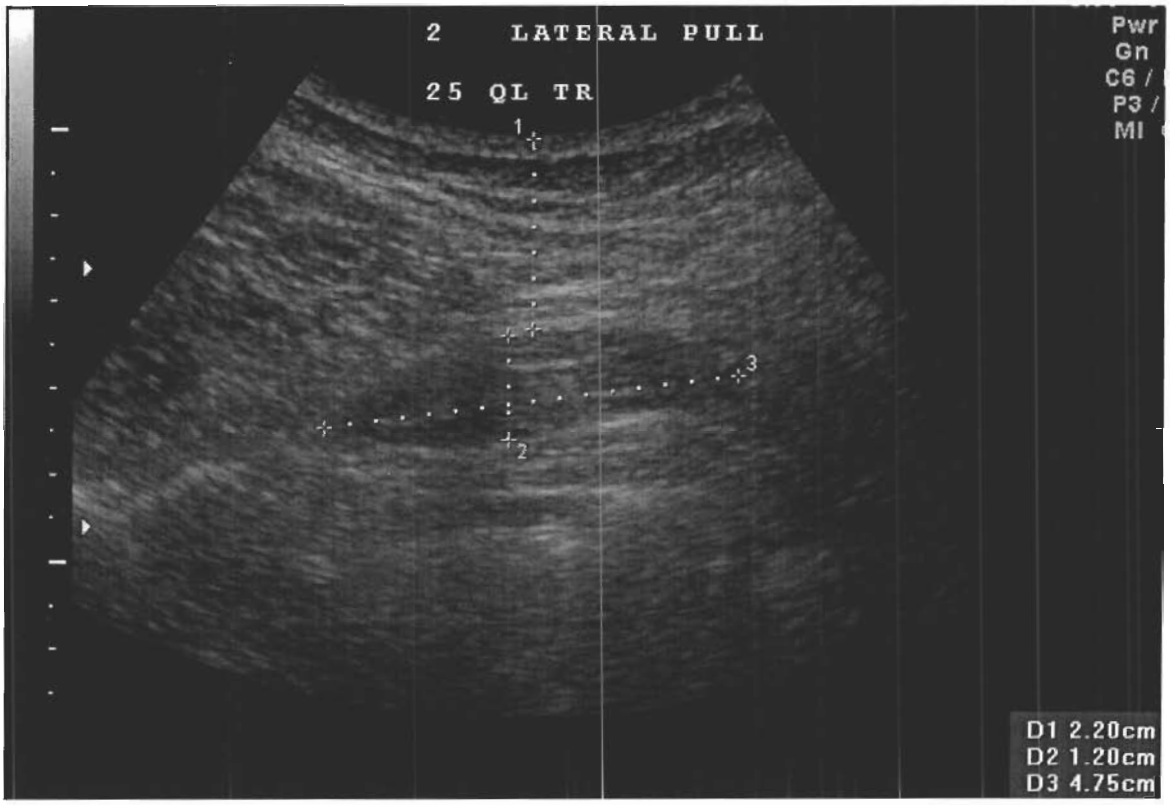

The fourth region was located at the iliac spine and included the three muscles of the abdominal group (external oblique, internal oblique and transversus abdominis). The transducer was oriented to obtain an image in the transverse plane, with the lower border of the transducer placed immediately superior to the iliac crest (Fig. 3.11).

Figure 3.11 Example of structures imaged in the fourth scan region.

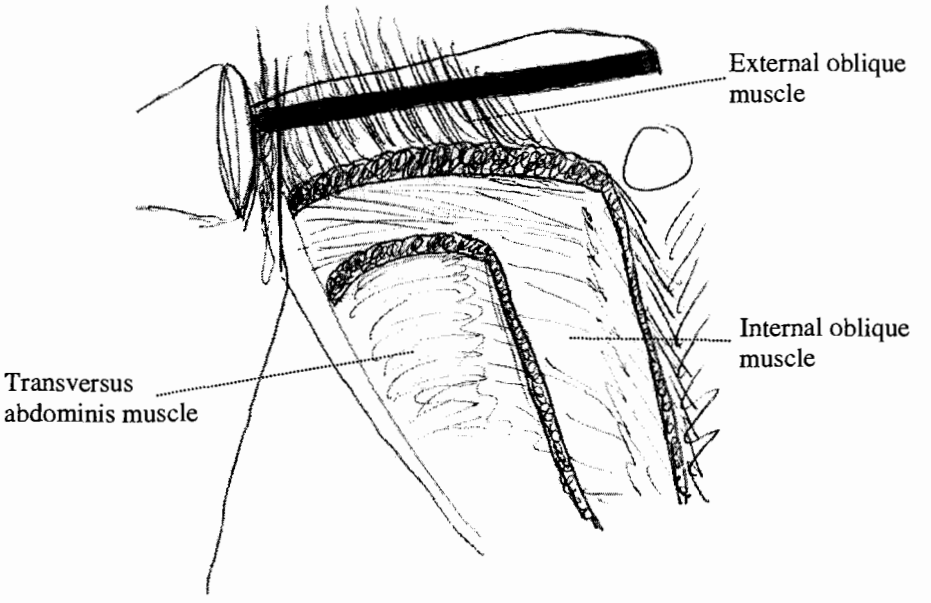

The lateral tip of the transversus abdominis aponeurosis appeared at the left side of the image. The subject was instructed to breath in then breath out naturally without forced exhalation and finally to hold their breath. The pressure on the transducer was reduced to the minimum while still maintaining contact with the skin surface since the abdominal muscles are deformed by transducer pressure. There were three caliper measurements made from the image of the fourth region. All measurements are obtained from an M-L plane located 2 cm to the right of the lateral tip of the transversus abdominis aponeurosis. Figure 3.12 shows caliper placement #1 (Region #4; Experiment 1): The M-L diameter of the external oblique muscle (inside to inside). Caliper placement #2 (Region #4; Experiment 1): The M-L diameter of the internal oblique muscle (inside to inside). Caliper placement #3 (Region #4; Experiment 1): The M-L diameter of the transversus abdominis muscle (inside to inside). In every image from every region the

caliper placement accuracy was optimized by measuring all images at the largest scale size possible.

Figure 3.12 **Example of caliper placement #1 (Region #4; Experiment 1) (D2), caliper placement #2 (Region #4; Experiment 1) (D3) and caliper placement #3 (Region #4; Experiment 1) (D4). Measuring the M-L thickness of the external oblique, internal oblique and transversus abdominis muscles**

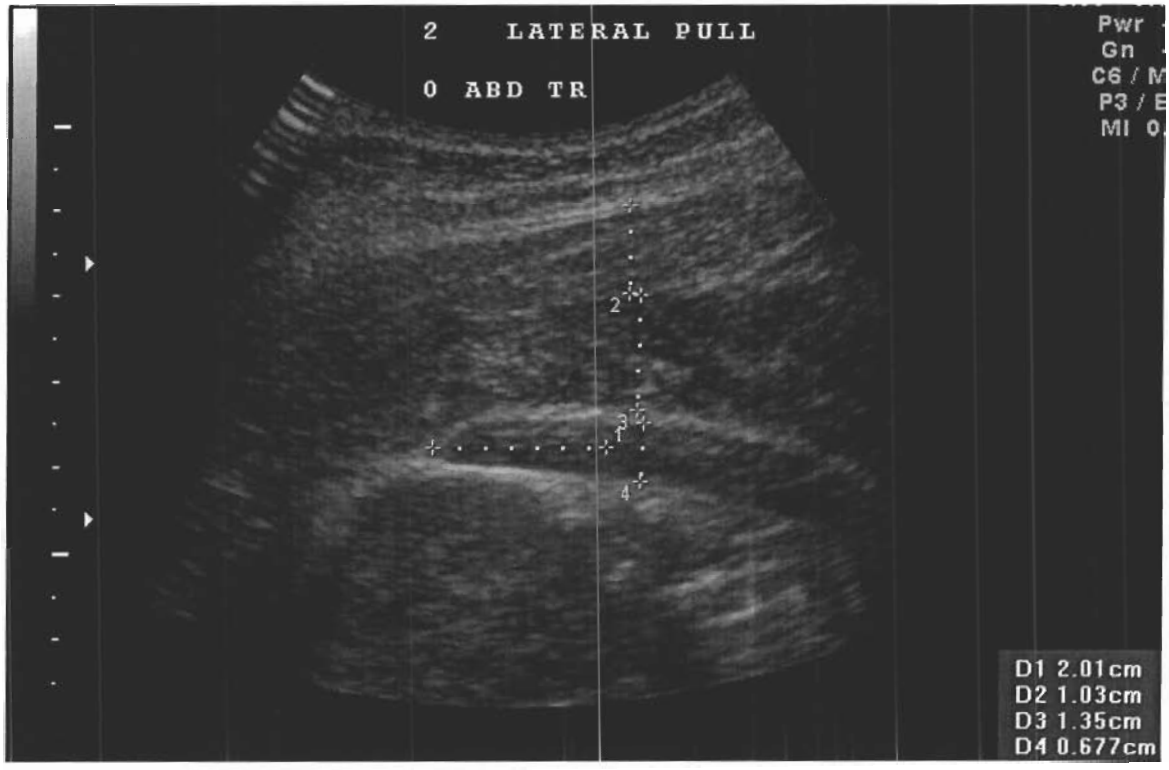

The first two regions were scanned when the subject pulled in extension. All four regions were scanned when the subject pulled in lateral flexion. The caliper measurements were made directly after each scan the entire protocol. This allowed us to re-scan if the image was not optimal for caliper placements. There were 72 scans for Experiment 1 (2 scan regions for extension x 4 force levels x 3 repeats + 4 scan regions for lateral flexion x 4 force levels x 3 repeats).

In Experiment 2, the subject contracted the trunk muscles isometrically in lateral flexion. The experimenter released the electromagnet at a random time during the contraction, causing the trunk to be rapidly displaced by about 5° as the springs shortened. The duration of the displacement ranged from 70 ms to 160 ms depending on the subjects trunk inertia. Two-dimensional ultrasound images of the vertebrae (L1-L2) were recorded during the displacement at a 57 Hz frame rate. Although it would have been preferable to use the 3D capability of the ultrasound probe, frame rates were too low (15 Hz) to capture the motion. This required that the ultrasound transducer be taped to the skin over the designated scanning region to prevent excess motion of the transducer relative to the skin during the perturbation. The sonographer positioned the transducer to obtain a scan of Region #1 with the best possible images of L1-L2 transverse processes. A long strip (1m) of duct tape was centered and applied to the base of the transducer on one side of the cable. The tape was then wrapped around the subject's torso while the sonographer maintained an optimal image of L1-L2 transverse processes. A second strip of tape similarly held the base of the transducer on the other side of the cable. The transducer head was taped in a similar manner. Shorter strips of duct tape (0.5m) were placed along the inferior and superior surfaces of the transducer and secured caudally and rostrally along the subjects torso, respectively. Finally, we placed a very short strip of duct tape around the shaft of the transducer to regulate the slack in the longer strips of tape. The sonographer could adjust the pressure of the transducer on the skin by adjusting this last strip of tape. The best images during the test perturbations were obtained if the tape was not so tight as to prevent the sonographer from making adjustments after taping. Despite taping the transducer the image of the transverse processes was blurred due to

motion between the skin and transducer. However, image frames prior to onset of the perturbation and image frames located at the point where motion changed direction were clear enough to make accurate caliper measurements. The cini-loop was deemed "good" and was permanently recorded if the transverse processes were seen throughout the perturbation (pre, during and after the perturbation). The caliper placement was as described in Ledsome et al. (1996). There were two caliper placements; one caliper placement prior the perturbation (pre-perturbation) and one at the first change in direction of vertebral motion during the perturbation. The point of direction change was determined from reduction in image blur. The cini-loop images of the transverse processes increase in quality and suddenly stop for 1-2 frames and then change direction of motion. This was assumed to be the point of maximum displacement between the L1 and L2 transverse processes. Figure 3.13 shows caliper placement #1 (Region #1; Experiment 2): Pre-perturbation point distance between the L1 and L2 transverse processes was obtained by placing one caliper on the leading edge echo from the surface of the lateral tip of the L2 transverse process and measuring the distance from here to the second caliper placement that lies along the leading edge echo from the surface of the lateral tip of the L1 transverse process. The pre-perturbation measurement was performed on the non-blurred image in the cini-loop that lies one frame prior to the onset of perturbation. The onset of perturbation was defined as the first frame where the image was blurred therefore, it was easily identified.

Figure 3.13 Example of caliper placement #1 (Region #1; Experiment 2). Distance between the L1-L2 transverse processes before perturbation.

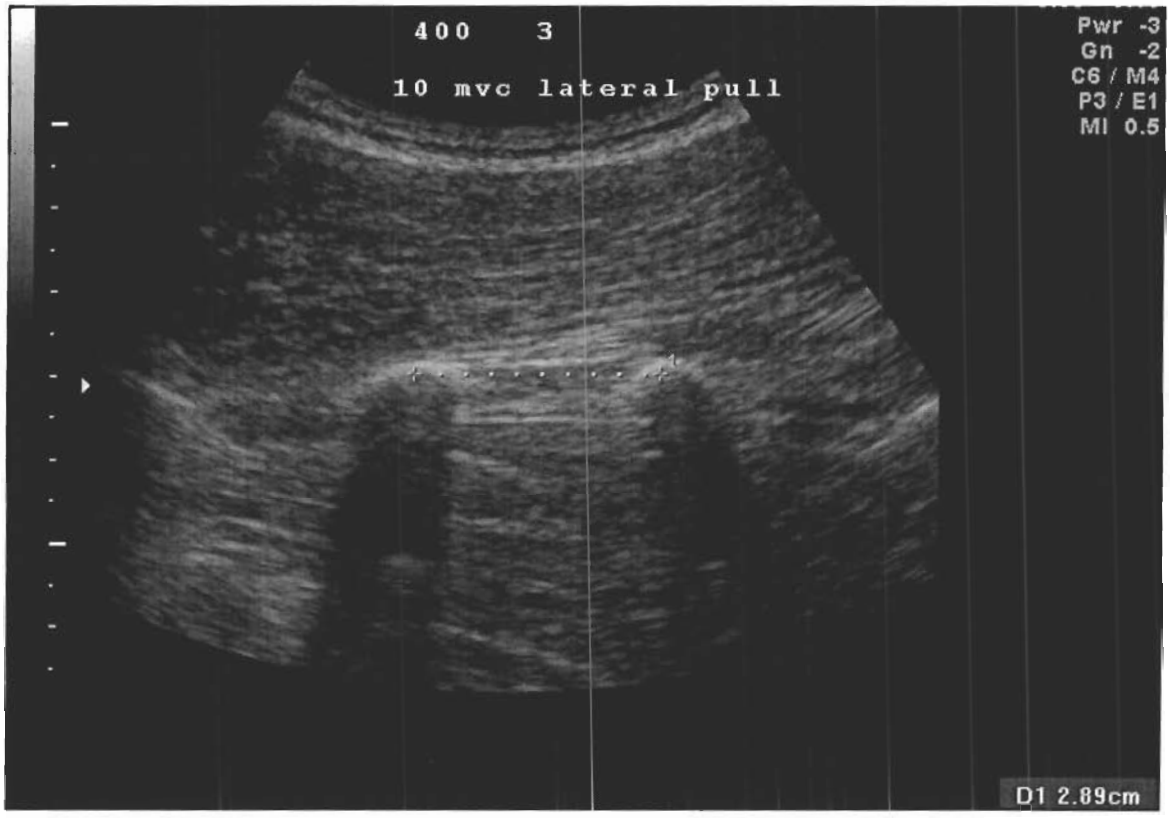

Figure 3.14 shows caliper placement #2 (Region #1; Experiment 2): Distance between the L1 and L2 transverse processes are the point of maximum displacement was obtained by placing one caliper on the leading edge echo from the surface of the lateral tip of the L2 transverse process and measuring the distance from here to the second caliper placement that lies along the leading edge echo from the surface of the lateral tip of the L1 transverse process. This measurement was made from the image in the cini-loop that situated at the point where the direction of motion changed. This frame number was also recorded. We recorded a total of 12 scans for Experiment 2 (4 force levels x 3 repeats).

Figure 3.14 Example of caliper placement #2 (Region #1; Experiment 2). Distance between the L1-L2 transverse processes at maximum displacement during the perturbation.

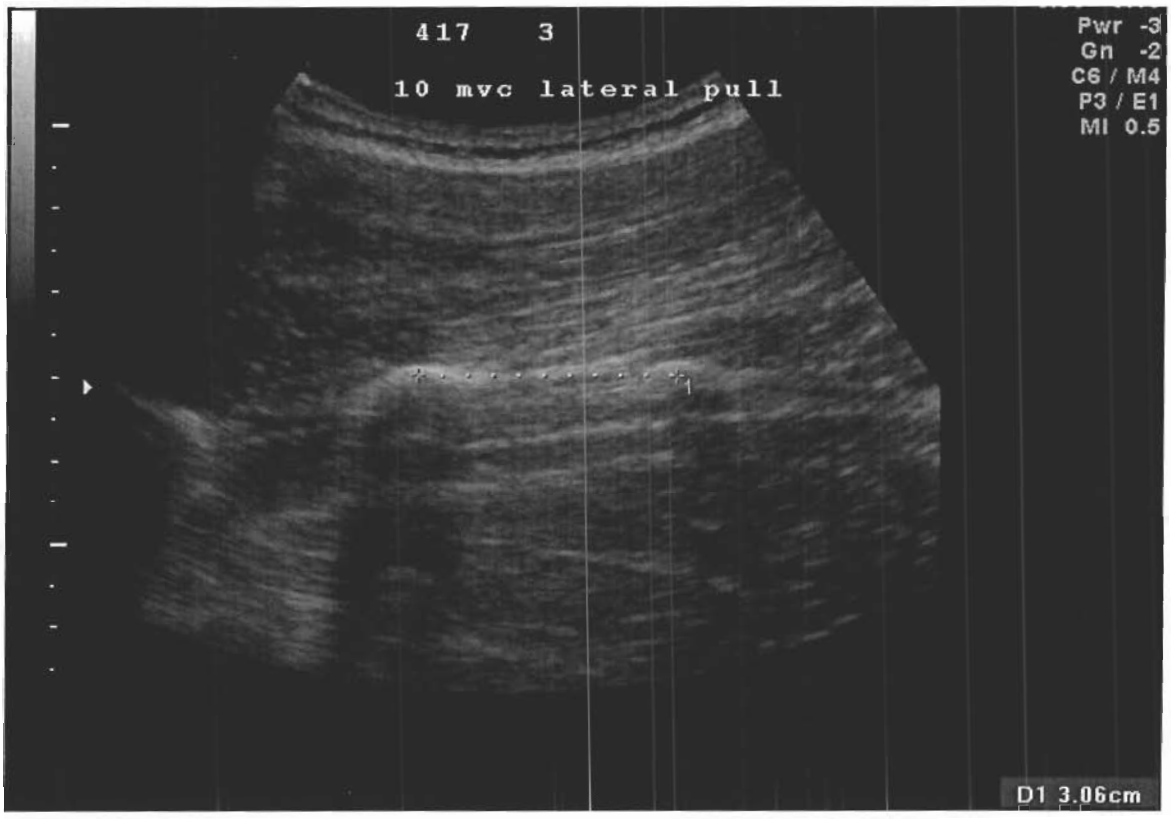

3.6 Data Analysis

Data from Experiment 1 were used to determine whether there were correlations between the ultrasound measurements and trunk force. Linear regression was performed both with the individual subject data normalized to parameter values at 10% MVC and the average data of all subjects.

Data from Experiment 2 were used to estimate L1-L2 joint stiffness. When the springs of the apparatus are released they cause a force impulse (torque impulse at the vertebrae) that acts to accelerate the torso. A sample calculation of the torque impulse can be found in Appendix E. The resistance to this imposed motion consists mainly of inertia and stiffness which determine the angular velocity of the vertebrae. We assumed that the

torque produced by damping is small compared to that produced by the inertia and stiffness. This assumption is based on studies of the mechanical impedance at the ankle (Weiss et al., 1988) and knee (Dhaher et al., 2004). The initial angular velocity of the vertebrae is zero when the subject is pulling isometrically with a constant force. We assumed that the angular velocity is again zero at the point where the relative motion of the transverse processes reversed direction (See Protocol – Experiment 2). This assumption is based on the observation that the image of the transverse processes was not blurred at this point, suggesting that neither was moving. From these assumptions then, the change in angular momentum from the initial starting point to the point at which the direction of the vertebral motion reverses is zero. The change in angular momentum is given by the following equation

$$I\omega(T) - I\omega(0) = \int_0^T \tau(t) - K(\theta(t) - \theta_i)dt$$

where $\tau(t)$ is the torque applied to the L1-L2 joint by the springs, which is computed from the measured force, $K(\theta(t)- \theta_i)$ is the torque due to stiffness of the vertebral joint at the L1-L2 level. The stiffness included contributions from all of the soft tissue surrounding the joint, as well stiffness due to reflex muscle activation. Time 0 represents a time where the vertebrae are stationary prior to the onset of the perturbation and time T represents the time at which motion reverses direction with θ_i being the angle prior to onset of the perturbation and $\theta(t)$ being the angle at any time t.

The term on the left side of the equation is zero because the angular velocity at $t=T$ and $t=0$ is zero. Therefore, we have

$$\int_0^T \tau(t)dt = K\int_0^T (\theta(t) - \theta_i)dt$$

In order to solve for K we also need to know θ_i which we can obtain from the pre-perturbation images and $\theta(t)$. Because we cannot measure $\theta(t)$ due to the limited sampling rate and possible movement of the transducer with respect to the skin we can only solve for K if we assume that $\theta(t)$ has a known profile. A reasonable approximation for this profile may be a sinusoid since we are assuming that the joint behaves like a second-order mechanical system with little damping. The constraints on the sinusoid would be that its velocity and acceleration are zero at t=0 and that the velocity, but not the acceleration is again zero at t=T. It is not actually possible to fulfill these constraints with a sinusoid, but they can be fulfilled if the sinusoid is slightly modified so that it is phase-advanced by $\pi/2$, offset and set equal to zero prior to t=0. This forces all derivatives to be zero at t=0.

To estimate the change in angle between the vertebrae, normative data of the geometry of the vertebral bodies and their associated processes were used to obtain values for the length of the transverse processes and distance to the centre point of the vertebral disk located between L1-L2 vertebral bodies (Zhou et al., 2000; Tan et al., 2002; Wolf et al., 2001; Panjabi et al., 1992, Davies et al., 1989; Berry et al., 1987). Trigonometry can then be used to calculate the angles prior to the onset of the perturbation, θ_i, and at the point at which motion reverses direction, θ_{max}. The angle itself is formed by the assumed axis of rotation of the L1-L2 joint and the tips of the transverse processes of these same vertebrae. Assumptions required for this calculation included using normative morphological lumbar vertebrae data to estimate the actual size of the

vertebrae although rough anthropometric data could be matched. We also needed to assume where the axis of rotation of the L1-L2 joint occurred. A range of values spanning the center of the joint to the edge of the vertebral body were chosen. Our calculations estimate that up to 31% of the uncertainty of the stiffness estimate would be due to the uncertainty of the axis of rotation. A sample vertebrae angle calculation can be found in Appendix F.

3.7 Statistical Analysis

As mentioned in section 3.6 several different statistical measures were used in analyzing the data. The coefficient of variation is the ratio between the standard deviation divided by the mean for a repeated measurement. It is a unit-less quantity that was used as a measure of the reliability of a repeated measurement, expressed as a percentage of the mean. In Experiment 1, we used the coefficient of variation of repeated measurements of the same ultrasound variable for individual subjects as a measure of the reliability of different ultrasound measurements (Tables 4.3 and 4.4). The ability of the ultrasound measurements to provide reliable information about a given anatomical feature was assessed from the coefficient of variation computed across all subjects (Tables 4.5 and 4.6).

In Experiment 1 we also performed linear regression to determine whether a given ultrasound measurement was correlated with trunk force, i.e., whether there were systematic changes in the measurement that could be used to predict the trunk force. This was assessed from the R^2 value. The slope of the linear regression was also tested for significance. If the p-value indicated statistical significance (p-value < 0.05) then the

slope of the regression relation was non-zero or a significant linear trend between the two variables existed.

In Experiment 2, we examined how the distance between the L1-L2 transverse processes was affected by trunk force. We used both analysis of variance and linear regression. In general, the purpose of analysis of variance (ANOVA) was to test whether trunk force could account for significant differences between more than two means. Linear regression analysis then established whether trunk force could be used to reliably predict those differences.

4 RESULTS

4.1 Ultrasound Images – Preliminary Testing

4.1.1 Resolution

The resolution of the Voluson 730 Expert from GE Medical Systems using model RAB4-8P sonography transducing probe is 0.3019 mm/pixel. Since two features would have to be at least 1 pixel apart to distinguish them as separate, the accuracy of our measurements cannot be better than 0.6038 mm, assuming that we are measuring the center to center distance. However, as discussed previously axial (in the direction of beam penetration) and lateral (in the direction of beam sweep) resolutions depend on additional factors besides the pixel size. For example, axial resolution refers to structures lying along the penetration path of the sound beam and is determined by the pulse duration PD, which is the number of cycles divided by the transducer frequency. Since most modern ultrasound machines use three cycles we can determine from our central transducer frequency of 4.5 MHz that the pulse duration is 6.67×10^{-7} s. Only if the time taken to travel from one structure to the next deepest structure is greater than this can they can be separated during image reconstruction. Using the average speed of sound in the human body, axial resolution equals approximately 1mm (1540 m/s x 6.67×10^{-7} s) despite the 0.3019 mm/pixel resolution. Since the speed of sound in muscle increases to 1600 m/s the axial resolution in muscle is reduced to 1.1 mm.

Lateral resolution refers to the ability to distinguish two closely spaced reflectors perpendicular to the ultrasound beam, i.e., along the direction of the beam sweep.

Determining lateral resolution is slightly more complex than axial resolution since the beam narrows at its focal point and then expands, i.e. the beam cross-section changes somewhat like an hour glass. This plays a significant role since objects that are larger than the beam width will be distinguished in the image but objects that are narrower than the beam width will not be clearly distinguished. The best lateral resolution will occur with objects located at the narrowest portion (focal zone) of the beam. The section of the beam from the transducer to the focal zone is termed the 'near field' and has a larger width than the focal zone. The section extending beyond the focal zone is termed the 'far field' and also has a larger width. The focal zone is not only the narrowest section of the beam but it is also the section of the beam that will reflect most strongly since it is also the section that has the least destructive or constructive sound wave interference (Zagzebski, 1996). The near field length (NFL) or distance from the transducer to the center of the focal zone can be estimated as the square of the diameter of the transducer divided by four times the wave length of the sound beam. Hence, NFL for our system equals 14.1 cm (wave length = 3.4×10^{-4} m; diameter of transducer = 65 mm). However, the NFL can be electronically focused to change the distance of the NFL over an object of interest. The width of the beam at the focal zone can also be estimated by multiplying the wave length by 1.22 and dividing this product by the diameter of the transducer. Hence, lateral resolution at the center of the focal zone was approximately 6 mm. However, keep in mind that any sound scatter from an object can contribute to the image reconstruction based on the fact that the scattered waves will be amplified by the sensitive ultrasound equipment and can be picked up from objects as small as or smaller

than the wave length. Thus an object may be reconstructed from scattered waves even though the object has a smaller diameter than the given lateral or axial resolution.

Since resolution depends on many factors it is difficult to determine accuracy based on theoretical calculations alone. Essentially, we can say that in order to reliably detect changes in muscle shape the change itself should be larger than the limit of the image resolution. Based on the theoretical calculations discussed above, this would imply that the limit for structures changing shape in the direction of penetration of the ultrasound beam (axial resolution) is 1.1 mm and 6 mm for structures changing shape in the direction lying in the sweep direction of the ultrasound beam (lateral resolution). However, the resolution is best determined from calibration tests. We conducted calibration tests to compare the known distances between wires embedded with in a calibrated phantom with those measured with the software calipers on the image display.

4.1.2 Phantom Calibration

To ensure valid ultrasound measurements taken with electronic calipers, calibration of the ultrasound images and associated equipment was conducted on the Voluson 730 Expert from GE Medical Systems. The sonography transducing probe used was model RAB4-8P. This probe has a broad bandwidth and software adjustable scanning frequency range from 4 to 8 MHz. The central image frequency is 4.5 Hz. The pre-settings used here were maintained throughout the duration of the study. They are as follows:

Global Settings: Main, 2D, Pediatric Abdomen

Angle: 70 Degrees

Focal Zone: 1 focal point placed at the level of interest or just inferior.

Scale Size: 6.8 or 8.7

Frame rate: Acquisition rates varied from 25 to 70 Hz.

Mechanical Index: Maintained between 0.7 to 0.5

"*Global Settings*" are defined as the software determined pre-settings that alter the image quality based on the type of scan being performed. The professional sonographer judged that that Main, 2D (also see protocol) and Paediatric Abdomen were best for the purposes of scanning muscle and were, therefore, used for the calibration procedure. "*Angle*" refers to the width of field of view displayed on the image. It was set to the machine's maximum of 70 degrees. "*Focal Zone*" refers to the focal point of the image. We placed the focal point at the position which gave the best image quality. "*Scale size*" refers to the depth of field of the scan. The greater the depth of field, the slower the frame rate and the worse the image. Hence, we minimized depth of field to get the best image.

"*Mechanical Index*" is a quantity related to the potential for mechanical effects (cavitation) of the sound wave on soft tissue during a diagnostic ultrasound examination. A sound wave travelling away from the source (transducer) fills the affected medium (human soft tissue) with vibrational energy. A 'snap shot' of the event in time would look like the figure below.

Figure 4.1 Mechanical effects of diagnostic ultrasound on human soft tissues. Rarefraction measures are used in the calculation of "Mechanical Index"

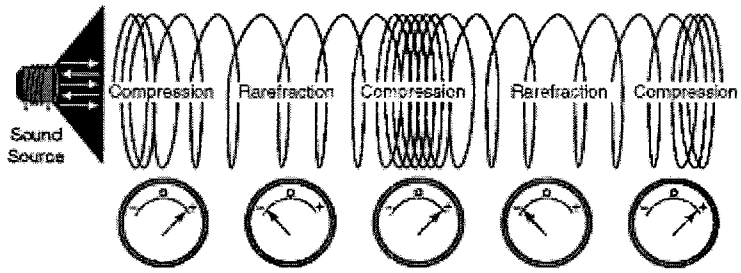

Source: Picture permitted for use by Sarayoot Eaimkhong of the School of Chemistry, University of Bristol. This copyright can be found at the following internet address www.chm.bris.ac.uk/ webprojects2004/eaimkhong/ultrasound.htm.

Mechanical Index then, is given by the ratio of the largest value in the ultrasound beam of any rarefractional pressure to the square root of the transducer frequency. A higher Index value of this mechanical 'energy' has been known to cause damage to deeper tissues in animal models (Baggs et al., 1996; Dalecki et al., 1999). Hence, Health Canada recommends that the displayed Mechanical Index (MI) does not exceed 1 (Health Canada, 2001).

The phantom used for calibration was a General Purpose Multi-Tissue Ultrasound Phantom (Model 40) manufactured by CIRS Tissue Simulations Technology Inc. The phantom material is chosen to have sound transmission properties similar to that of biological tissue, i.e. the speed of sound in the phantom is the same as that of the average biological tissue medium (1540 m/s). Arrays of 0.1 mm wires are embedded in the phantom running perpendicular to the plane of the scan.

All calibration tests were based on images taken from a single scan. In the first procedure, we tested the distance given by the caliper measurement against the known values of the distances between the vertical plane target group (depth calibration). These comprised of 16 x 0.1 mm (9 are shown in Fig. 4.2) diameter nylon monofilament wires

placed 1 cm apart. As can be seen in Fig. 4.2, all 9 wires are clearly seen. As well, the calipers placed on the first and last wire read 7.99 cm. This suggests that the resolution based on the reconstruction of scattered sound waves is approximately 0.1 mm. Since this less than the pixel size, we assume the axial resolution cannot be greater than the width one pixel in the image (0.3019 mm).

Figure 4.2 **Image from phantom calibration testing. Vertical plane target group. (9 x 0.1 mm diameter wires separated by 1 cm). Caliper measurement is displayed in bottom right corner.**

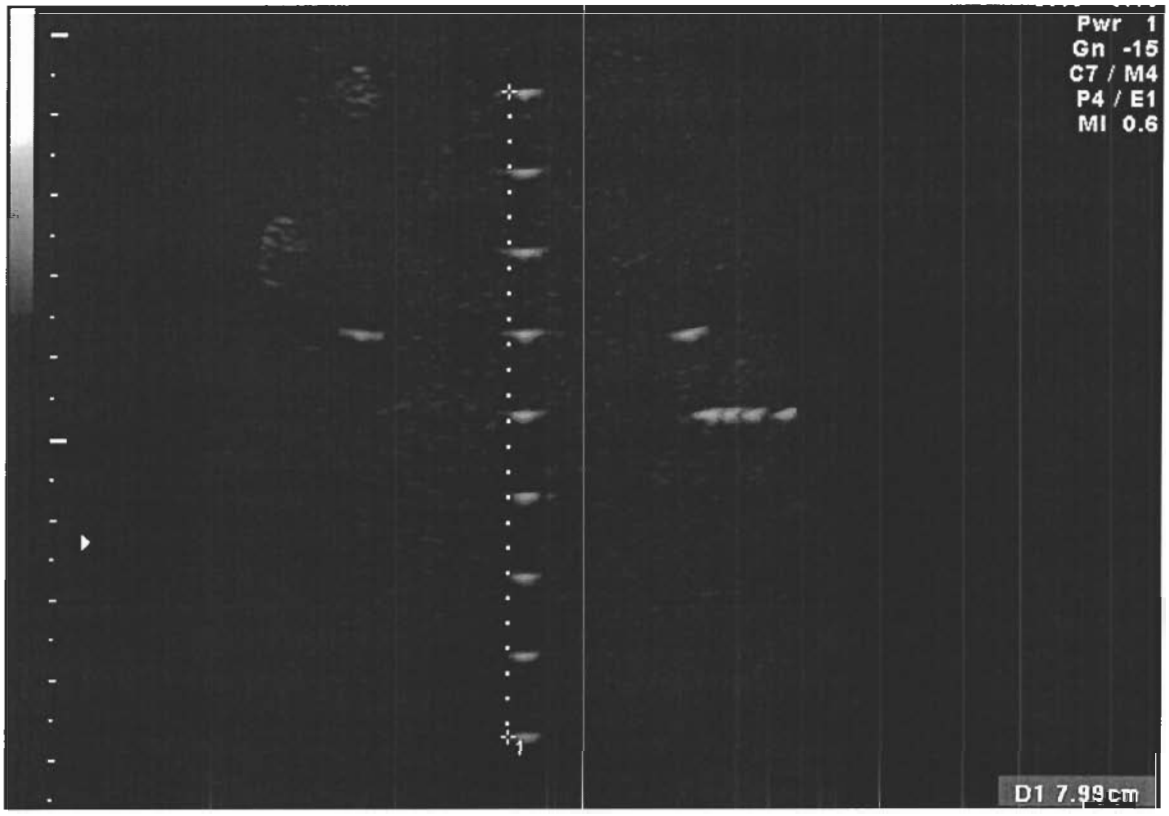

Near field resolution refers to the closest image that can be clearly distinguished in the image. The wire next to the arrow in Figure 4.3 depicts a 0.1 mm diameter nylon monofilament wire located 1 mm from the surface of the phantom. It was clearly

distinguishable suggesting that any reflector greater than 1 mm from the surface of the skin should be seen in the reconstructed image.

Figure 4.3 Near field resolution image from phantom testing of 0.1 mm diameter wire located 1mm from the surface of the phantom (arrow).

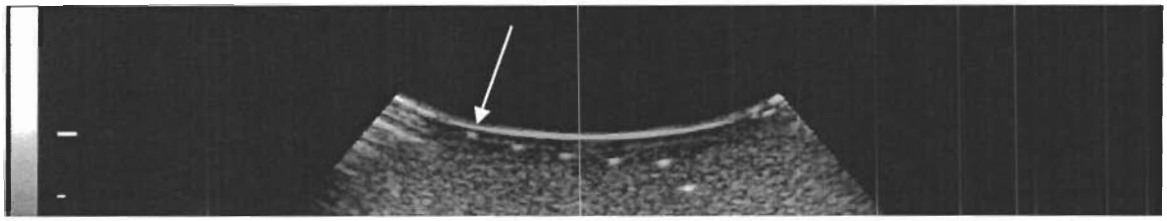

Next, using a single scan we tested the axial resolution (up and down in the image) group of wires, i.e., we attempted to distinguish between 0.1 mm diameter wires lying in the plane of the ultrasound beam as they are placed farther and farther apart (Fig. 4.4), with the near wire always at the same depth from the surface of the phantom (2.5 cm). Going from the center of the image (arrow) to the left edge the distance between wires increased from 0.5 to 5 mm. In the axial resolution test, the 0.5 mm spread of the two 0.1 mm diameter wires could not be distinguished, but the 1 mm spread was clearly distinguishable. This suggests that the axial resolution is between 0.5 mm and 1.0 mm. In this same image, we checked the lateral distance measurement accuracy of the calipers by placing them across 5 x 0.1 mm wires placed at 2 cm intervals at a 9 cm fixed depth from the surface of the phantom. The calipers measured 10.09 cm across this 10 cm test grid. The number of significant figures given in the measurement again suggests that the resolution based on the reconstruction of scattered sound waves is 0.1 mm (Fig. 4.4). However, since this cannot be achieved the axial resolution becomes that of one pixel in

the image (0.3019 mm). Rounding off to the nearest 0.5 mm, the measurement becomes 10.1 cm, which indicates that the accuracy is about 1%.

Figure 4.4 **Axial (horizontal) resolution image from phantom testing of 6 x 0.1 mm diameter wires separated by 2 cm; 2 x 0.1 mm wires separated by 0.5 mm (arrow). Caliper measurement is displayed in bottom right corner.**

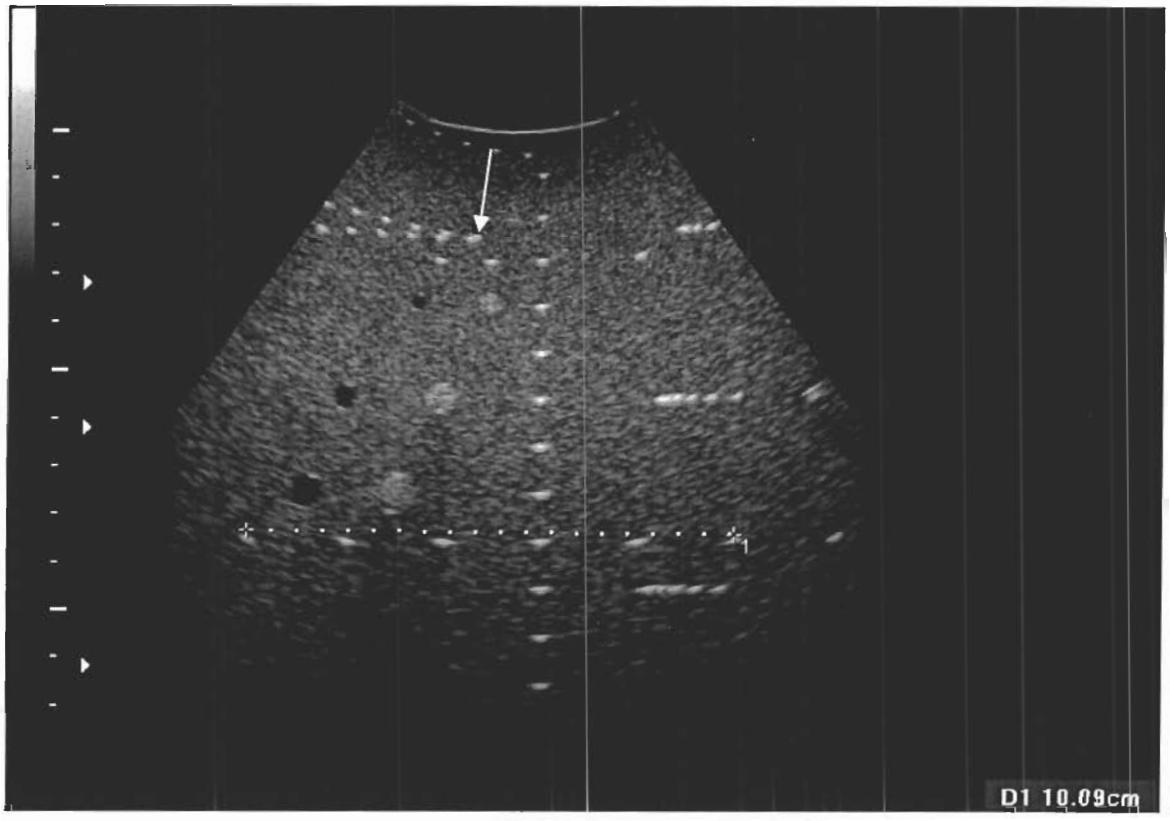

Finally, we tested the lateral resolution (left and right in the image), which indicates how close two wires that lie in the direction of the sweep of the ultrasound beam can be placed to one another while still being distinguishable and to compare how the resolution of identically placed groups of wires changes at different depths (Fig. 4.5). The six wires within one group (arrow) were located 1, 2, 3, 4 and 5 mm apart starting from the center of the image moving to the right. Three groups of six wires were placed at three different depths (2.5, 6 and 10 cm). From Figure 4.5 we see that the 2.5 cm wires

are not all distinguishable. Although the 1 mm separation is not distinguishable, the wires separated by 2 mm can be clearly distinguished. Similarly, the 1 mm separation at 6 and 10 cm depths is not distinguishable. In addition, the wires separated by 2 mm at 10 cm depth are not distinguishable. This suggests that at 2.5 cm and 6 cm depths the lateral resolution is between 1 mm and 2 mm. However, at a depth of 10 cm the lateral resolution drops to between 2mm and 3mm. This reduction in lateral resolution as the beam penetrates the phantom is likely due to both sound beam attenuation and the pre-set focal zone.

Figure 4.5 **Lateral resolution image from phantom testing with 3 groups of 6 x 0.1 mm wire placed at 3 different depths and lateral orientation.**

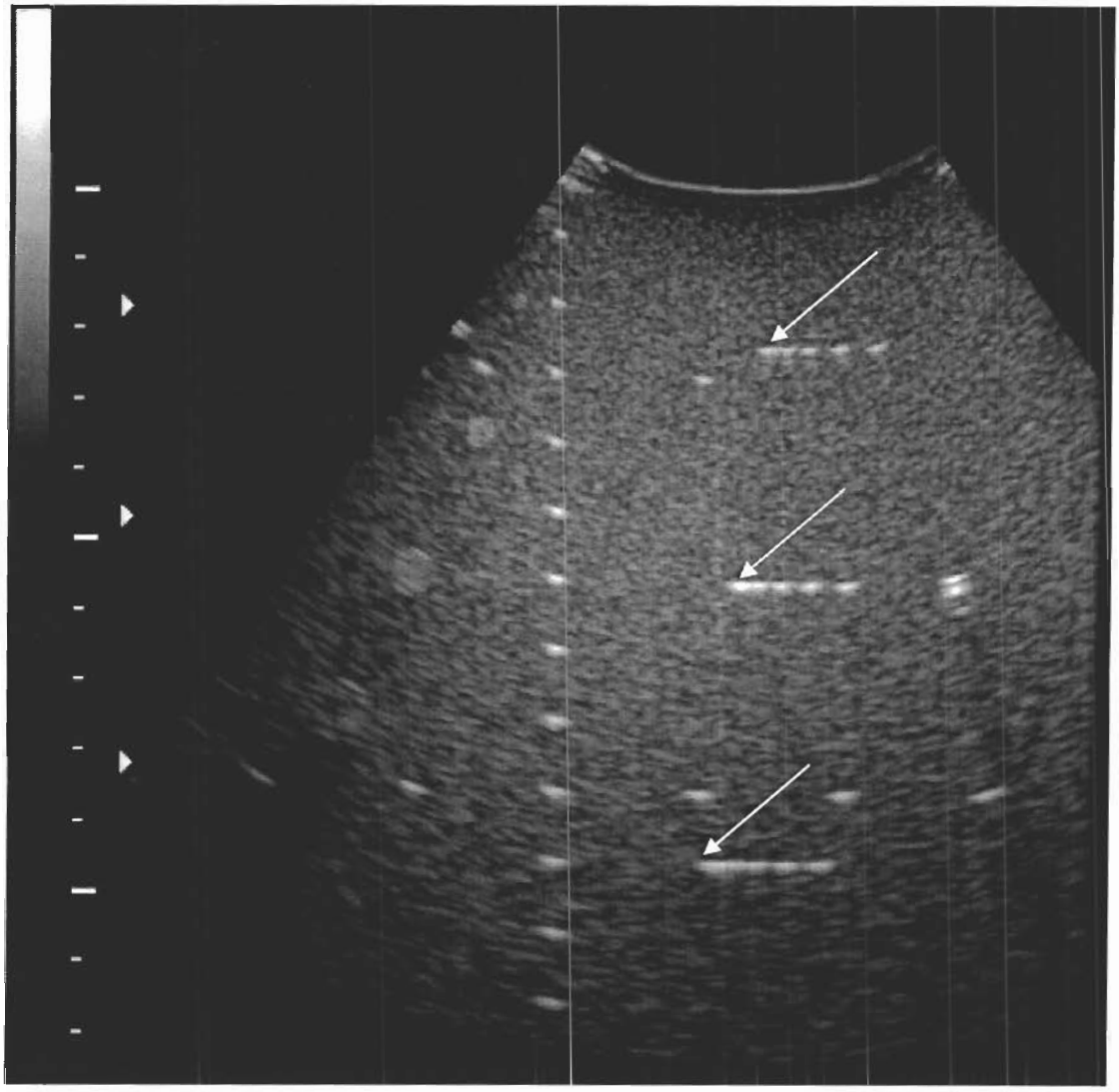

As previously mentioned the sound beam undergoes attenuation as the sound beam penetrates further into a given medium. Typically, additional amplification of the returning wave is required to reconstruct an image of improved quality. However, when we penetrate deeper into a tissue we are also increasing the number of interfaces the sound beam interacts with, causing increased amounts of refraction leading to an increase

in beam 'noise'. This means as we increase the amplitude of the returning sound waves we also amplify the noise as well.

Hence, the images reconstructed from sound waves returning from deeper tissues in the far field are of lower quality than those reconstructed from waves returning from more superficial structures lying in the focal zone. This may have implications on measurements made on muscles that run parallel to the transmitted sound wave. In Figure 4.5 the focal zone was placed over the group of wires placed at a 2.5 cm depth.

Despite the fact of our original calculations estimated an axial resolution of 1.1 mm and a lateral resolution of 6 mm they did not account for the sensitivity of the ultrasound system to reconstruct scattered waves from objects smaller than the calculated resolutions. Our results with the RAB4-8P ultrasound probe indicate that the axial and lateral resolutions are about 1 mm and 2 mm, respectively. This also places a limit on the accuracy because it cannot be greater than the resolution. Despite being able to adjust the position of the calipers in 1 pixel increments (~ 0.3 mm), the accuracy is much lower. In order to make reliable caliper measurements, changes in features which are being compared should be at least 1 mm for axial (along the direction of beam penetration) measurements and at least 2 mm for lateral measurements (along the direction of the beam scan).

4.1.3 Pilot Tests of Ultrasound Imaging

We performed pilot testing of the lumbar region of the spine and determined that it was possible to identify the following structures: psoas, quadratus lumborum, iliocostalis lumborum, longissimus thoracis, external oblique, internal oblique and

transverse abdominis muscles and the transverse processes with associated articular regions of the L1-L3 lumbar vertebrae. We observed changes in several features of the images with muscle contraction. These included pennation angle, fascicle length, muscle thickness, circumference, cross sectional area and distance from the skin (Table 4.1). Not all of these could be measured in each muscle but at least 2 parameters could be measured for each muscle except for the spinalis and iliocostalis muscles (erector spinae).

Table 4.1 Pilot test results of ultrasound imaging.

Muscle	Location	Scan Plane	Pennation	Circumference	Area	Diameter	Distance from Skin
Longissimus thoracis	L1-L2	Sagittal	Y	-	-	Y	-
Erector spinae	L2	Transverse	-	?	?	Y	-
Quadratus lumborum	L3	Transverse	-	Y	Y	Y	Y
Psoas major	L1-L2	Transverse	-	Y	Y	Y	Y
External obliques	Iliac Crest	Transverse	Y	-	-	Y	Y
Internal obliques	Iliac Crest	Transverse	Y	-	-	Y	Y
Tranversus abdominis	Iliac Crest	Transverse	-	-	-	Y	Y

Y, Measured and applied in this study; -, Measurement could not be achieved; ?, Difficult to achieve this measurement

Figure 4.6 depicts how muscle shape can change during contraction. In the section of the figure labeled 'A', the quadratus lumborum is relaxed and in section 'B' the subject is exerting approximately 50% of maximal right lateral flexion force. The most obvious change in the features of the ultrasound image between the two conditions is the medial-lateral (M-L) thickness.

Figure 4.6 **Quadratus lumborum (right side) relaxed (A) and during exertion of 50% of maximal right lateral flexion force (B). Both images show the distance from the muscle to the skin (D1) A-P thickness (D2) and M-L thickness (D3).**

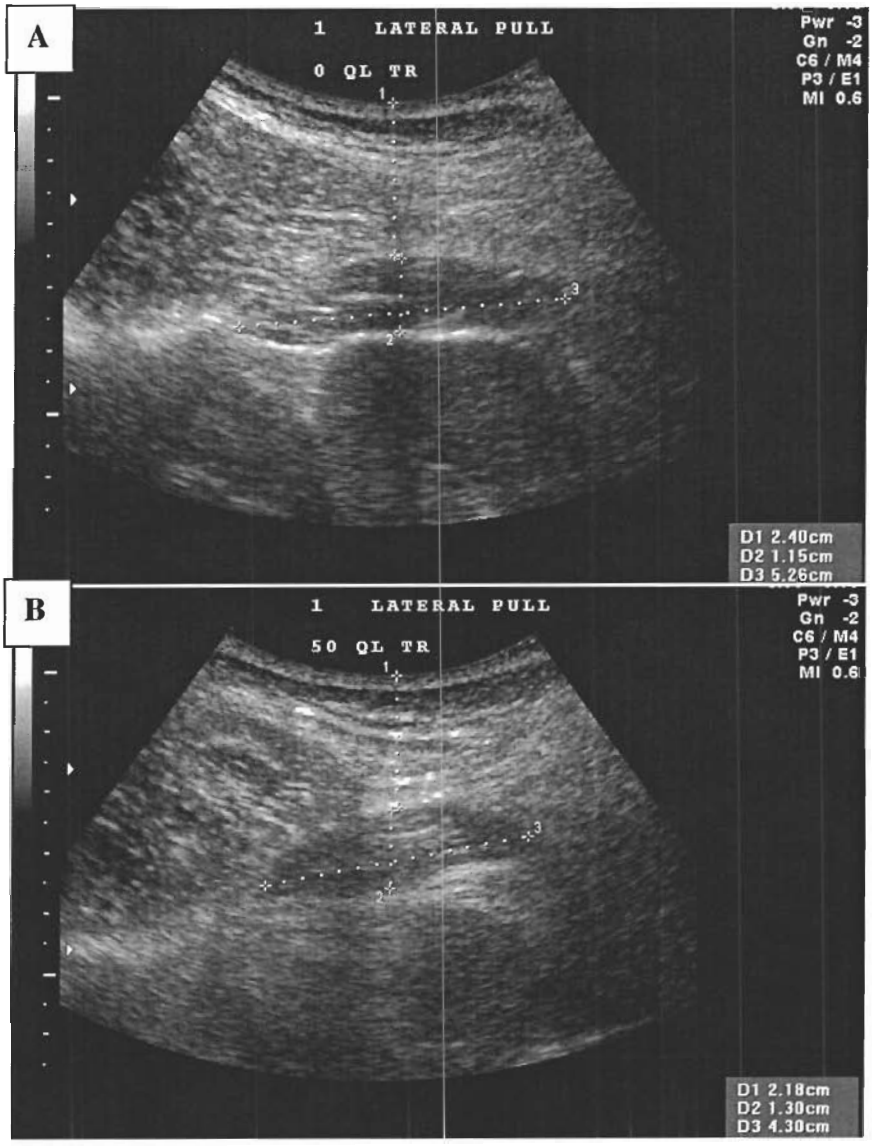

Figure 4.7 depicts contraction of the longissimus throracis. The two most obvious features that change are the muscles thickness and the pennation angle. As the muscle contracts and shortens the muscle begins to thicken when viewed in the sagittal plane. As well, pennation angle increases.

Figure 4.7 **Longissimus thoracis relaxed (A) and during exertion of 50% of maximal trunk extension force (B). Both images give the pennation angle (a) in the bottom right corner.**

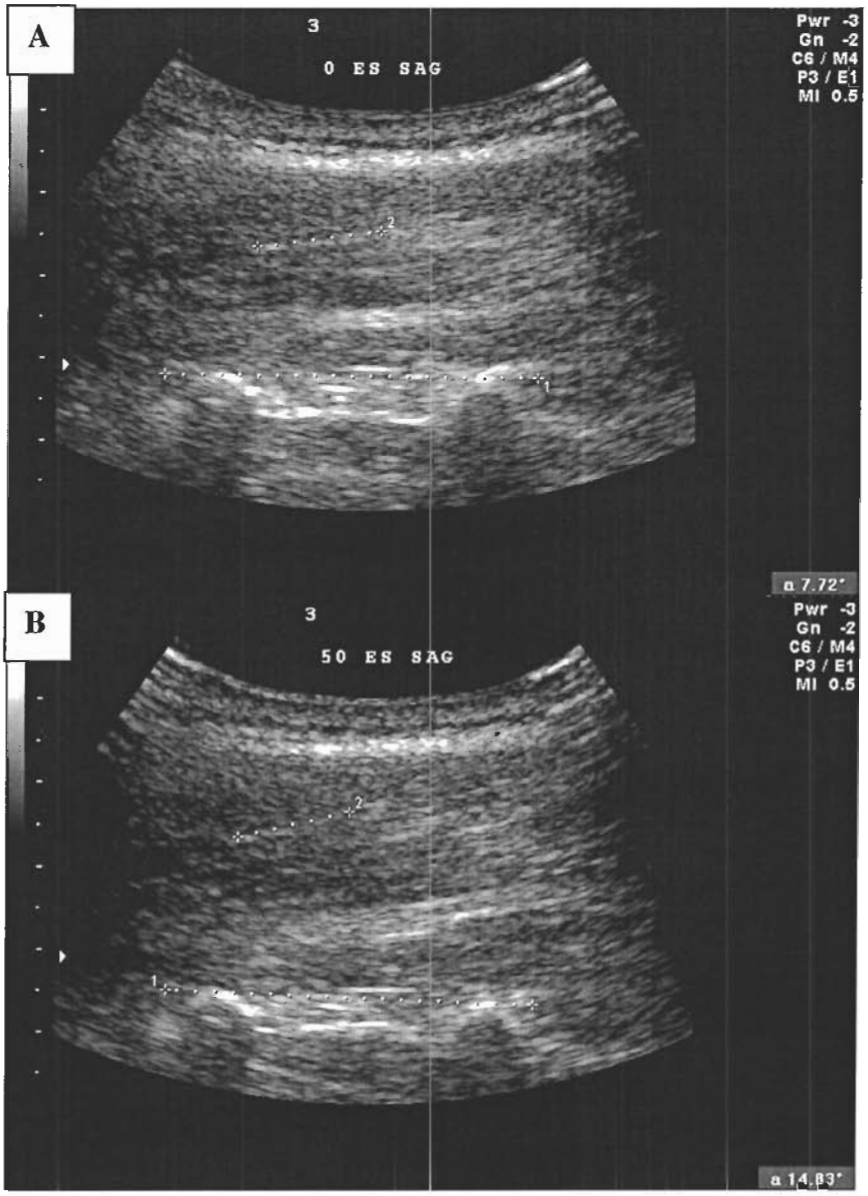

In addition, we were able to measure the distance between transverse processes for different trunk postures. Figure 4.8 illustrates the displacement of the tips of the transverse processes that occurs when moving the torso from a vertical orientation to one that is laterally flexed.

Figure 4.8 **Tips of the transverse processes of L1-L2 (right side) when torso is oriented vertically (A) and laterally flexed to the left (B). Both images give the distance between the tips of the transverse processes (D1) in the bottom right corner.**

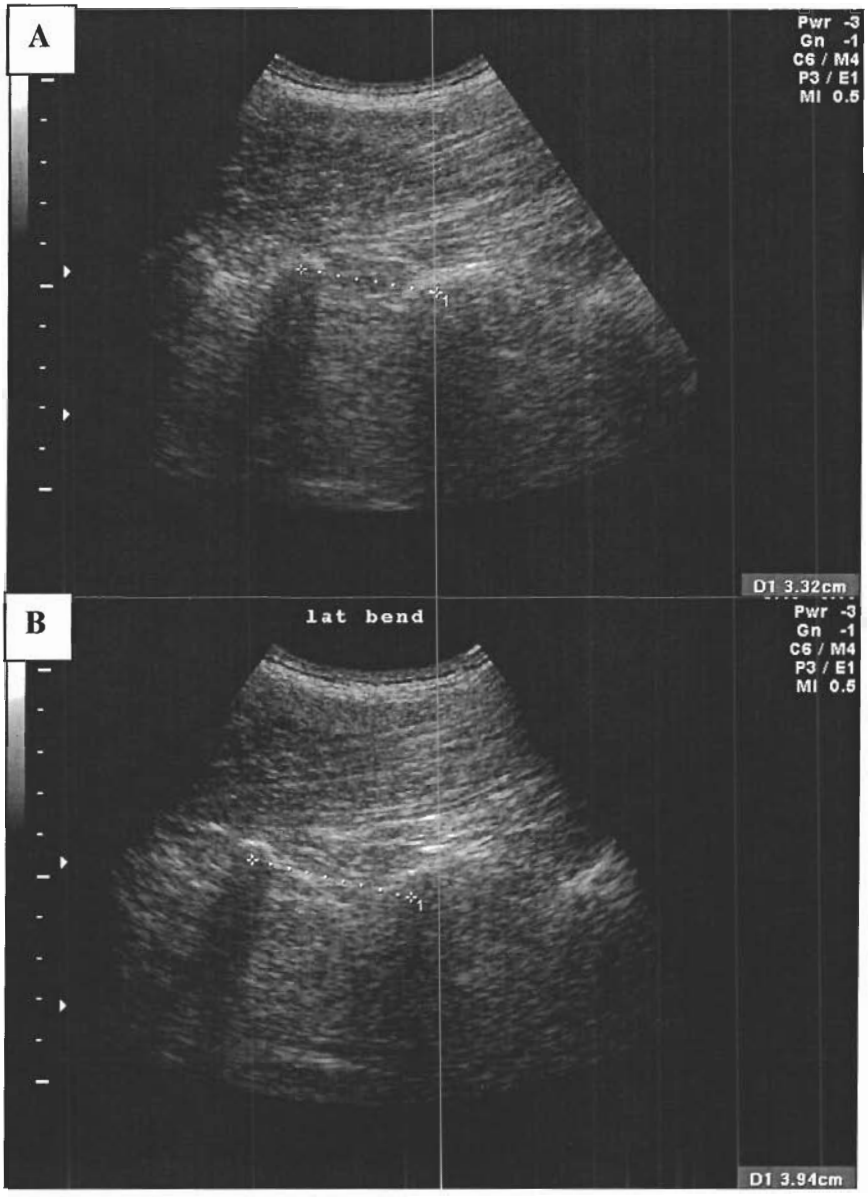

Such differences in the distance between transverse processes were not found for torso extension – flexion. Therefore, we concluded that trunk perturbations should be performed in the coronal plane and pull the subject in lateral flexion. Figure 4.9 shows images obtained during pilot tests of trunk perturbation in the lateral direction. For the situation depicted in Figure 4.9 there is close to 3 mm difference in the distance between

the tips of the transverse processes before the perturbation occurs and at maximum displacement.

Figure 4.9 **Tips of the transverse processes of L1-L2 (right side) when torso is oriented vertically and subject is contracting in lateral flexion to the right at 25% MVC (A) and at the point where the direction of motion changes during perturbation as previously described (B). Both images give the distance between the tips of the transverse processes (D1) in the bottom right corner.**

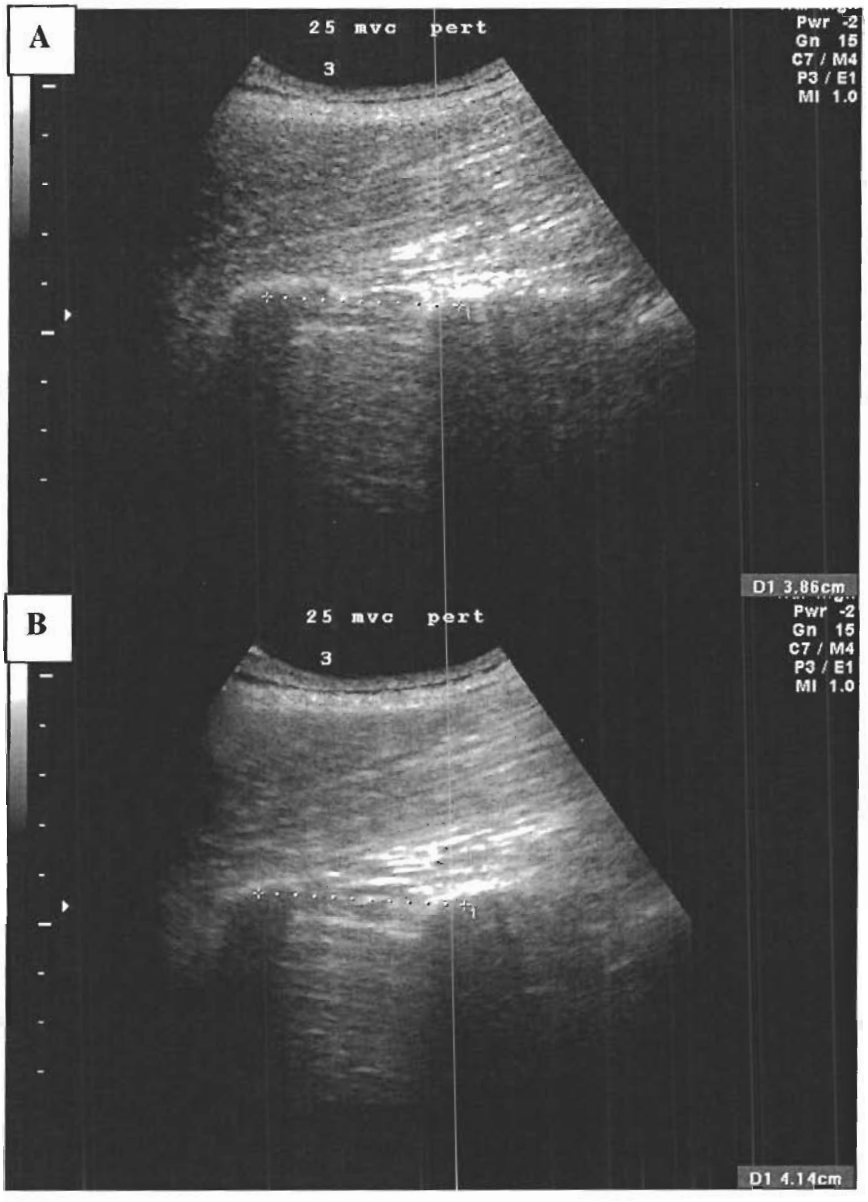

4.2 Ultrasound Images - Descriptive Statistics

Table 4.2 summarizes the types of electronic caliper measurements used in the study. The table lists measurements actually used in the study, measurements that were achievable but not used in the study and for completeness, measurements that were not attempted for the study.

Table 4.2 Summary of measurements made from ultrasound images.

Structure Imaged	Location	Scan Plane	Pennation	Diameter (d)	Distance from Skin (s)	Distance b/w structures
Longissimus thoracis (LT)	L1-L2	Sagittal	Y	Y (x2 – L1-L2)	§	N/A
Erector spinae (ES)	L2	Transverse	§	Y (x2 – Med.-Lat.)	§	N/A
Quadratus lumborum (QL)	L3	Transverse	§	Y (x2 – ML-AP)	Y	N/A
External oblique (EO)	Iliac Crest	Transverse	#	Y	#	N/A
Internal oblique (IO)	Iliac Crest	Transverse	#	Y	#	N/A
Transversus abdominis (TA)	Iliac Crest	Transverse	#	Y	#	N/A
Vertebral transverse processes	L1-L2	Sagittal	N/A	§	#	Y

Measured and applied in this study (Y); Not used in this study (#); Not attempted (§).

The individual calculated coefficients of variation of the measurements recorded for both extension and lateral flexion averaged from 10 subjects individual data (6 female and 4 male) are listed in Tables 4.3 and 4.4.

Table 4.3 Coefficients of Variation for raw data of each ultrasound variable measured at each contraction level for lateral flexion averaged from individual values for 10 subjects.

Structure Imaged	Ultrasound Measurement	Coefficient of Variation
Longissimus thoracis	0% MVC Pennation	0.12
(deg)	10% MVC Pennation	0.14
	25% MVC Pennation	0.17
	50% MVC Pennation	0.13
Longissimus thoracis	0% MVC Diameter (d) - L1	0.05
(cm)	10% MVC Diameter (d) - L1	0.03
	25% MVC Diameter (d) - L1	0.05
	50% MVC Diameter (d) - L1	0.04
Longissimus thoracis	0%MVC Diameter (d) - L2	0.04
(cm)	10%MVC Diameter (d) - L2	0.04
	25%MVC Diameter (d) - L2	0.04

	50%MVC Diameter (d) - L2	0.03
Erector spinae	0%MVC Diameter (d) – Medial	0.04
(cm)	10%MVC Diameter (d) - Medial	0.05
	25%MVC Diameter (d) - Medial	0.05
	50%MVC Diameter (d) - Medial	0.04
Erector spinae	0% MVC Diameter (d) - Lateral	0.05
(cm)	10% MVC Diameter (d) - Lateral	0.04
	25% MVC Diameter (d) - Lateral	0.03
	50% MVC Diameter (d) - Lateral	0.02
Quadratus lumborum	0%MVC Diameter (d) - ML	0.07
(cm)	10%MVC Diameter (d) - ML	0.06
	25%MVC Diameter (d) - ML	0.05
	50%MVC Diameter (d) - ML	0.06
Quadratus lumborum	0%MVC Diameter (d) - AP	0.06
(cm)	10%MVC Diameter (d) - AP	0.05
	25%MVC Diameter (d) - AP	0.06
	50%MVC Diameter (d) - AP	0.05
Quadratus lumborum	0%MVC Distance from Skin (s)	0.03
(cm)	10%MVC Distance from Skin (s)	0.04
	25%MVC Distance from Skin (s)	0.06
	50%MVC Distance from Skin (s)	0.04
External oblique	0%MVC Diameter (d)	0.09
(cm)	10%MVC Diameter (d)	0.09
	25%MVC Diameter (d)	0.10
	50%MVC Diameter (d)	0.05
Internal oblique	0%MVC Diameter (d)	0.11
(cm)	10%MVC Diameter (d)	0.08
	25%MVC Diameter (d)	0.07
	50%MVC Diameter (d)	0.07
Transversus abdominis	0%MVC Diameter (d)	0.18
(cm)	10%MVC Diameter (d)	0.17
	25%MVC Diameter (d)	0.12
	50%MVC Diameter (d)	0.10

From these results we can see that the least reliable ultrasound measurements for lateral flexion are the longisimus thoracis pennation angle and the transversus abdominis diameter, having average coefficients of variation (CVa) of approximately 0.14. The most reliable ultrasound measurements were the longisimus thoracis – L1 diameter, longisimus thoracis – L2 diameter, erector spinae - lateral diameter and quadratus lumborum – distance from skin all with an average CVa of approximately 0.04.

Table 4.4 Coefficients of Variation for raw data of each ultrasound variable measured at each contraction level for extension averaged from individual values for 10 subjects.

Structure Imaged	Ultrasound Measurement	Coefficient of Variation
Longissimus thoracis	0% MVC Pennation	0.12
(deg)	10% MVC Pennation	0.14
	25% MVC Pennation	0.17

	50% MVC Pennation	0.14
Longissimus thoracis	0% MVC Diameter (d) - L1	0.05
(cm)	10% MVC Diameter (d) - L1	0.02
.04	25% MVC Diameter (d) - L1	0.05
	50% MVC Diameter (d) - L1	0.04
Longissimus thoracis	0%MVC Diameter (d) - L2	0.04
(cm)	10%MVC Diameter (d) - L2	0.04
	25%MVC Diameter (d) - L2	0.04
	50%MVC Diameter (d) - L2	0.03
Erector spinae	0%MVC Diameter (d) - Medial	0.05
(cm)	10%MVC Diameter (d) - Medial	0.05
	25%MVC Diameter (d) - Medial	0.04
	50%MVC Diameter (d) - Medial	0.04
Erector spinae	0% MVC Diameter (d) - Lateral	0.05
(cm)	10% MVC Diameter (d) - Lateral	0.04
	25% MVC Diameter (d) - Lateral	0.03
.04	50% MVC Diameter (d) - Lateral	0.02

As in lateral flexion, the longissimus thoracis pennation angle had the largest average CVa (0.14), where as the longisimus thoracis – L1 diameter, longissimus thoracis – L2 diameter and erector spinae - lateral diameter had the smallest average CVa (0.04).

The means, standard deviations and calculated coefficients of variation of the measurements recorded for both extension and lateral flexion averaged over 10 subjects (6 female and 4 male) are listed in Tables 4.5 and 4.6.

Table 4.5 Means, Standard Deviations and Coefficients of Variation for raw data of each ultrasound variable measured at each contraction level for lateral flexion computed for 10 subjects.

Structure Imaged	Ultrasound Measurement	Mean	Standard Deviation	Coefficient of Variation
Longissimus thoracis	0% MVC Pennation	16.4	4.9	0.29
(deg)	10% MVC Pennation	15.5	5.9	0.38
	25% MVC Pennation	15.3	5.0	0.33
	50% MVC Pennation	17.3	6.3	0.36
Longissimus thoracis	0% MVC Diameter (d) - L1	2.6	0.4	0.19
(cm)	10% MVC Diameter (d) - L1	2.6	0.4	0.19
	25% MVC Diameter (d) - L1	2.5	0.3	0.12
	50% MVC Diameter (d) - L1	2.6	0.4	0.19
Longissimus thoracis	0%MVC Diameter (d) - L2	2.9	0.4	0.14
(cm)	10%MVC Diameter (d) - L2	2.8	0.4	0.14
	25%MVC Diameter (d) - L2	2.8	0.4	0.14
	50%MVC Diameter (d) - L2	3.0	0.4	0.13
Erector spinae	0%MVC Diameter (d) – Medial	2.1	0.4	0.19
(cm)	10%MVC Diameter (d) - Medial	2.0	0.3	0.15
	25%MVC Diameter (d) - Medial	2.1	0.3	0.14
	50%MVC Diameter (d) - Medial	2.1	0.3	0.14
Erector spinae	0% MVC Diameter (d) - Lateral	2.9	0.5	0.17
(cm)	10% MVC Diameter (d) - Lateral	3.0	0.4	0.13

	25% MVC Diameter (d) - Lateral	3.0	0.4	0.13
	50% MVC Diameter (d) - Lateral	3.1	0.4	0.13
Quadratus lumborum	0%MVC Diameter (d) - ML	3.7	0.9	0.24
(cm)	10%MVC Diameter (d) - ML	4.0	0.9	0.23
	25%MVC Diameter (d) - ML	3.8	1.1	0.29
	50%MVC Diameter (d) - ML	3.9	1.1	0.28
Quadratus lumborum	0%MVC Diameter (d) - AP	1.2	0.4	0.33
(cm)	10%MVC Diameter (d) - AP	1.2	0.4	0.33
	25%MVC Diameter (d) - AP	1.2	0.4	0.33
	50%MVC Diameter (d) - AP	1.3	0.5	0.38
Quadratus lumborum	0%MVC Distance from Skin (s)	2.7	0.9	0.33
(cm)	10%MVC Distance from Skin (s)	2.7	0.8	0.30
	25%MVC Distance from Skin (s)	2.5	1.0	0.40
	50%MVC Distance from Skin (s)	2.8	1.0	0.36
External oblique	0%MVC Diameter (d)	0.9	0.2	0.22
(cm)	10%MVC Diameter (d)	1.0	0.2	0.20
	25%MVC Diameter (d)	1.1	0.2	0.10
	50%MVC Diameter (d)	1.2	0.3	0.18
Internal oblique	0%MVC Diameter (d)	1.0	0.2	0.20
(cm)	10%MVC Diameter (d)	1.3	0.4	0.31
	25%MVC Diameter (d)	1.5	0.5	0.33
	50%MVC Diameter (d)	1.9	0.4	0.21
Transversus abdominis	0%MVC Diameter (d)	0.4	0.1	0.25
(cm)	10%MVC Diameter (d)	0.5	0.2	0.40
	25%MVC Diameter (d)	0.6	0.2	0.33
	50%MVC Diameter (d)	0.6	0.2	0.33

Compared to the individual data we again see that one of the least consistent ultrasound measurements for lateral flexion was the longisimus thoracis pennation angle with an average CVa of 0.34. However, the CVa of most other variables was also high, indicating that a major source of variation is variability across subjects rather than variability in being able to make repeatable measurements. The most consistent ultrasound measurements across subjects were the erector spinae lateral and longisimus thoracis – L2 diameters with an average CVa = 0.14.

Table 4.6 Means, Standard Deviations and Coefficients of Variation for raw data of each ultrasound variable measured at each contraction level for extension computed for 10 subjects.

Structure Imaged	Ultrasound Measurement	Mean	Standard Deviation	Coefficient of Variation
Longissimus thoracis	0% MVC Pennation	16.5	4.8	0.29
(deg)	10% MVC Pennation	16.2	4.1	0.25
	25% MVC Pennation	17	5.3	0.25
	50% MVC Pennation	18.1	5.0	0.28
Longissimus thoracis	0% MVC Diameter (d) - L1	2.6	0.5	0.19
(cm)	10% MVC Diameter (d) - L1	2.6	0.4	0.15

	25% MVC Diameter (d) - L1	2.7	0.5	0.19
	50% MVC Diameter (d) - L1	2.8	0.6	0.21
Longissimus thoracis	0%MVC Diameter (d) - L2	2.9	0.4	0.14
(cm)	10%MVC Diameter (d) - L2	3.0	0.4	0.13
	25%MVC Diameter (d) - L2	3.1	0.5	0.16
	50%MVC Diameter (d) - L2	3.3	0.5	0.15
Erector spinae	0%MVC Diameter (d) - Medial	2.1	0.4	0.19
(cm)	10%MVC Diameter (d) - Medial	2.2	0.4	0.18
	25%MVC Diameter (d) - Medial	2.2	0.5	0.23
	50%MVC Diameter (d) - Medial	2.4	0.5	0.21
Erector spinae	0% MVC Diameter (d) - Lateral	2.9	0.5	0.17
(cm)	10% MVC Diameter (d) - Lateral	3.1	0.5	0.16
	25% MVC Diameter (d) - Lateral	3.3	0.5	0.15
	50% MVC Diameter (d) - Lateral	3.4	0.6	0.15

Compared to the individual data we again see that one of the least consistent ultrasound measurements for lateral flexion was the longisimus thoracis pennation angle with a CVa of 0.27 whereas the longisimus thoracis – L2 diameter had the smallest CVa (0.14).

4.3 Linear Regression Analysis

4.3.1 Individual Subject Data

Linear regression analysis was conducted to determine the correlation between ultrasound measurements and trunk force. First, linear regressions of individual data were performed. In order to take into account individual differences in resting anatomy the data were normalized by dividing all values by the average value of the 10% MVC measurements for each subject. Figures 4.10 through to 4.13 show scatter plots of some of these data. Table 4.7 summarizes the results of linear regressions performed on the individual subject data. The heading "%Significance" indicates the percentage of individual linear regression results out of 10 subjects that were found to be significant ($p < 0.05$). The p-value refers to the relation of the x (independent) and y (dependent) variables, which are force and ultrasound measurement, respectively. If the p-value

indicates statistical significance then the slope of the regression relation is non-zero or a significant correlation between the two variables exists.

Figure 4.10 Scatter plot of the ultrasound variable with the lowest correlation with trunk force in extension (longissimus thoracis – pennation angle) from 1 subject. (Normalized to 10% MVC)

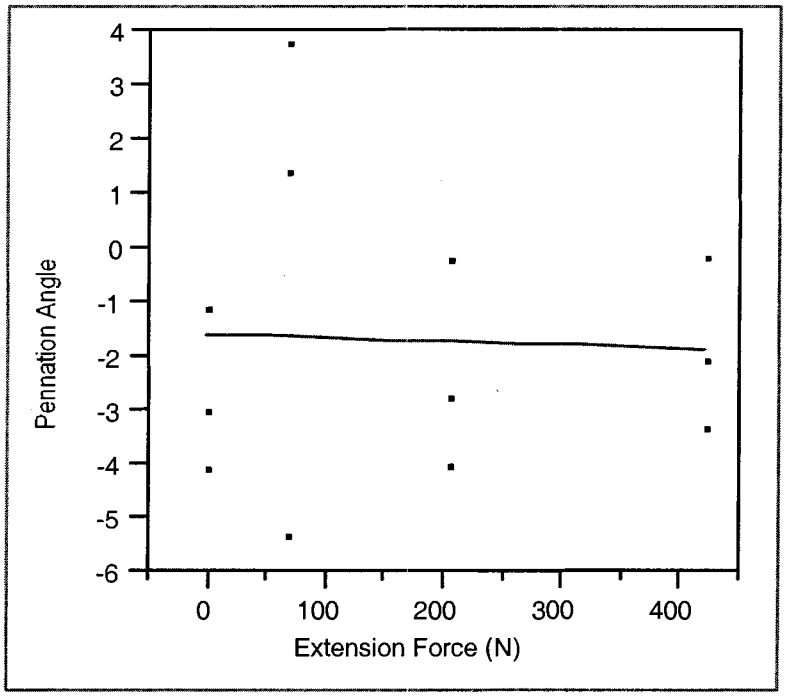

Figure 4.11 Scatter plot of the ultrasound variable with the highest correlation with trunk force in extension (erector spinae - lateral) from 1 subject. (Normalized to 10% MVC)

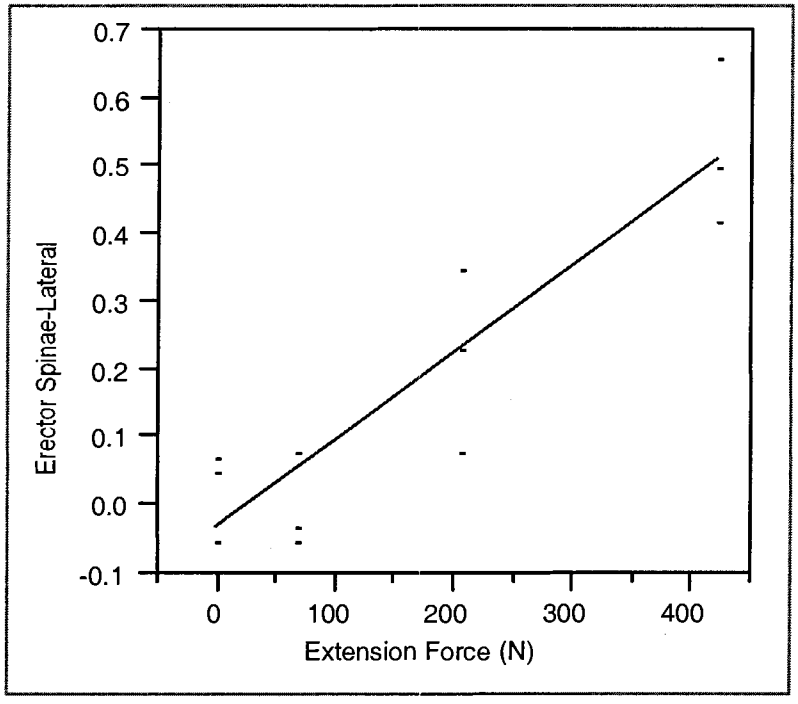

Figure 4.12 Scatter plot of the ultrasound variable with the lowest correlation with trunk force in lateral flexion (longissimus thoracis – L1) from 1 subject. (Normalized to 10% MVC)

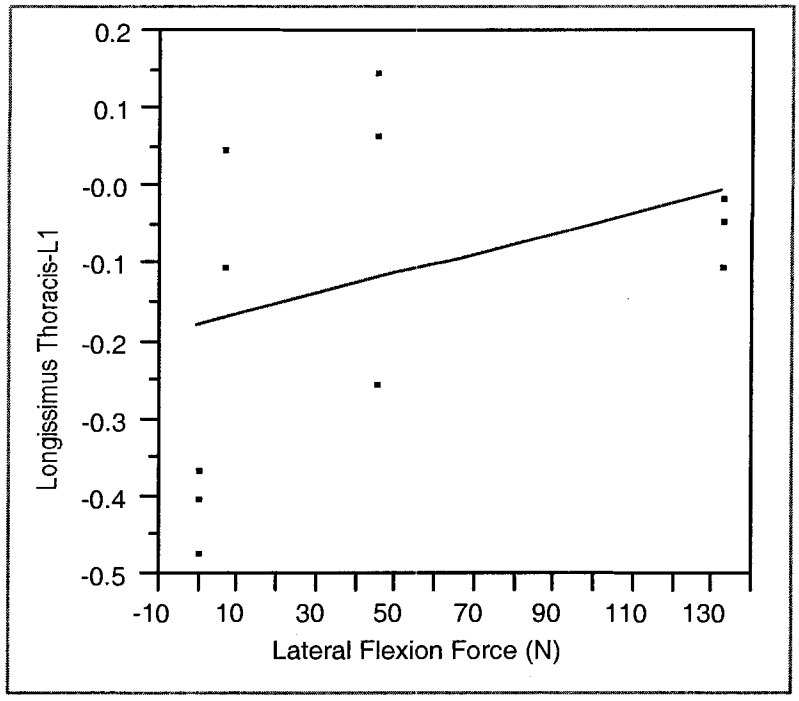

Figure 4.13 Scatter plot of the ultrasound variable with the highest correlation with trunk force in lateral flexion (internal oblique diameter) from 1 subject. (Normalized to 10% MVC)

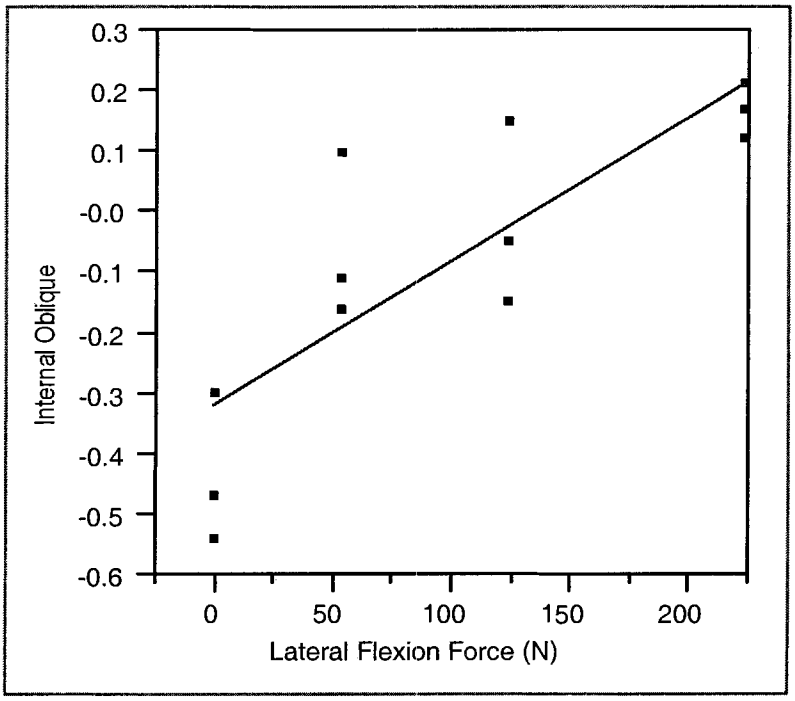

Table 4.7 Average linear regression parameters for individual subject data.

Abbreviations for measured variables are explained in Table 4.2.

INDIVIDUAL DATA (Normalized to 10% MVC)											
EXTENSION	LT-Pennation	LT-L1	LT-L2	ES-Medial	ES-Lateral						
%Significant	20	60	80	70	80						
Mean R^2 (N=10)	0.167	0.341	0.411	0.433	0.604						
STDEV R^2	0.235	0.309	0.267	0.228	0.321						
Mean P-value	0.355	0.250	0.143	0.037	0.013						
STDEV P-value	0.318	0.358	0.303	0.062	0.113						
LATERAL FLEXION	LT-Pennation	LT-L1	LT-L2	ES-Medial	ES-Lateral	QL-Dis.to Skin	QL-AP	QL-ML	EO	IO	TA
%Significant	30	10	20	20	50	40	40	40	70	100	60
Mean R^2 (N=10)	0.244	0.165	0.173	0.206	0.323	0.181	0.302	0.248	0.406	0.682	0.418
STDEV R^2	0.260	0.154	0.184	0.165	0.297	0.203	0.350	0.260	0.283	0.259	0.310
Mean P-value	0.265	0.244	0.318	0.208	0.237	0.366	0.298	0.319	0.076	0.003	0.133
STDEV P-value	0.295	0.212	0.305	0.256	0.316	0.389	0.364	0.379	0.133	0.005	0.233

Abbreviations

LT-Pennation - Longissimus thoracis pennation angle
LT-L1 - Longissimus thoracis diameter measured at lumbar vertebra 1
LT-L2 - Longissimus thoracis diameter measured at lumbar vertebra 2
ES-Medial - Erector spinae diameter measured at facet
ES-Lateral - Erector spinae diameter measured at tip of L2 transverse process
QL—Dis. to Skin – Distance from skin to posterior plane of quadratus lumborum
QL—AP – Diameter of quadratus lumborum in anterior-posterior plane
QL—ML – Diameter of quadratus lumborum in medial-lateral plane
EO - External oblique diameter
IO - Internal oblique diameter
TA - Transversus abdominis diameter

We found that the erector spinae lateral thickness was the best predictor of trunk extension force (average $R^2 = 0.604$) and that the internal oblique diameter was the best predictor of lateral flexion force (average $R^2 = 0.682$). Longisimus thoracis pennation angle was least correlated with trunk extension force (average $R^2 = 0.167$) and longissimus thoracis L1 thickness was least correlated with lateral flexion force (average $R^2 = 0.165$).

Table 4.7 also indicates characteristic differences between certain measurements. Specifically, reliability and variability comparisons can be made. For example, in extension longissimus thoracis L2 thickness and erector spinae medial have similar R^2 average and variances, indicating that the spread of data points around the regression line are similar in both measurements. However, the average p-values are 0.143 (longisimus thoracis L2 thickness) and 0.037 (erector spinae medial thickness), indicating that the relationship between force and muscle thickness is much stronger for the medial measurement. Further, the standard deviation of the p – value for the longisimus thoracis L2 thickness is quite large indicating that for some subjects the p-value is very low and for others very high. This is indicative of an unreliable measurement.

4.3.2 Data Averaged over all Subjects

A second linear regression analysis was performed using the same data as in section 4.3.1 but averaged over all subjects. As before, in order to reduce the effect of individual differences in resting anatomy the data for each subject were first normalized by the average value at 10% MVC for that subject. Figures 4.14 through to 4.17 show scatter plots of some of these data. Table 4.8 summarizes the linear regression results.

Figure 4.14 **Mean (dot), ±1 standard error (solid bar) and ±1 standard deviation (broken bar) for scatter plot of the ultrasound variable with the lowest correlation with trunk force in extension (longissimus thoracis – pennation angle) averaged over 10 subjects. (Normalized to 10% MVC)**

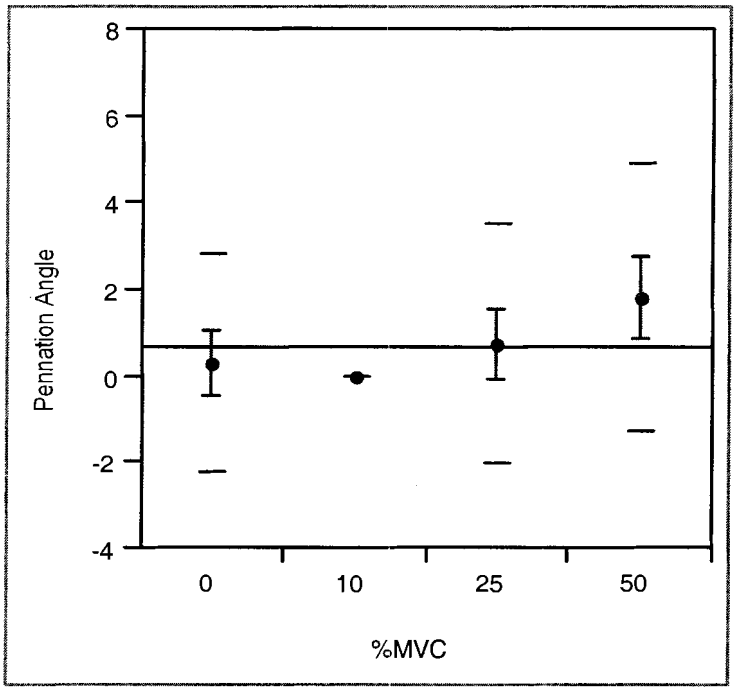

Figure 4.15 **Mean (dot), ±1 standard error (solid bar) and ±1 standard deviation (broken bar) for scatter plot of the ultrasound variable with the highest correlation with trunk force in extension (erector spinae - medial) averaged over 10 subjects. (Normalized to 10% MVC)**

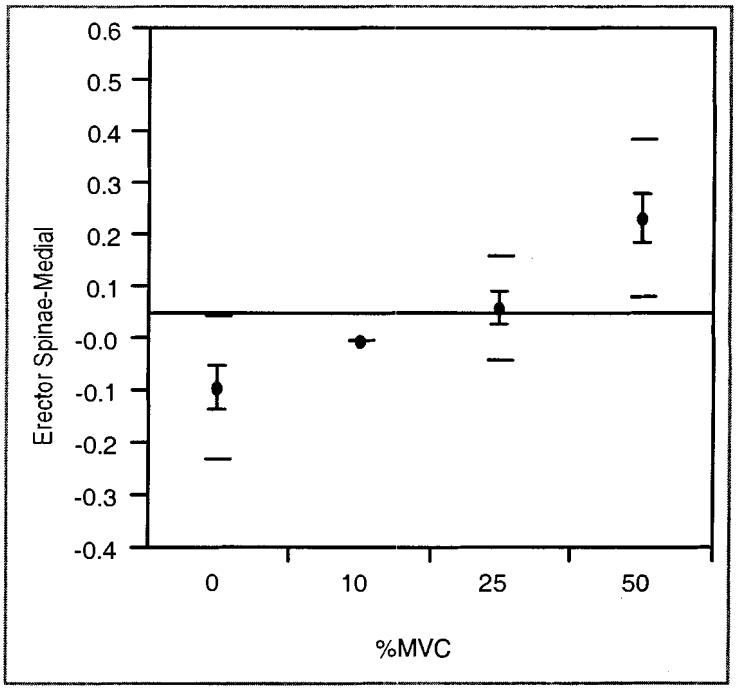

Figure 4.16 Mean (dot), ±1 standard error (solid bar) and ±1 standard deviation (broken bar) for scatter plot of the ultrasound variable with the lowest correlation with trunk force in lateral flexion (longissimus thoracis – L1) averaged over 10 subjects. (Normalized to 10% MVC)

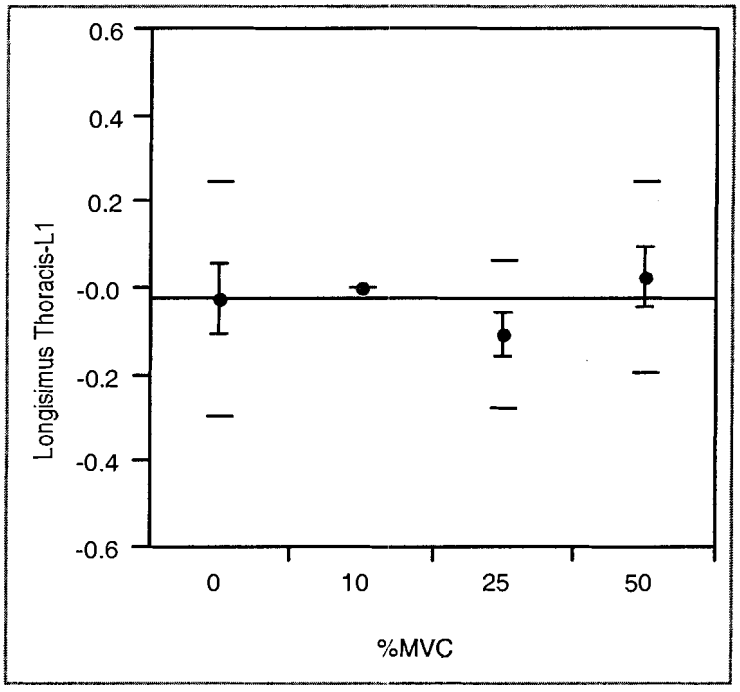

Figure 4.17 Mean (dot), ±1 standard error (solid bar) and ±1 standard deviation (broken bar) for scatter plot of the ultrasound variable with the highest correlation with trunk force in lateral flexion (internal oblique diameter) averaged over 10 subjects. (Normalized to 10% MVC)

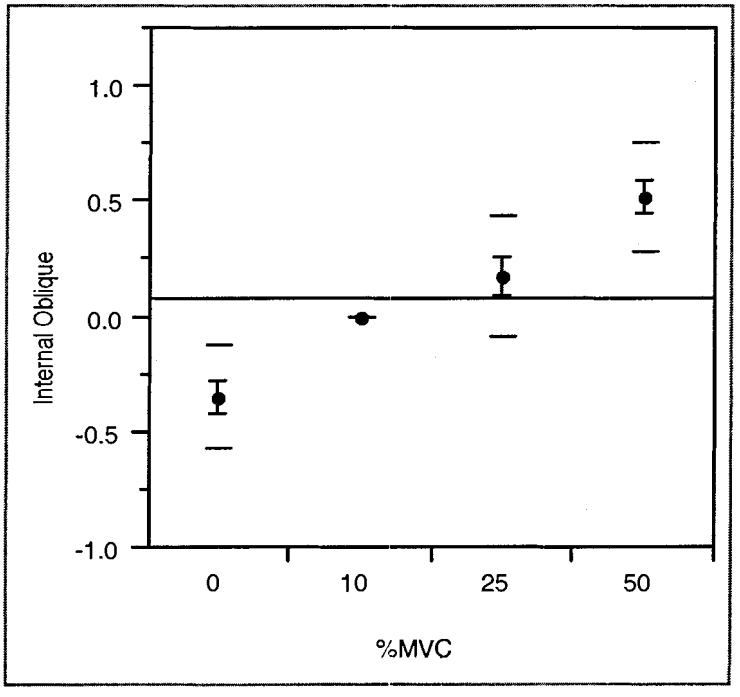

Table 4.8 Summary of linear regressions on averaged data.

DATA AVERAGED OVER ALL SUBJECTS (Normalized to 10% MVC)											
EXTENSION	LT-Pennation	LT-L1	LT-L2	ES-Medial	ES-Lateral						
R^2	0.047	0.452	0.406	0.560	0.480						
P-value	0.181	<0.0001	<0.0001	<0.0001	<0.0001						
LATERAL FLEXION	LT-Pennation	LT-L1	LT-L2	ES-Medial	ES-Lateral	QL-Dis.to Skin	QL-AP	QL-ML	EO	IO	TA
R^2	0.001	0.001	0.017	0.003	0.233	0.018	0.200	0.070	0.486	0.606	0.484
P-value	0.794	0.836	0.417	0.738	0.002	0.413	0.004	0.097	<0.0001	<0.0001	<0.0001

Abbreviations

LT-Pennation - Longissimus thoracis pennation angle
LT-L1 - Longissimus thoracis diameter measured at lumbar vertebra 1
LT-L2 - Longissimus thoracis diameter measured at lumbar vertebra 2
ES-Medial - Erector spinae diameter measured at facet
ES-Lateral - Erector spinae diameter measured at tip of L2 transverse process
QL—Dis. to Skin – Distance from skin to posterior plane of quadratus lumborum
QL—AP – Diameter of quadratus lumborum in anterior-posterior plane
QL—ML – Diameter of quadratus lumborum in medial-lateral plane
EO - External oblique diameter
IO - Internal oblique diameter
TA - Transversus abdominis diameter

We expected all of the muscle parameters being measured in the extension condition to be significantly correlated with trunk extension force since the ultrasound measurements were selected to quantify changes in muscle geometry that occurred during contraction. In contrast to the individual subject data, the data averaged across subjects produced significant relations between all measured variables and extension force ($p < 0.0001$) except for the pennation angle of the longisimus thoracis ($p = 0.1807$).

Lateral flexion was not the primary function of most of the muscles that could be examined so we did not expect that all of the measured variables would be significantly correlated with lateral trunk flexion force. The parameters that were significantly related to lateral flexion force were the erector spinae lateral thickness ($p = 0.002$), quadratus lumborum – anterior/posterior thickness ($p = 0.004$), external oblique thickness ($p < 0.0001$), internal oblique thickness ($p < 0.0001$) and the transversus abdominis thickness ($p < 0.0001$). However, only one of the three parameters measured for the quadratus lumborum was statistically significant. The quadratus lumborum - medial/lateral diameter and quadratus lumborum – distance to skin were not significantly correlated with lateral flexion force ($p = 0.097$ and 0.413, respectively). Most of the parameters for the erector spinae muscles were also not significantly correlated with lateral flexion force.

4.4 Ultrasound Images – Dependence on Trunk Orientation

To determine whether some of the variance of our data might be due to variation in trunk orientation during the experiment, a post-hoc test (Post-hoc Test #1) was designed to measure trunk orientation. One additional subject completed the procedure of Experiment 1 (See Section 3.5 "Protocol") with one modification, namely that trunk

orientation was recorded for each trial. Trunk orientation was represented as the distance from a reference point on the frame of the apparatus to the mid portion of the subjects' sternum. The change in orientation was calculated as the difference between the measured distance on a given trial and the distance on the first trial in the 0% MVC condition. Regression relations were calculated between the orientation measure and each ultrasound parameter over all contraction levels. Figures 4.18 and 4.19 show scatter plots of the ultrasound measurements which were best and least correlated with changes in trunk orientation and Table 4.9 summarizes the results for all measurements.

Figure 4.18 Scatter plot of the ultrasound variable with the lowest correlation with trunk orientation (longissimus-thoracis – L2) from 1 subject.

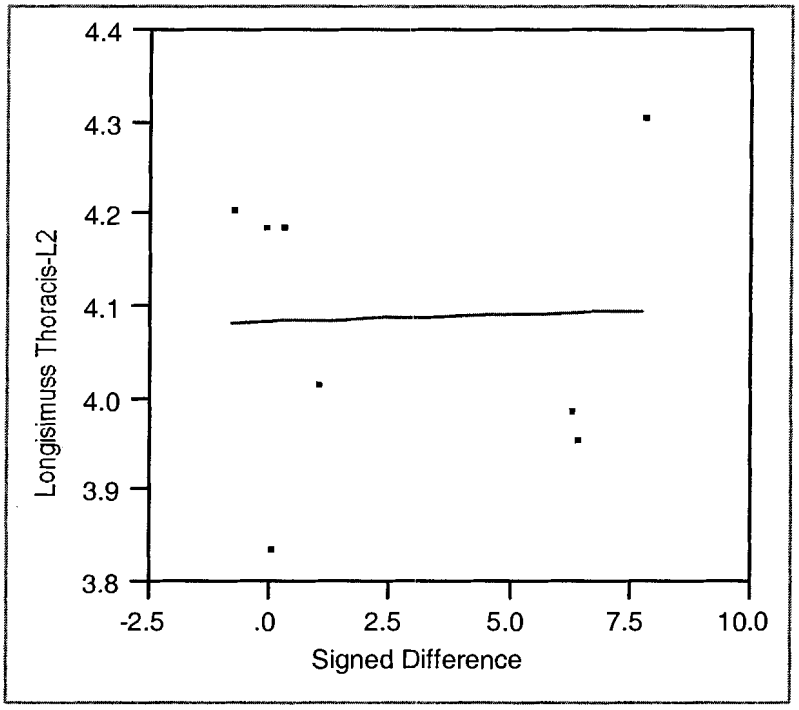

Figure 4.19 Scatter plot of the ultrasound variable with the highest correlation with trunk orientation (external oblique) from 1 subject.

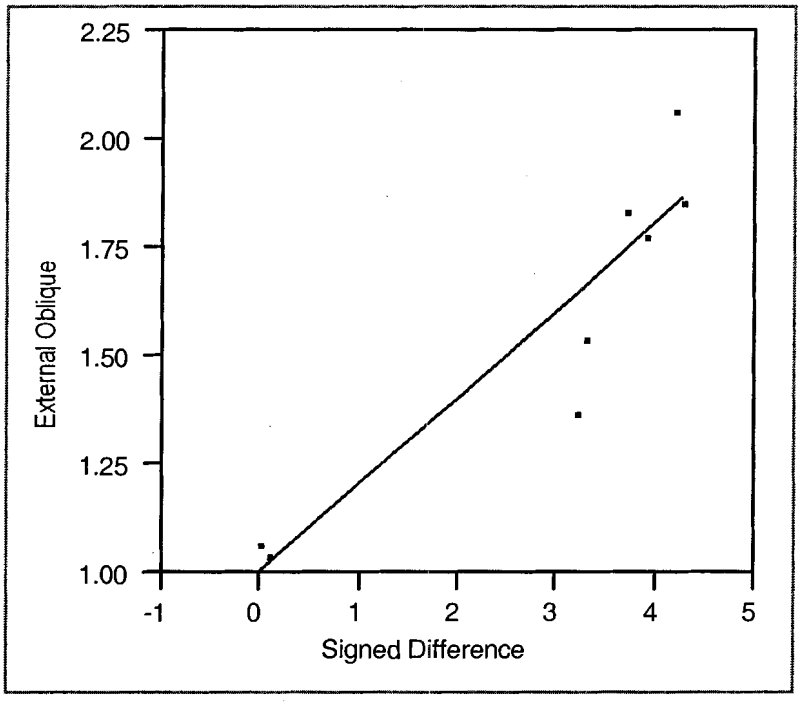

Table 4.9 Summary of linear regression analysis with the subject of post-hoc test #1Trunk Orientation)

Trunk Orientation vs. Ultrasound Measurement												
EXTENSION		LT-Pennation	LT-L1	LT-L2	ES-Medial	ES-Lateral						
Signed Difference	R^2	0.207	0.169	0.001	0.009	0.353						
	P-value	0.257	0.312	0.939	0.816	0.120						
Absolute Value	R^2	0.228	0.171	0.008	0.009	0.143						
	P-value	0.232	0.309	0.829	0.818	0.356						
LATERAL FLEXION		LT-Pennation	LT-L1	LT-L2	ES-Medial	ES-Lateral	QL-Dis.to Skin	QL-AP	QL-ML	EO	IO	TA
Signed Difference	R^2	0.701	0.682	0.036	0.831	0.580	0.143	0.397	0.047	0.848	0.775	0.815
	P-value	0.009	0.012	0.655	0.002	0.028	0.355	0.094	0.607	0.001	0.004	0.002
Absolute Value	R^2	0.701	0.682	0.036	0.831	0.580	0.174	0.418	0.074	0.848	0.775	0.815
	P-value	0.009	0.012	0.655	0.002	0.028	0.304	0.083	0.515	0.001	0.004	0.002

Abbreviations

LT-Pennation - Longissimus thoracis pennation angle
LT-L1 - Longissimus thoracis diameter measured at lumbar vertebra 1
LT-L2 - Longissimus thoracis diameter measured at lumbar vertebra 2
ES-Medial - Erector spinae diameter measured at facet
ES-Lateral - Erector spinae diameter measured at tip of L2 transverse process
QL—Dis. to Skin – Distance from skin to posterior plane of quadratus lumborum
QL—AP – Diameter of quadratus lumborum in anterior-posterior plane
QL—ML – Diameter of quadratus lumborum in medial-lateral plane
EO - External oblique diameter
IO - Internal oblique diameter
TA - Transversus abdominis diameter

In extension, no measured ultrasound parameter was significantly correlated with trunk orientation. However, in lateral flexion seven of eleven ultrasound parameters were significantly correlated with trunk orientation. The longissimus thoracis pennation angle ($p = 0.009$), the longisimus thoracis L1 thickness ($p = 0.012$), the erector spinae medial thickness ($p = 0.002$), the erector spinae lateral thickness ($p = 0.028$), the external oblique thickness ($p = 0.001$), the internal oblique thickness ($p = 0.004$) and the transversus abdominis thickness ($p = 0.002$) all varied significantly with changes in trunk orientation.

4.5 Lumbar Stiffness Estimation

In Figures 4.20-4.22, the distance between the L1 and L2 transverse processes before perturbation (Figure 4.20), at maximum displacement (the point at which relative motion of the transverse processes appeared to reverse direction) (Figure 4.21) and the difference between the two distances (Figure 4.22) are shown as a function of lateral flexion force.

Figure 4.20 Distance between the L1-L2 transverse processes vs %MVC at the time just prior to torso perturbation.

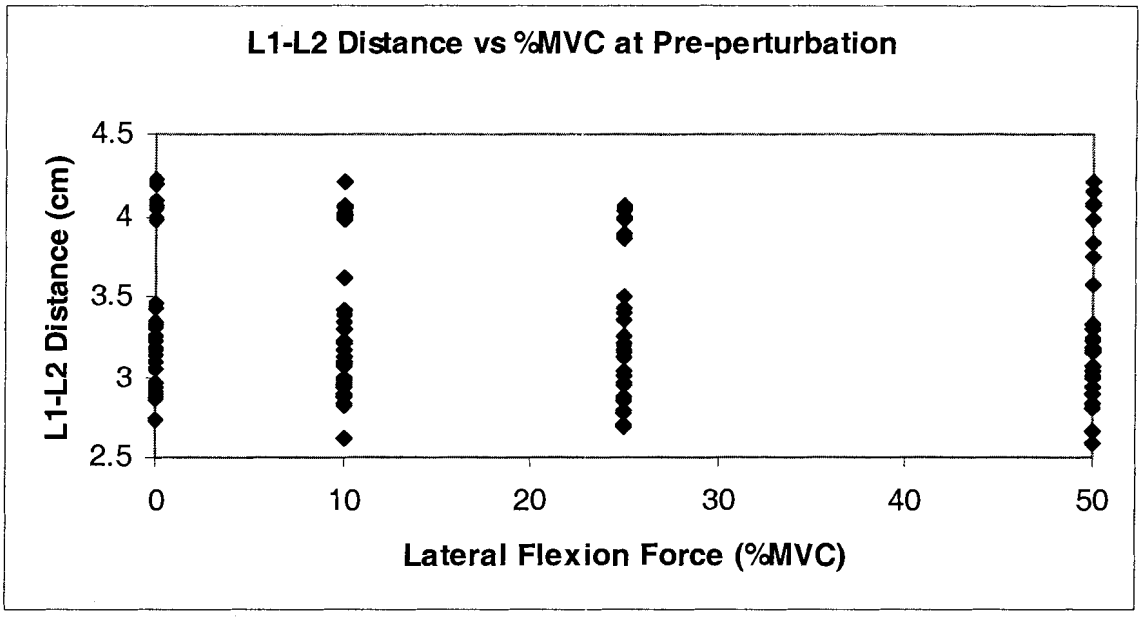

Repeated measures ANOVA showed that the distance between the L1-L2 transverse processes in lateral flexion as measured with ultrasound during the pre-perturbation period was affected by lateral flexion force ($p < 0.0001$). However, according to linear regression analysis of the same data it was shown that the slope of the relation was not significantly different from zero ($p = 0.32$). This indicates that there was no systematic effect of trunk force on L1-L2 separation distance.

Figure 4.21 Distance between the L1-L2 transverse processes vs %MVC at the time of maximum displacement during torso perturbation.

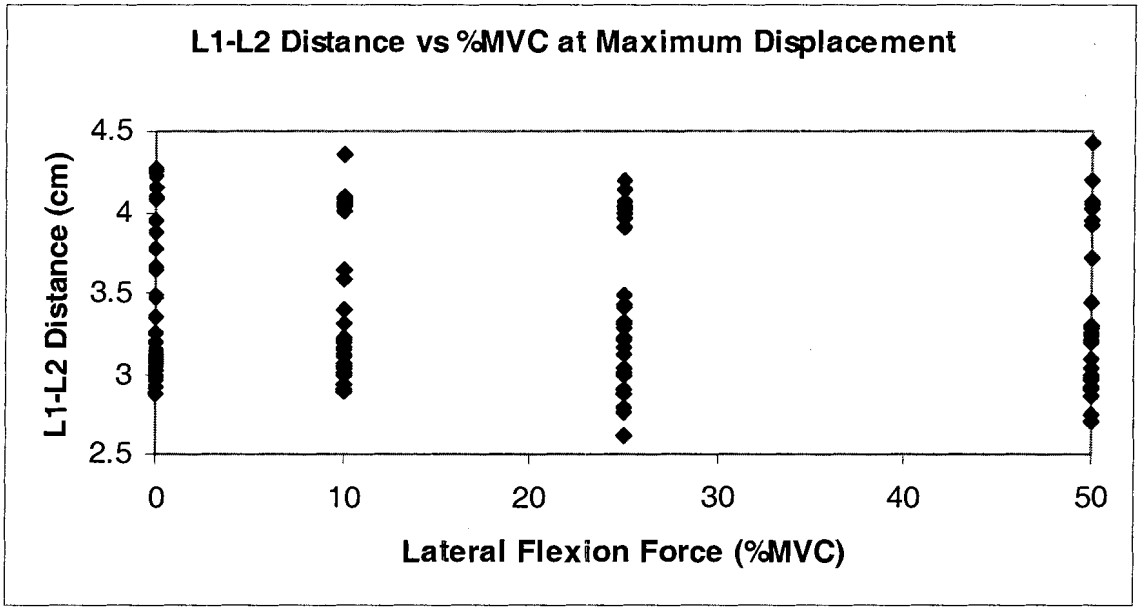

Similarly, the distance between the L1-L2 transverse processes at maximum L1-L2 displacement during the perturbation was also significantly affected by trunk force according to the repeated measures ANOVA ($p < 0.0001$). However, the slope computed from the linear regression analysis was not significantly different from zero ($p = 0.65$).

Figure 4.22 Change in distance between the L1-L2 transverse processes vs %MVC at the time of maximum displacement compared to pre-perturbation.

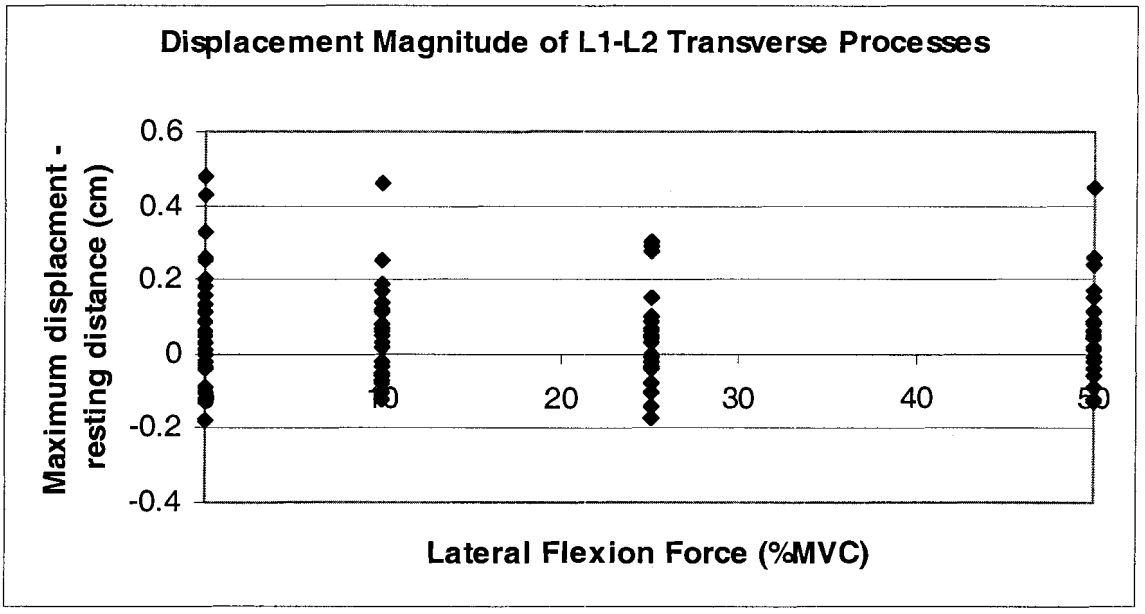

There was no relation between the change in distance between the L1-L2 transverse processes from pre-perturbation to maximum displacement and the lateral flexion force based on linear regression analysis ($p = 0.71$). From figure 4.22 it is apparent that there were many cases in which the difference between the two values was negative. A negative value for this measurement means that the estimated L1-L2 joint angle would have actually decreased during the displacement. This did not coincide with the observation that that lateral displacement of the trunk produced by the perturbation decreased noticeably as the initial lateral flexion force increased.

4.6 EMG, Force and Ultrasound

After the technical problems outlined in Appendix G were solved the entire protocol for experiment 1 (See Methods Section) was repeated with one subject. As before, linear regression analysis was conducted to determine the relation between

ultrasound measurements and trunk force (Post-hoc Test #2). However, since better EMG data were available, relations between EMG, ultrasound measurements and force were also computed (Post-hoc Test #3). Linear regressions involving all of the individual trials were performed. As before, the data were normalized by dividing all values by the average value of the 10% MVC measurements. Table 4.10 summarizes the results of linear regressions performed between ultrasound measurements and trunk force for extension and lateral flexion (Post-hoc Test #2).

Table 4.10 Linear regression parameters for the subject of post-hoc test #2 (Ultrasound Measurement vs. Trunk Force).

INDIVIDUAL DATA (Normalized to 10% MVC)											
EXTENSION	LT-Pennation	LT-L1	LT-L2	ES-Medial	ES-Lateral						
R^2	0.544	0.751	0.669	0.129	0.547						
P-value	0.006	0.0003	0.001	0.252	0.006						
LATERAL FLEXION	LT-Pennation	LT-L1	LT-L2	ES-Medial	ES-Lateral	QL-Dis.to Skin	QL-AP	QL-ML	EO	IO	TA
R^2	0.221	0.517	0.153	0.308	0.315	0.173	0.606	0.022	0.837	0.703	0.245
P-value	0.125	0.008	0.209	0.061	0.058	0.179	0.003	0.642	<0.0001	0.001	0.121

Abbreviations

LT-Pennation - Longissimus thoracis pennation angle
LT-L1 - Longissimus thoracis diameter measured at lumbar vertebra 1
LT-L2 - Longissimus thoracis diameter measured at lumbar vertebra 2
ES-Medial - Erector spinae diameter measured at facet
ES-Lateral - Erector spinae diameter measured at tip of L2 transverse process
QL—Dis. to Skin – Distance from skin to posterior plane of quadratus lumborum
QL—AP – Diameter of quadratus lumborum in anterior-posterior plane
QL—ML – Diameter of quadratus lumborum in medial-lateral plane
EO - External oblique diameter
IO - Internal oblique diameter
TA - Transversus abdominis diameter

EMG data were quantified by computing the root mean square (rms). Linear regression was then performed between the rms EMG and force and between rms EMG and ultrasound measurements (Post-hoc Test #3). Linear regression was performed between the longissimus thoracis, external oblique and internal oblique EMG and extension force. As expected, there was a significant relation only between longissimus thoracis EMG and extension force ($p = 0.0097$ (LT-EMG); $p = 0.052$ (EO-EMG) and $p = 0.10$ (IO-EMG)). However, in lateral flexion the electrical activity of all muscles (longissimus thoracis, external oblique, internal oblique) was related to lateral flexion force ($p = 0.0034$, $p = 0.0071$ and $p = 0.0086$, respectively). These relationships are consistent with the actions of the muscles and the direction of the isometric force.

Table 4.11 summarizes the results of linear regressions performed between ultrasound measurements and rms EMG for extension and lateral flexion (Post-hoc Test #3). In the extension condition, none of the erector spinae ultrasound measurements varied significantly with the longissimus thoracis EMG. However, in lateral flexion all erector spinae ultrasound measurements except the longissimus thoracis L2 thickness varied significantly with longissimus thoracis EMG. As well, external oblique and internal oblique ultrasound measurements were significantly correlated with the respective muscle EMG.

Table 4.11 Linear regression parameters for the subject of post-hoc test #3 (Ultrasound Measurement vs. EMG)

INDIVIDUAL DATA								
EXTENSION		LT-Pennation	LT-L1	LT-L2	ES-Medial	ES-Lateral		
Erector Spinae-EMG	R^2	0.090	0.214	0.358	0.091	0.252		
	P-value	0.370	0.152	0.052	0.368	0.116		
LATERAL FLEXION		LT-Pennation	LT-L1	LT-L2	ES-Medial	ES-Lateral	EO	IO
Erector Spinae-EMG	R^2	0.771	0.914	0.012	0.853	0.675		
	P-value	0.0004	<0.0001	0.750	<0.0001	0.002		
External Oblique-EMG	R^2						0.849	
	P-value						<0.0001	
Internal Oblique-EMG	R^2							0.694
	P-value							0.002

Abbreviations

LT-Pennation - Longissimus thoracis pennation angle
LT-L1 - Longissimus thoracis diameter measured at lumbar vertebra 1
LT-L2 - Longissimus thoracis diameter measured at lumbar vertebra 2
ES-Medial - Erector spinae diameter measured at facet
ES-Lateral - Erector spinae diameter measured at tip of L2 transverse process
QL—Dis. to Skin – Distance from skin to posterior plane of quadratus lumborum
QL—AP – Diameter of quadratus lumborum in anterior-posterior plane
QL—ML – Diameter of quadratus lumborum in medial-lateral plane
EO - External oblique diameter
IO - Internal oblique diameter
TA - Transversus abdominis diameter

5 DISCUSSION

Although the relations between various muscle thicknesses and trunk force were statistically significant, the correlation coefficients were generally low suggesting that changes in the shape of muscles at the lumbar level do not provide a good indication of the force being produced by the trunk muscles. In general, muscle thickness was the only muscle parameter measured that correlated with trunk force. Pennation angle did not change with trunk force. This is in marked contrast to studies measuring pennation angle in muscles surrounding the ankle and the elbow (Herbert and Gandevia 1995; Narici et al. 1996; Maganaris et al. 1998; Ito et al., 1998; Maganaris and Baltzopoulos 1999; Hodges et al. 2003). However, changes in pennation angle from rest to MVC can be very small, depending on the joint angle. In particular, Ito et al. (1998) and Maganaris and Baltzopoulos (1999) show that changes in pennation angle of the tibialis anterior can be as small as 2 deg. Since the resting fascicle length of the longissimus thoracis (Delp et al., 2001) is about twice that of the tibialis anterior differences in the pennation angle between the two muscles might be expected. Post hoc analysis demonstrated that the orientation of the trunk changed with increasing trunk force, particularly from rest. Therefore, trunk angle and perhaps curvature of the spine could change with increasing force. Therefore, changes in the muscle length due to changes in the angle or curvature of the spine may have obscured any systematic change in pennation angle with trunk force.

Further, the results of the descriptive statistics and the linear regression analysis showed that our CV values were larger and our R^2 values for the linear regressions were

lower compared to CV's and R^2 values of similar studies of the lower limb (Fukunaga et al., 1997; Kawakami et al., 1998; Rutherford et al., 1992; Narici et al., 1996; Maganaris et al., 1998; Maganaris et al., 1999; Muramatsu et al., 2002). This indicates greater variance in our data. It was hypothesized that the greater variance could be due to 1) compliance in the apparatus; 2) equipment adjustability limitations; 3) the complexity of the joints over which we were measuring; 4) the muscles being scanned were not contracting and 5) the pressure of other contracting muscles or increased intra-abdominal pressure caused the changes in muscle thickness.

Compliance in the apparatus prevented precise control over the orientation of the subjects' torso during testing. Although in extension none of the variables tested significantly correlated with changes in trunk posture, many ultrasound parameters were correlated significantly in lateral flexion. It is, therefore, possible that the failure to control trunk orientation could have increased the variance making it a factor that could have added to other sources of variance. There were multiple sources of compliance in the apparatus. There was compliance in the material of the harness worn by the subject, compliance in the loops of the cable the harness was attached to at low forces, as well as compliance of the soft tissues of the torso. The former two sources of compliance could be addressed in future research by 1) simply hand sewing or purchasing a backpack that is comprised of stiffer material and 2) adding an additional un-looped cable in parallel with the current cable.

Equipment adjustability issues consisted of difficulty in altering the cable length and the coarseness of the adjustment. Both contributed to the problem of keeping the subjects' torso identically oriented on every trial. This proved especially difficult when

the subjects increased their isometric trunk force. Based on the post-hoc analysis the greatest change in orientation was between the 0% MVC and 10% MVC conditions. This was one reason for normalizing the data by the value at 10% MVC, the other being that trunk orientation was more variable at 0% MVC than at 10% MVC and higher force levels. A finer adjustment could be designed into future versions of the subject apparatus. For example, a very fine toothed (< 0.5 cm) winch attached to the cable of the harness to perfectly adjust cable length at each force level to compensate for compliance in the apparatus.

When comparing our results to those of lower limb studies it should be noted that the entire group of lower limb studies involved muscles crossing only one or two joints. Although, the knee and ankle have several degrees of freedom, they were constrained to move about a single axis of rotation with the possibility of translational motion mainly along one axis in those studies. In contrast, each joint of the spine, two vertebrae and an intervertebral disk, possesses a total of 6 absolute degrees of freedom (3 rotational axes + 3 translational axes). It is quite likely that the curvature of the spine changed with increasing force. However, we did not try to account for this. Instead we made simplifying assumptions about the actual torque being applied at the L1-L2 joint, which were not necessary in the studies of the leg.

In addition to changes in trunk orientation there are a number of other possible explanations for low correlations between ultrasound measurements and trunk force. An unlikely possibility is that the muscles being imaged were not contracting. Unfortunately, we were not able to verify the activation of these muscles with intramuscular EMG. We attempted to record intramuscular EMG from several of these muscles but the two

subjects willing to participate could not tolerate the discomfort during contraction. Instead, we opted to proceed with the project using surface EMG as an independent measure of muscle activation. Hodges et al., (2003) discuss other factors that can reduce the correlation between muscle shape changes and activation. In particular, muscle deformation by variations in the pressure applied to the skin by the transducer and deformation of inactive muscles by neighbouring active muscles or by changes in internal pressure of the abdominal cavity. We also discovered this to be the case, especially over the abdominal muscles. Hence, careful attention to not only the amount of pressure being applied to the transducer by the sonographer but also to the subjects' breathing is required when obtaining measurements of the abdominal wall. To control for this, we standardized the protocol by applying the minimal amount of pressure to the transducer to achieve the necessary image and instructing the subjects to hold their breath after the end of a natural exhalation during image acquisition.

Hodges et al. (2003) reported that the relation between muscle thickness and EMG is non-linear, with most of the change occurring in the range of 20-30% MVC. Unfortunately, we do not have EMG data from a group of subjects, which would be needed for comparison. Although Hodges et al. (2003) did examine three of the same muscles, namely the external oblique, internal oblique and transversus abdominis, they performed the scans from the anterior rather than the latero-posterior surface of the body as we did, i.e., they were viewing the muscles from the front rather than from the side. Furthermore, they had the subjects perform isolated contractions of the abdominal wall, whereas our subjects performed isometric lateral flexion. Hence, the two experiments are not directly comparable. Hodges et al. (2003) reported that the thickness of the external

oblique muscle was not strongly correlated with contraction level (R=0.23). In contrast, we found that the thickness of the external oblique was relatively highly correlated with trunk force (R=0.70 for mean subject data). This may be an anomaly of ultrasound measurements relating to trunk orientation instead of trunk force. However, a recent study in which EMG of external oblique, internal oblique and extensor muscles of the trunk was recorded found that external oblique is maximally activated during lateral flexion and multifidus during extension (Ng et al., 2002). None of the other muscles were maximally activated in these directions. This would correspond to the relatively strong correlation of external oblique thickness with trunk force during lateral flexion. We were unable to obtain clear images of multifidus due to its proximity to the vertebrae so we could not confirm a similar relation for extension. Thickness of the erector spinae muscles, including the longissimus thoracis muscle may have been affected by similar factors to those discussed for pennation angle, although Watanabe et al. (2004) have shown that the thickness of erector spinae muscles increases with trunk extension, during slow movement of the trunk. As well, it is more difficult to distinguish the boundaries of erector spinae muscles than the muscles of the abdominal wall which are more echogenic because of the surrounding aponeuroses. Thus, measurements tended to be less accurate for erector spinae muscles, introducing variability.

Andersson et al. (1996) and McGill et al. (1996) performed fundamental studies looking at the activation patterns of the quadratus lumborum. Analysis of the individual subject data showed that none of the three parameters for the quadratus lumborum (QL) were correlated with lateral flexion force, although averaged across all subjects the quadratus lumborum – anterior/posterior thickness was significantly correlated. The QL

originates from the iliolumbar ligament, the transverse processes of the lumbar vertebrae and the twelfth rib and inserts on the posterior portion of the iliac crest. These lines of action would act to extend and laterally flex the torso as in our protocol. However, our measurements do not indicate this as they did not correlate strongly with either trunk extension or lateral flexion force. Andersson et al. (1996) showed that the QL is active for both dynamic trunk extension and lateral flexion activities, although these results cannot be strictly compared to the results of our study as our protocol involved isometric versions of these actions. McGill et al. (1996) showed that for lifting tasks the QL was activated to 74% of its MVC, on average. The same study also showed that for isometric side support postures where the body is held horizontally, almost parallel to the ground as the subjects supported themselves on one elbow and both feet, the QL was on average activated to 54% of its MVC. However, both studies did comment that even though the QL was generally active during extension and lateral flexion its activity depended on the specificity of the tasks. Although there is some evidence for contraction of the QL during the period of isometric lateral flexion, the results are equivocal. One explanation may lie in the ultrasound measurement itself. From Tables 4.3 and 4.5 it is evident that although the CVs for the three QL measurements are relatively low when compared to other individual measurements the ability of the QL measurements to provide reliable information about the QL itself was not confirmed when averaged across all subjects. This is related to the ability of the QL ultrasound measurements to provide reliable information about a given anatomical feature across subjects rather than reproducibility of a measurement on one individual. Figure 3.10 clearly shows that the lateral border of the muscle is not as echogenic as the rest of the cross section of the muscle. This is a

function of the angle of incidence of the ultrasound beam. When the transducer angle is altered the image of the lateral border improves. However, the medial border no longer reflects with intensity strong enough to be seen. Hence, the image used to measure QL shape changes across all subjects was less than ideal for this case.

Although we could develop a mathematical nonlinear relation by combining more than one measurement and performing numerical operations on the parameters of muscle shape to improve the correlations with trunk force, a better measure of muscle activation than trunk force is also needed to serve as a standard, i.e., intramuscular EMG should be recorded at the same time.

We attempted to record intramuscular EMG and although our first two subjects tolerated insertion of the hypodermic needles well, the number of insertion points needed was greater than anticipated. The larger muscles of the lower back required a 2 cm space between electrodes in order to obtain a representative electrical signal of overall muscle activation. Therefore, two insertion points were required for each muscle. Initially, we planned to record intramuscular EMG from the six muscles being imaged in order to confirm muscle activity levels. Since this would have required twelve insertion points we decided to record from only four muscles. However, this still required eight insertion points and after some time during the recording, both subjects felt that the discomfort due to the intramuscular electrodes during contraction was too severe to continue the experiment. In addition, it was extremely difficult to recruit and maintain subjects' interest in the study when asking them to under go an invasive technique like intramuscular recording. Furthermore, we could not find inexpensive commercially available pre-sterilized intramuscular electrodes. Therefore, we manufactured and

sterilized the intramuscular electrodes in the Neuromuscular Control Laboratory at Simon Fraser University. This may have had an impact on our study. In testing the electrodes we encountered significant problems with 60 Hz noise that was independent of the data acquisition system. Hence, given the reluctance of subjects to participate and the technical difficulty getting clean signals, the protocol without intramuscular recording was adapted because of these difficulties which allowed the study to proceed.

In experiment 2, the failure to find a significant correlation between displacement of the L1-L2 transverse processes and trunk force suggests that this measure is not a good indicator of intervertebral stiffness. Intervertebral stiffness should increase with the force exerted by the trunk since muscle stiffness increases with muscle force and joint stiffness increases when the muscles surrounding it increase activity. One factor that has a significant bearing on the result is that the change in distance between the transverse processes produced by the perturbation was very small. The mean across all force levels and subjects was only 0.05 cm. This is well below the limit of the resolution of the caliper measurements in the direction of the beam scan (~ 0.2 cm), as determined from calibration procedures. Another important factor is that the transverse processes can only be visualized by the shadows they cast since they reflect most of the incident sound energy. Because the shadows are quite broad and smooth there are no distinct or reproducible features that can be used as landmarks for accurate tracking of motion. In addition, if blurring of the image during the perturbation was due to movement of the transducer over the skin then the scan plane probably shifted as well. This could cause the shadows cast by the transverse processes to shift position in the image independently of any relative motion of the vertebrae. This is suggested by the large number of negative

values computed for the change in displacement of the transverse processes. Unless we can be absolutely certain that the scanned images are in the same plane throughout the perturbation we cannot have confidence that the measurements represent distances between identical points on the transverse processes in pre-perturbation images and the image in the frame where maximum displacement of the transverse processes is assumed to occur. Out of plane motion of the vertebrae would have had a similar effect on the measurement. Originally, we had hoped to be able to use the 3D capability of the Voluson 730 to circumvent that problem. However, the frame rate (15 Hz) was much too low to freeze the motion of the transverse processes. Even though we attained a frame rate of 57 Hz with 2D acquisition we were only able to find one or two frames where the motion appeared to be frozen. Given that architectural features of the erector spinae muscles and muscles close to the vertebrae cannot be clearly distinguished in ultrasound images and that images of bony structures lack detailed features we must unfortunately conclude that B-mode ultrasound cannot be used to obtain the measurements necessary to compute intervertebral or muscle stiffness.

Since we only have clean surface EMG from a single subject, we are limited in comparing ultrasound images of muscles and EMG of those same muscles. Nonetheless, special attention was paid to trunk orientation and EMG signal to noise ratio so, tentative findings are interesting. As previously mentioned, we were able to confirm the classic positive correlation between the EMG of muscles that produce isometric force about a joint. Hence, as expected, only longissimus thoracis EMG was related significantly to extension force. As well, although correlations were low, significant relations were found between erector spinae ultrasound measurements (Pennation, LT-L1, LT-L2, ES-Med.,

ES-Lat.) and trunk force in extension. However, despite these findings there were no significant relationships between longissimus thoracis EMG and erector spinae ultrasound variables (Pennation, LT-L1, LT-L2, ES-Med., ES-Lat.) in extension. This may be due to muscles other than those being recorded from being responsible for the extension force (e.g. quadratus lumborum) or the primary role of the muscles being recorded from could be for spine stabilization as opposed to prime movers of the trunk or muscle activity could be highly task specific. These possibilities could account for our findings of low correlations between erector spinae ultrasound variables and extension force.

Again, in lateral flexion we were able to confirm the classic positive correlation between the EMG of muscles that produce isometric force about a joint. Hence, all muscles being recorded from (longissimus thoracis, external oblique, internal oblique) were related to lateral flexion force. These relationships are consistent with the actions of the muscles recorded from and the direction of the isometric force. Accordingly, high correlations were found between all erector spinae ultrasound parameters and longissimus thoracis EMG except longissimus thoracis L2. High correlations between external oblique and internal oblique thickness and the EMG of the respective muscles were also found. These findings also support the conclusion that ultrasound measurements are better correlated with parameters of lumbar mechanics in lateral flexion than extension and suggest that ultrasound may be used as a substitute for electromyography as a means of estimating certain non-superficial muscle activity.

Post hoc tests of the cleaner data show that only two ultrasound variables (longissimus thoracis pennation and longissimus thoracis L1 thickness) in extension had

higher correlations (> 1SD) than the averaged individual data listed in Table 4.7. However, the longissimus thoracis pennation angle was negatively correlated rather than positively correlated which did not correspond to our hypothesis. One ultrasound variable (erector spinae-medial thickness) was found to be one standard deviation below the average across all individual subjects for the noisier signals (Table 4.7). As well, in lateral flexion only two ultrasound variables (longissimus thoracis-L1 thickness and external oblique thickness) had higher correlations (> 1SD) than the averaged individual data found in Table 4.7. Hence, conclusions can be made that although the cleaner data may lead to better overall correlations the large majority of relationships seen are well within one standard deviation of the average computed with nosier data, summarized in Table 4.7. Although, good laboratory practice and improvements in correlations are undisputable arguments to always collect as clean data as possible, comparisons between clean data and original data shows that assumptions and conclusions made on original data are valid and accurate.

Comparing coefficients of variation of individual ultrasound measurements (Tables 4.3 and 4.4) to that of the coefficients of variation from averaged ultrasound measurements made over 10 subjects (Tables 4.5 and 4.6) we see that similar measurements (quadratus lumborum and abdominal measurements) are similarly high. As well, subject variance accounts for approximately 0.1 of the averaged coefficient of variance. More importantly, are the changes in the means of individual ultrasound measurements in Tables 4.5 and 4.6 and how they relate to the linear regression findings. As previously mentioned our calibration results with the RAB4-8P ultrasound probe indicate that the axial and lateral resolutions are about 1 mm and 2 mm, respectively.

Therefore, in order to make reliable caliper measurements, changes in features being analyzed should be at least 1 mm for axial (along the direction of beam penetration) measurements and at least 2 mm for lateral measurements (along the direction of the beam scan). Hence, the mean changes from 0% to 50% MVC for axial lateral flexion measurements are LT-L1 (1 mm), LT-L2 (1 mm), ES-Medial (0 mm), ES-Lateral (2 mm), QL-AP (1 mm), QL-Distance from skin (1 mm), EO (3 mm), IO (9mm) and TA (2 mm). We could predict then that the ultrasound measurements with the largest change from 0% to 50% MVC might also achieve the greatest regression scores. Comparing Table 4.8 we see that this is indeed the trend. The single ultrasound measurement that is computed perpendicular to beam penetration is QL-ML which has a mean change of 2 mm and is also significantly related to trunk force.

Mean changes for extension measurements computed in the axial plane are LT-L1 (2 mm), LT-L2 (4 mm), ES-Medial (3 mm), ES-Lateral (5 mm) as such they are all highly related to trunk force.

Mean changes in pennation angle for both extension and lateral flexion are 1.6 and 0.9 deg respectively. Since our resolution computations could not cover the error that might be introduced to the angle calculation of the ultrasound machine when computing pennation it is difficult to say whether or not this is large enough to detect changes. However, it should be noted that the landmarks used to make the measurements (Figure 3.5) were made perpendicular to beam penetration making the resolution 2 mm at best. This may have had an effect on our correlates for this measurement.

This information tells us that despite whether or not a muscle is contributing to trunk force the change in shape that is detected by ultrasound measurements using

electronic calipers must be larger than 1 mm in axial resolution and 2 mm in lateral resolution in order to be linearly related to trunk force. Hence, it is a prerequisite to interpreting any findings or conclusions.

6 CONCLUSIONS

- Ultrasound measurements were better correlated with parameters of lumbar mechanics in lateral flexion than extension.
- There was a statistically significant linear trend between change in thickness and trunk force, although the correlation coefficients were generally low.
- Resolution of changes in pennation angle of erector spinae muscles was not sufficient to correlate with trunk force.
- Conventional B-mode ultrasound was not able to track displacement of the transverse processes during the sudden perturbation.
- Ultrasound measurements of distances between transverse processes were not sufficiently reliable to be useful in estimating intervertebral joint stiffness.
- Although further research is required, findings indicate that muscle thickness measured by ultrasound may be used as a substitute for electromyography in estimating isometric activity of some muscles.
- In this study, many ultrasound measurements were very close to resolution limits (Axial 1 mm; Lateral 2 mm), which precluded being able to find changes with different levels of trunk force.

7 FUTURE RESEARCH

Areas that require expansion and further investigation are:

1) Further investigation the patterns of recruitment of deep muscles during different actions of the trunk using ultrasound measurements is worthwhile. Such information would be useful in developing more comprehensive models of spinal mechanics that could be applied to injury risk assessment.

2) The technique used to estimate intervertebral joint stiffness in this study is not yet sufficiently reliable to be used to obtain accurate estimates of parameters related to spine biomechanics. A better method to attach the ultrasound transducer to the skin could result in less motion between the two, leading to better quality images during the perturbation trials. A suggestion is to place a hole in a firm but flexible piece of foam to fit the dimensions of the transducer head and then shape and tape the piece of foam to the skin.

3) Noise in the force signal and freezing of the force display during the 5 second data acquisition period resulted in fluctuations in the force produced by the subject due to difficulty in holding the target force without visual feedback. Correcting these problems would improve the reliability of the data.

4) Intramuscular recording could be achieved if no more than one muscle is investigated in any given research protocol. This would permit direct investigation of the relation between changes in muscle dimensions and muscle activity.

REFERENCES

Abenhaim, L., and Suissa, S. (1987). Importance and economic burden of occupational back pain: a study of 2,500 cases representative of Quebec. *J Occup Med, 29*(8), 670-4.

American Institute of Ultrasound in Medicine (AIUM) (1994). Medical ultrasound safety. Rockville, MD: AIUM Publications.

American Institute of Ultrasound in Medicine/National Electrical Manufacturers Association (AIUM/NEMA). (1998b). Standard for real time display of thermal and mechanical acoustic output indices on diagnostic ultrasound equipment, Revision 1. Laurel MD: AIUM Publications.

Andersson GB. (1999) Epidemiological features of chronic low-back pain. *Lancet, 354*, 581-5.

Andersson EA, Oddsson LE, Grundstrom H, Nilsson J, Thorstensson A. (1996) EMG activities of the quadratus lumborum and erector spinae muscles during flexion-relaxation and other motor tasks. *Clinical Biomechanics, 11*(7), 392-400.

Baggs R, Penney DP, Cox C, Child SZ, Raeman CH, Dalecki D and Carstensen EL. (1996). Thresholds for ultrasonically induced lung hemorrhage in neonatal swine. *Ultrasound in Med. and Bio,* 22:119-128.

Bergmark A. (1989). Stability of the lumbar spine. A study in mechanical engineering. Acta Orthop Scand Suppl, 230, 1-54. Review

Biedermann, H. J., Shanks, G. L., Forrest, W. J., and Inglis, J. (1991). Power spectrum analyses of electromyographic activity. Discriminators in the differential assessment of patients with chronic low-back pain. *Spine, 16*(10), 1179-84.

Biering-Sorensen, F. (1983). A prospective study of low back pain in a general population. I. Occurrence, recurrence and aetiology. *Scand J Rehabil Med, 15*(2), 71-9.

Bigos SJ, Spengler DM, Martin NA et al., (1986). Back injuries in industry: a retrospective study. II. Injury factors. *Spine, 11,* 246-51.

Bly SHP, Vlahovich S, Mabee PR, and Hussey RG. (1992). Computed estimates of maximum temperature elevations in fetal tissues during transabdominal pulsed Doppler examinations. *Ultrasound in Med. and Biol,* 18:389-397.

Cady EB, Gardner JE, Edwards RHT. (1983) Ultrasonic tissue characterisation of skeletal muscle. *Eur J Clin Sci, 13,* 469-473.

Clague JE, Roberts N, Gibson H, Edwards RH, (1995). Muscle imaging in health and disease. *Neuromuscul Disord, 5*(3), 171-8. Review.

Cholewicki, J., Panjabi, M. M., and Khachatryan, A. (1997). Stabilizing function of trunk flexor-extensor muscles around a neutral spine posture. *Spine, 22*(19), 2207-12.

Cholewicki J and McGill SM. (1996). Mechanical stability of the in vivo lumbar spine: implications for injury and chronic low back pain. *Clin Biomech (Bristol, Avon) 11*, 1-15.

Crisco, J. J., Panjabi, M. M., Yamamoto, I., and Oxland, T. R. (1992). Euler stability of the human ligamentous lumbar spine: Part II experiement. *Clinical Biomechanics, 7*, 27-32.

Dalecki C, Child SZ, Raeman CH, and Cox C. Hemmorage in murine fetuses exposed to pulsed ultrasound. *Ultrasound in Med. and Bio*, 25:1139-1144.

Davies KM, Recker RR, Heaney RP. (1989). Normal vertebral dimensions and normal variation in serial measurements of vertebrae. *J Bone Miner Res, 4*(3), 341-349.

Delp SL, Survanaravanan S, Murray WM, Uhlir J, Triolo RJ. (2001) Architecture of the rectus abdominis, quadratus lumborum, and erector spinae. *J Biomech*, 34:371-375.

Dhaher YY, Tsoumanis AD, Houle TT, Rymer WZ. (2004). Neuromuscular reflexes contribute to knee stiffness during valgus loading. *J Physiol,* (In press).

Doody C, Porter H, Duck F and Humphry V. (1999) *In vitro* heating of in vivo human vertebra by pulsed diagnostic ultrasound. *Ultrasound in Med. and Bio,*25:1289-1294.

Dugan MP, Liggins GC, and Barnett BC. (1995). Ultrasonic heating of the brain of the fetal sheep *in utero. Ultrasound in Med. and Bio,* 21:553-560.

Ferrell WG, Crowe N, Walker FO, Donofrio PD, Williams D. (1989) Force/diameter relationships in human muscle: an EMG and sonographic study. *Muscle Nerve, 12*, 759.

Fischer AQ, Carpenter DW, Hartlage PL, Carroll JE, Stephens S. (1988) Muscle imaging in neuromuscular disease using computerized real-time sonography. *Muscle Nerve, 11*, 270-275.

Frymoyer JW and Cats-Baril W. (1987). Predictors of low back pain disability. *Clin Orthop,* 89-98.

Fukunaga T, Ichinose Y, Ito M, Kawakami Y, and Fukashiro S. (1997). Determination of fascicle length and pennation in a contracting human muscle in vivo. *J Appl Physiol, 82*, 354-8.

Fukunaga T, Kawakami Y, Shinya K, Funato K, Fukashiro S. (1997). Muscle architecture and function in humans. *J Biomech, 30*(5), 457-463.

Fukunaga T, Kubo K, Kawakami Y, Fukashiro S, Kaneshisa H, Maganaris CN. (2001). In vivo behaviour of human muscle tendon during walking. *Proc R Soc Lond, 268*, 229-233.

Gardner-Morse M, Stokes IA. (2004) Structural behaviour of human lumbar spinal motion segments. *J Biomech,* 37, 205-212.

Gardner-Morse M, Stokes IA, Laible JP. (1995). Role of muscles in lumbar spine stability in maximum extension efforts. *J Orthop Res, 13*(5), 802-8.

Goldstein R, Filly R, Simpson G. (1987). Pitfalls in femur length measurements. *J Ultrasound Med, 6*(4), 203-7.

Granata KP and Marras WS. (2000). Cost-benefit of muscle cocontraction in protecting against spinal instability. *Spine 25*, 1398-404.

Granata KP, Marras WS, Kirking B. (1996). Influence of Experience on Lifting Kinematics and Spinal Loading. *Proc. Am. Soc. Biomech.*.

Greenough, C. G., Oliver, C. W., and Jones, A. P. (1998). Assessment of spinal musculature using surface electromyographic spectral color mapping. *Spine, 23(16)*, 1768-74.

Health Canada (2001) Guidelines for the Safe Use of Diagnostic Ultrasound. Minister of Public Works and Government Services Canada. ISBN 0-662-30974-x.

Heckmatt JZ, Dubowitz V. (1988) Realtime ultrasound imaging of muscles. *Muscle Nerve, 11*, 56-65.

Heckmatt JZ, Pier N, Dubowitz V. (1988) Real-time ultrasound imaging of muscles. *Muscle Nerve, 11,* 56-65.

Herbert RD. Gandevia SC. (1995) Changes in pennation with joint angle and muscle torque: in-vivo measurements in human brachialis muscle. *J Physiol,* 484:523-532.

Herrin GD, Jaraiedi M, and Anderson CK. (1986). Prediction of overexertion injuries using biomechanical and psychophysical models. *Am Ind Hyg Assoc J, 47*, 322-30.

Hide JA, Stokes MJ, Saide M, Jull GA, Cooper DH. (1994). Evidence of lumbar multifidus muscle wasting ipsilateral to symptoms in patients with acute/subacute low back pain. *Spine, 19*(2), 165-72.

Hodges PW, Pengel LHM, Herbert RD, Gandevia SC. (2003) Measurement of muscle contraction with ultrasound imaging. *Muscle Nerve, 27*, 682-692.

Ichinose Y, Kawakami Y, Ito M, Fukunaga T. (1997) Estimation of active force-length characteristics of human vastus lateralis muscle. *Acta Anat (Basel) 159*(2-3), 78-83.

Ito M, Kawakami Y, Ichinose Y, Fukashiro S, Fukunaga T (1998) Nonisometric behaviour of fascicles during isometric contractions of a human muscle. *J Appl Physiol,* 85:1230-1235.

Jonsson, B. (1978). *Vocational electromyography*. Amsterdam: Cobband WA.

Kawakami Y, Abe T, Fukunaga T. (1993). Muscle fiber pennation angles are greater in hypertrophied than in normal muscles. *J Appl Physiol, 74*(6), 2740-4.

Kawakami Y, Ichinose Y, Fukunaga T. (1998). Architectural and functional features of human triceps surae muscles during contraction. *J Appl Physiol, 85*(2), 398-404.

Kawakami Y, Kubo K, Kanehisa H, Fukunaga T. (2002). Effect of series elasticity on isokinetic torque-angle relationship in humans. *Eur J Appl Physiol 87*, 381-387.

Kremkau FW, (2002). Diagnostic ultrasound: principles, insruments and exercises, 6th ed. Philadelphia, PA: Saunders; 2002.

Kubo K, Kanehisa H, Fukunaga T. (2002) Effect of stretching training on the viscoelastic properties of human tendon structures in vivo. *J Appl Physiol, 92*, 595-601.

Kubo K, Kanehisa H, Kawakami Y, Fukunaga T. (2001). Influence of static stretching on viscoelastic properties of human tendon structures in-vivo. *J Appl Physiol, 90*, 511-519.

Kubo K, Kanehisa H, Takeshita D, Kawakami Y, Fukashiro S, Fukunaga T. (2000). In vivo dynamics of human medial gastrocunemius muscle-tendon complex during stretch-shortening cycle exercise. *Acta Physiol Scand, 170*(2), 127-35.

Kumar, S., and Narayan, Y. (1998). Spectral parameters of trunk muscles during fatiguing isometric axial rotation in neutral posture. *J Electromyogr Kinesiol, 8(4)*, 257-67.

Lafortune D, Norman R, McGill S. (1988). Ensemble averages of linear enveloped EMGs during lifting. Proceedings of the 5th Biannual Conference of the Canadian Society for Biomechanics, Ottawa, Ontario, 16-18 August.

Lariviere C, Gagnon D, and Loisel P. (2000). The comparison of trunk muscles EMG activation between subjects with and without chronic low back pain during flexion-extension and lateral bending tasks. *J Electromyogr Kinesiol, 10,* 79-91.

Ledsome JR, Lessoway V, Susak LE, Gagnon FA, Gagnon R, Wing PC. (1996). Diurnal changes in lumbar intervertebral distance, measured using ultrasound. *Spine, 21*(14), 1671-5.

Maganaris CN. (2002). Tensile properties of in vivo human tendinous tissue. *J Biomech, 35*, 1019-1027.

Maganaris CN and Baltzopoulos V. (1999). Predictability of in vivo changes in pennation angle of human tibialis anterior muscle from rest to maximum isometric dorsiflexion. *Eur J Appl Physiol, 79*, 294-7.

Maganaris CN, Baltzopoulos V, Sargeant AJ. (1998) In vivo measurements of the triceps surae complex architecture in man: implications for muscle function. *J Physiol, 512*(2), 603-614.

Maganaris CN, Narici MV, Reeves ND. (2004). In vivo human tendon mechanical properties: effect of resistance training in old age. J Musculoskelet Neuronal Interact, 4(2), 204-8. Review.

Maganaris CN, Paul JP. (2000). In vivo human tendinous tissue stretch upon maximum muscle force generation. *J Biomech, 33*(11), 1453-9.

Maganaris CN, Paul JP. (2002). Tensile properties of the in vivo human gastrocnemius tendon. *J Biomech, 35*(12), 1639-46.

Mallows C.L. (1973). Some comments on Cp. *Technometrics, 15*(4), 661-675.

Mannion, A. F. (1999). Fibre type characteristics and function of the human paraspinal muscles: normal values and changes in association with low back pain. *J Electromyogr Kinesiol, 9(6)*, 363-77.

Marras WS, Davis KG, Ferguson SA, Lucas BR, and Gupta P. (2001). Spine loading characteristics of patients with low back pain compared with asymptomatic individuals. *Spine, 26*, 2566-74.

McGill, S. M. (1998). Low back exercises: evidence for improving exercise regimens. *Phys Ther, 78(7)*, 754-65.

McGill S, Jucker D, Kropf P. (1996) Quantitative intramuscular myoelectric activity of quadratus lumborum during a wide variety of tasks. *Clinical Biomechanics, 11*(3), 170-172.

McKenzie DK, Gandevia SC, Gorman RB, Southon FC. (1994) Dynamic changes in the zone of apposition and diaphragm length during maximal respiratory efforts. *Thorax, 49*(7), 634-8.

McMeeken JM, Beith ID, Newham DJ, Milligan P, Critchley DJ. (2004). The relationship between EMG and change in thickness of transversus abdominis. *Clinical Biomechanics, 19*, 337-342.

Muramatsu T, Muraoka T, Kawakami Y, and Fukunaga T. (2002). Intramuscular variability of the architechture in human medial gastrocnemius muscle in vivo and its functional implications. *Adv Exerc Sports Physiol, 8,* 17-21.

Muramatsu T, Muraoka T, Kawakami Y, Shibayama A, and Fuknaga T. (2002). In vivo determination of fascicle curvature in contracting human skeletal muscles. *J Appl Physiol, 92*, 129-34.

Muraoka T, Muramatsu T, Fukunaga T, Kanehisa H. (2004). Influence of tendon slack on electromechanical delay in the human medial gastrocnemius in vivo. *J Appl Physiol, 96*, 540-544.

Muraoka T, Muramatsu T, Fukunaga T, Kanehisa H. (2005). Elastic properties of human Achilles tendon are correlated to muscle strength. J Appl Physiol, In Press.

Muraoka T, Muramatsu T, Takeshita D, Kawakami Y, Fukunaga T. (2002). Length change of human gastrocnemius aponeurosis and tendon during passive joint motion. *Cells Tissues Organs 171*, 260-268.

Murphy, P. L., and Volinn, E. (1999). Is occupational low back pain on the rise? *Spine, 24(7)*, 691-7.

Narici MV, Binzoni T, Hiltbrand E, Fasel J, Terrier F, Cerretelli P. (1996). In vivo human gastrocnemius architecture with changing joint angle at rest and during graded isometric contraction. *J Physiol, 496*, 287-97.

Ng JK, Kippers V, Parnianpour M, Richardson CA. (2002) EMG activity normalization for trunk muscles in subjects with and without back pain. *Med Sci Sports Exerc,* 34:1082-1086.

Panjabi MM. (1992). The stabilizing system of the spine. Part I. Function, dysfunction, adaptation, and enhancement. *J Spinal Disord, 5*, 383-9.

Panjabi, M., Abumi, K., Duranceau, J., and Oxland, T. (1989). Spinal stability and intersegmental muscle forces. A biomechanical model. *Spine, 14(2)*, 194-200.

Panjabi MM, Goel V, Oxland T, Takata K, Duranceau J, Krag M, Price M. (1992). Human Lumbar vertebrae. Quantitative three-dimensional anatomy. *Spine, 17*(3), 299-306.

Porter, R. W. (1989). Mechanical disorders of the lumbar spine. *Ann Med, 21(5),* 361-6.

Radebold, A., Cholewicki, J., Panjabi, M. M., and Patel, T. C. (2000). Muscle response pattern to sudden trunk loading in healthy individuals and in patients with chronic low back pain. *Spine, 25(8)*, 947-54.

Radebold A, Cholewicki J, Polzhofer GK, and Greene HS. (2001). Impaired postural control of the lumbar spine is associated with delayed muscle response times in patients with chronic idiopathic low back pain. *Spine, 26,* 724-30.

Rainville, J., Ahern, D. K., Phalen, L., Childs, L. A., and Sutherland, R. (1992). The association of pain with physical activities in chronic low back pain. *Spine, 17(9)*, 1060-4.

Rainville, J., Sobel, J., Hartigan, C., Monlux, G., and Bean, J. (1997). Decreasing disability in chronic back pain through aggressive spine rehabilitation. *J Rehabil Res Dev, 34(4)*, 383-93.

Reeves NP, Cholewicki J, Milner TE. (2005). Muscle reflex classification of low-back pain. *J Electromyogr Kinesiol., 15(1)*, 53-60.

Reimers CD, Fleckenstein JL, Witt TN, Muller-Felber W, Pongratz DE. (1993a). Muscular ultrasound in idiopathic inflammatory myopathies of adults. *J Neurol Sci, 116*, 82-92.

Reimers K, Reimers CD, Wagner S, Paetzke I, Pongratz DE. (1993b). Skeletal Muscle sonography: a correlative study of echogenicity and morphology. *J Ultrasound Med, 12*, 73-7.

Richardson CA, Snijders CJ, Hides JA, Damen L, Pas MS, Storm J. (2002). The relation between the transversus abdonminis muscle, sacroiliac joint mechanics and low back pain. *Spine, 27*(4), 399-405.

Riley WA, (1996a). Physics and principles of ultrasound and instrumentation. In: Tegeler CH, Babikian VL, Gomez CR, editors. Neurosonology, 1st ed. New York: Mosby-Year-Book; 3-7.

Riley WA, (1996b). Ultrasonic B-mode imaging systems. In: Tegeler CH, Babikian VL, Gomez CR, editors. Neurosonology, 1st ed. New York: Mosby-Year-Book; 14-18.

Robinson D, Wilson L, Kossoff G. (1981). Shadowing and enhancement in ultrasonic echograms by reflection and refraction. *J Clin Ultrasound, 9*(4), 181-188.

Roland, M., and Fairbank, J. (2000). The Roland-Morris Disability Questionnaire and the Oswestry Disability Questionnaire. *Spine, 25(24)*, 3115-24.

Roy, S. H., De Luca, C. J., and Casavant, D. A. (1989). Lumbar muscle fatigue and chronic lower back pain. *Spine, 14(9)*, 992-1001.

Roy, S. H., De Luca, C. J., Emley, M., and Buijs, R. J. (1995). Spectral electromyographic assessment of back muscles in patients with low back pain undergoing rehabilitation. *Spine, 20(1)*, 38-48.

Roy, S. H., De Luca, C. J., Emley, M., Oddsson, L. I., Buijs, R. J., Levins, J. A., Newcombe, D. S., and Jabre, J. F. (1997). Classification of back muscle impairment based on the surface electromyographic signal. *J Rehabil Res Dev, 34(4)*, 405-14.

Roy, SH, De Luca, CJ, Snyder-Mackler, L, Emley, MS, Crenshaw, RL, and Lyons, JP. (1990). Fatigue, recovery, and low back pain in varsity rowers. *Med Sci Sports Exerc, 22(4)*, 463-9.

Rutherford OM, Jones DA. (1992) Measurement of fibre pennation using ultrasound in the human quadriceps in vivo. *Eur J Appl Physiol occup Physiol, 65*(5), 433-7.

Spengler, DM, Bigos SJ, Martin NA, Zeh J, Fisher L, Nachemson A. (1986). Back injuries in industry: a retrospective study. I. Overview and cost analysis. *Spine, 11*(3), 241-5.

Tan SH, Teo EC, Chua AC. (2002). Quantitative three-dimensional anatomy of lumbar vertebrae in Singaporean Asians. *Eur Spine J, 11*, 152-158.

Troup JD., Martin JW, Lloyd DC. (1981) Back pain in industry. A prospective survey. *Spine, 6*(1), 61-9.

Waddell, G. (1987). 1987 Volvo award in clinical sciences. A new clinical model for the treatment of low-back pain. *Spine, 12*(7), 632-44.

Walker FO. (1996) Normal neuromuscular sonography. In: Tegeler CH, Babikian VL, Gomez CR, editors. Neurosonology, 1st ed. New York: Mosby-Year-Book; 397-405.

Walker FO. (1998) Muscle Ultrasound: an AAEM workshop. Rochester, MN: American Association of Electrodiagnostic Medicine.

Walker FO, Cartwright MS, Ethan RW, James C. (2004). Ultrasound of nerve and muscle. *Clinical Neurophysiology, 115,* 495-507.

Walker FO, Harpold JG, Donofrio PD, Ferrell WG. (1990) Sonographic imaging of muscle contraction and fasciculations: a comparison with electromyography. *Muscle Nerve 13*, 33-9.

Walker FO and Jackson GH. (1997). Shoot first, draw later peroneal nerve palsy: a sonographic study. *J Neuroimaging, 7*(1), 54-5.

Watanabe K, Miyamoto K, Masuda T, Shimizu K. (2004) Use of ultrasonography to evaluate thickness of the erector spinae muscle in maximum flexion and extension of the lumbar spine. *Spine,* 29:1472-1477.

Webster's ninth new collegiate dictionary. (1986). Springfield, MA, Merriam Webster.

Weiss PL, Hunter IW, Kearney RE. (1988). Human ankle joint stiffness over the full range of muscle activation levels. *J Biomech, 21*(7), 539-44.

Wells PNT (1977). Biomedical Ultrasonics. New York, Academic Press.

Wolf A, Shoham M, Micheal S, Moshe R. Morphometric study of the human lumbar spine for operation-workspace specifications. *Spine, 26*(22), 2472-2477.

Worker's Compensation Board of British Columbia. (2001). *Statistics. 2001.,* Richmond, B.C.

Zagzebski, J, A. (1996). Essentials of Ultrasound Physics. Missouri, Mosby-Year Book, Inc.

Zarkowska, A. W. (1981). The Relationship Between Subjective and Behavioral Aspects of Pain in People Suffering from Low Back Pain. Unpublished master's thesis, University of London, London.

Zhou SH, McCarthy ID, McGregor AH, Coombs RRH, Hughes SPF. (2000). Geometrical dimensions of the lower lumbar vertebrae – analysis of data from digitised CT images. *Eur Spine J, 9*, 242-248.

APPENDIX A - DIAGNOSTIC ULTRASOUND SAFETY

There are no known detrimental effects on human patients subjected to diagnostic ultrasound for medical purposes using modern diagnostic ultrasound technology (Health Canada, 2001). However, specific guidelines have been put in place based on the current body of knowledge of the risks that exist. Some of the issues include deep tissue and brain temperature increases (Bly et al., 1992; Dugan et al., 1995; Doody et al., 1999) and mechanical damage (Baggs et al., 1996; Dalecki et al., 1999) in animal models. A concise version of these guidelines relevant to this study is presented here. This list is not complete. The complete list of recommendations can be found in Health Canada's Guidelines for the Safe Use of Diagnostic Ultrasound.

General Recommendations:

- Diagnostic ultrasound will not be used for non-medical/non-research applications or for producing pictures or videos for commercial purposes.
- Both the Thermal Index and Mechanical Index shall be displayed on the screen of the ultrasound device at all times and will remain under 1.
- Based on published (AIUM, 1998a) As Low As Reasonably Achievable (ALARA) principles the dosage of diagnostic ultrasound will be kept to a minimum and only for the purposes of the research protocol.

Thermal Recommendations:

- Exposure can be reduced by either reducing the Thermal Index by adjusting ultrasound device output controls or reducing dwell time, the amount of time that the transducer stays in one place (AIUM, 1994).

Mechanical Recommendations:

- Exposure can be reduced by lowering the Mechanical Index by adjusting ultrasound device output controls. Reducing dwell time is also useful if pressure thresholds have been exceeded.

Device Performance Recommendations:

- Diagnostic ultrasound devices should comply with the Output Display Standard (AIUM 1998a).
- Maximum attainable values for Mechanical Index should not exceed 1.9.

Quality Assurance Recommendations:

- The quality of diagnostic ultrasound information depends, in part, on operator training therefore, it is also recommended that sonographers be appropriately qualified and registered with the Canadian Association of Registered Diagnostic Ultrasound Professionals.

APPENDIX B – RESEARCH DESIGN

Table B.1 Research Design for Static Measurements (Experiment 1)

Static Measurements (Experiment 1)		
Orientation	90 Degree Sitting	90 Degree Sitting
Pulling Direction	Extension	Lateral Flexion
Scan Region	#1 and #2	#1, #2, #3 and #4
Set 1	3 x 100% (No Scan)	3 x 100% (No Scan)
Set 2	3 x rest	3 x rest
Set 3	3 x 10%	3 x 10%
Set 4	3 x 25%	3 x 25%
Set 5	3 x 50%	3 x 50%

Table B.2 Research Design for Dynamic Measurements (Experiment 2)

Dynamic Measurements (Experiment 2)	
Orientation	90 Degree Sitting
Pulling Direction	Lateral Flexion
Scan Region	#1
Set 1	3 x 100% (No Scan)
Set 2	3 x rest
Set 3	3 x 10%
Set 4	3 x 25%
Set 5	3 x 50%

APPENDIX C – RECRUITMENT POSTER

Ultrasound Imaging Study of Low Back Muscles

A study is currently being conducted at UBC, in collaboration with researchers from the School of Kinesiology at Simon Fraser University, to learn more about the reasons why individuals develop low back pain. The study will take place in the Robotics and Control Laboratory of the Department of Electrical and Computer Engineering.

Potential participants must be between 18 and 35 years of age with no history of low back pain or musculoskeletal injury affecting the trunk or neck. They must have normal corrected vision and be able to understand instructions in both written and spoken English.

Participation in the study will require two visits to the laboratory, lasting up to 4 hours each. Procedures will involve imaging of trunk muscles using medical ultrasound equipment while activating the trunk muscles under various conditions.

If you are interested in participating in this study, please contact Geoff Desmoulin by telephone at 604-291-3398 or by e-mail (geoffd@sfu.ca).

APPENDIX D – DATA ACQUISITION FORM

Condition **Subject Code:**
90 degree sitting **Date:**
Pull in extension
Muscle **Notes**
Erector spinae
Sagittal Plane U/S Scan

%MVC	Pennation Angle	Skin to trans proc. (L1)	Skin to trans proc. (L2)
0%			
0%			
0%			
10%			
10%			
10%			
25%			
25%			
25%			
50%			
50%			
50%			

Condition **Subject Code:**
90 degree sitting **Date:**
Pull in extension
Muscle **Notes**
Erector spinae
Transverse Plane U/S Scan (Medial)

%MVC	Skin to facet joint (L2)	Skin to transverse (L2)
0%		
0%		
0%		
10%		
10%		
10%		
25%		
25%		
25%		
50%		
50%		
50%		

Condition **Subject Code:**
90 degree sitting **Date:**
Pull in lateral flexion
Muscle **Notes**
Erector spinae

Sagittal Plane U/S Scan

%MVC	Pennation Angle	Skin to trans proc. (L1)	Skin to trans proc. (L2)
10%			
10%			
10%			
25%			
25%			
25%			
50%			
50%			
50%			

Condition **Subject Code:**

90 degree sitting **Date:**

Pull in lateral flexion

Muscle **Notes**

Erector spinae

Transverse Plane U/S Scan (Medial)

%MVC	Skin to facet joint (L2)	Skin to transverse (L2)
10%		
10%		
10%		
25%		
25%		
25%		
50%		
50%		
50%		

Condition **Subject Code:**
90 degree sitting **Date:**
Pull in lateral flexion
Muscle **Notes**
Quadratis Lumborum
Transverse Plane U/S Scan

%MVC	Skin to Muscle	Anterior-Posterior	Medial-Lateral
0%			
0%			
0%			
10%			
10%			
10%			
25%			
25%			
25%			
50%			
50%			
50%			

Condition **Subject Code:**
90 degree sitting **Date:**
Pull in lateral flexion
Muscle
Abdominals **Distance from Internal Oblique Fascia:**
Transverse Plane U/S Scan

%MVC	External Oblique	Internal Oblique	Transverse Abdominis
0%			
0%			
0%			
10%			
10%			
10%			
25%			
25%			
25%			
50%			
50%			
50%			

Condition **Subject Code:**
90 degree sitting **Date:**
Pull in lateral flexion
Perturbation Trials
DAQ Electromyography/Force Set-up: **Image Acquisition Frequency**
Ch#7: **Hz:**
Ch#6:
Ch#5:
Muscle
Erector Spinae
Sagittal Plane U/S Scan

%MVC	Pre - Transverse proc distance (L1-L2)	Post – Transverse proc distance (L1-L2)
0%	Frame #	Frame #
0%	Frame #	Frame #
0%	Frame #	Frame #
10%	Frame #	Frame #
10%	Frame #	Frame #
10%	Frame #	Frame #
25%	Frame #	Frame #
25%	Frame #	Frame #
25%	Frame #	Frame #
50%	Frame #	Frame #
50%	Frame #	Frame #
50%	Frame #	Frame #

APPENDIX E – TORQUE IMPULSE CALCULATION

Below is an example of a typical force trace during a perturbation trial.

Figure E.1 Typical force trace during a perturbation trial.

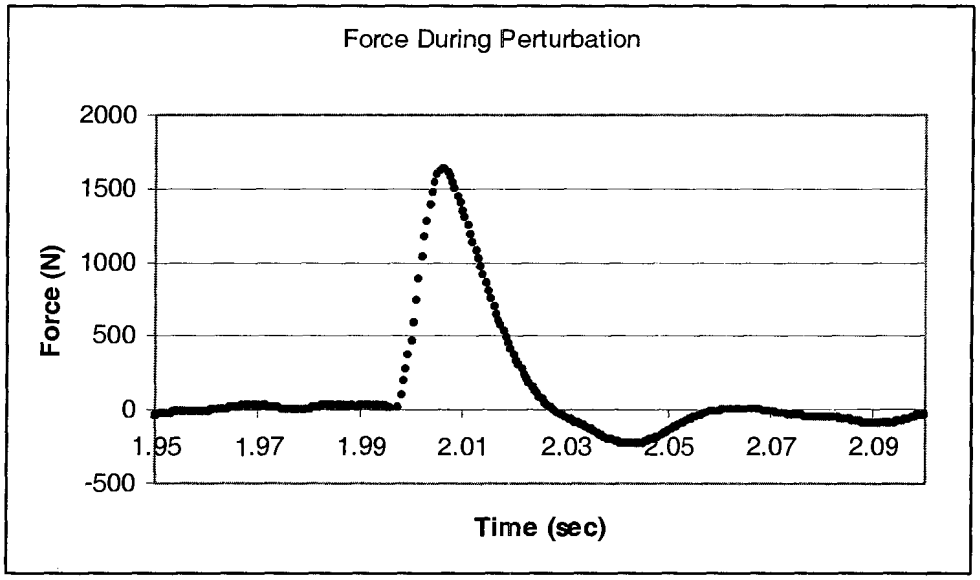

The torque impulse was calculated from the force trace transducer data using the following calculations. The integral of the force impulse can be calculated in part by using the following equation:

$$\text{Rectangle Area} = (\text{height})(\Delta t)$$

Where "height" equals the magnitude of the data point and Δt equals the time between data acquisition points (0.5 ms). Hence, the area under the curve can be calculated by the sum of the area of rectangles that exist beneath the force trace from the time of onset of perturbation to the time of the calculated turnaround point (See

Protocol). From here, greater accuracy in the integral calculation can be achieved if the area of the existing triangle is also included in the summation. Use the following equation:

$$\text{Triangle Area} = \tfrac{1}{2}(\text{difference})(\Delta t)$$

Where "difference" equals the difference between the magnitudes of 2 data acquisition points.

Figure E.2 Integral calculation of torque impulse.

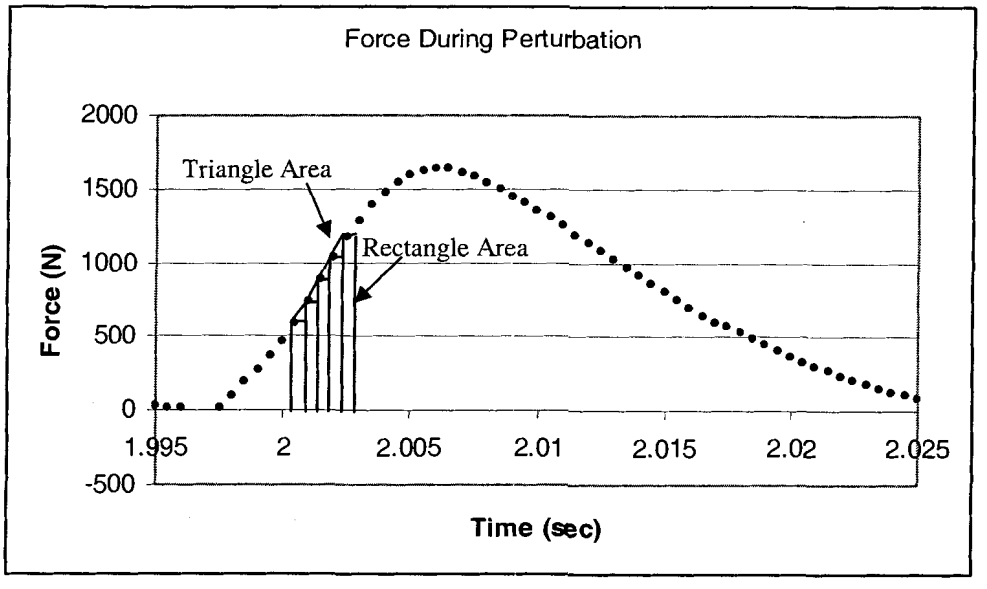

APPENDIX F – VERTEBRAE ANGLE CALCULATION

The angle formed by the tips of transverse processes of L1 and L2 with its vertex at the centre of rotation of the L1-L2 joint can be calculated using the following steps (Refer to Figure F.1):

1) Choose the appropriate L1 and L2 "Tip-to-Tip Distance" (T_{L1} and T_{L2}), "Vertebral Body Depth" (V_{L1} and V_{L2}) and "Disk Height" (D) from Table F.1 specific to the subject's characteristics.

2) Halve T_{L1} and T_{L2} and take the average of the two halves (T_{L1L2}). This is the number used to calculate the distance from the L1 or L2 tip to the centre of rotation of the L1-L2 joint in the transverse plane.

3) Sum V_{L1} with half of D (D_{VL1}). This is the distance from the superior surface of the L1 vertebral body to the centre of rotation about the L1-L2 joint.

4) Sum V_{L2} with half of D (D_{VL2}). This is the distance from the inferior surface of the L2 vertebral body to the centre of rotation about the L1-L2 joint.

5) Calculate the ratio between 3. and 4. (D_{VL1}/D_{VL2}). Multiply D_{VL1}/D_{VL2} by the "Ultrasound Measurement" (U) to split U into its L1 (U_{L1}) and L2 (U_{L2}) lengths.

6) Form the triangle for U_{L1} (opposite) and T_{L1L2} (adjacent). Calculate ½ of the L1-L2 joint angle using the formula:

$$\theta_1 = \tan^{-1}(U_{L1}/T_{L1L2})$$

7) Form the triangle for U_{L2} (opposite) and T_{L1L2} (adjacent). Calculate the other ½ of the L1-L2 joint angle using the formula:

$$\theta_2 = \tan^{-1}(U_{L2}/T_{L1L2})$$

8) The sum of θ_1 and θ_2 equals the L1-L2 joint angle (θ_{L1L2}) using the center of the disk in the coronal plane as the axis of rotation.

In summary,

$$\theta_{L1L2} = \theta_1 + \theta_2$$

Where

$\theta_1 = \tan^{-1}(U_{L1}/T_{L1L2})$

$\theta_2 = \tan^{-1}(U_{L2}/T_{L1L2})$

and

U_{L1} and U_{L2} equal the portion of the ultrasound measurement that reflects the distance from the tip of the transverse process to the center of the disk in the vertical plane for L1 and L2 respectively.

and

T_{L1L2} equals half of the averaged L1 and L2 tip to tip distance (See Figure F.1).

If you want to calculate the angles using the second axis of rotation at the edge of the vertebral body use the following steps:

1) Repeat #1 and #2 as stated above.

2) Choose the appropriate L1 and L2 vertebral width (W_{L1} and W_{L2}), from Table F.1 specific to the subject's characteristics.

3) Take the average of W_{L1} and W_{L2} (W_{L1L2}).

4) Halve W_{L1L2} and add it to T_{L1L2} (E_{L1L2}).

5) Calculate as above replacing T_{L1L2} with E_{L1L2}. (I.e. $\theta_1 = \tan^{-1}(U_{L1}/E_{L1L2})$

The difference in vertebral joint angle using typical vertebral dimensions for estimating the center of rotation at the center of the disk and at the edge of the disk can contribute up to 9 % of the variance in the stiffness estimation.

Figure F.1 Examples of vertebral parameters required for angle calculations.

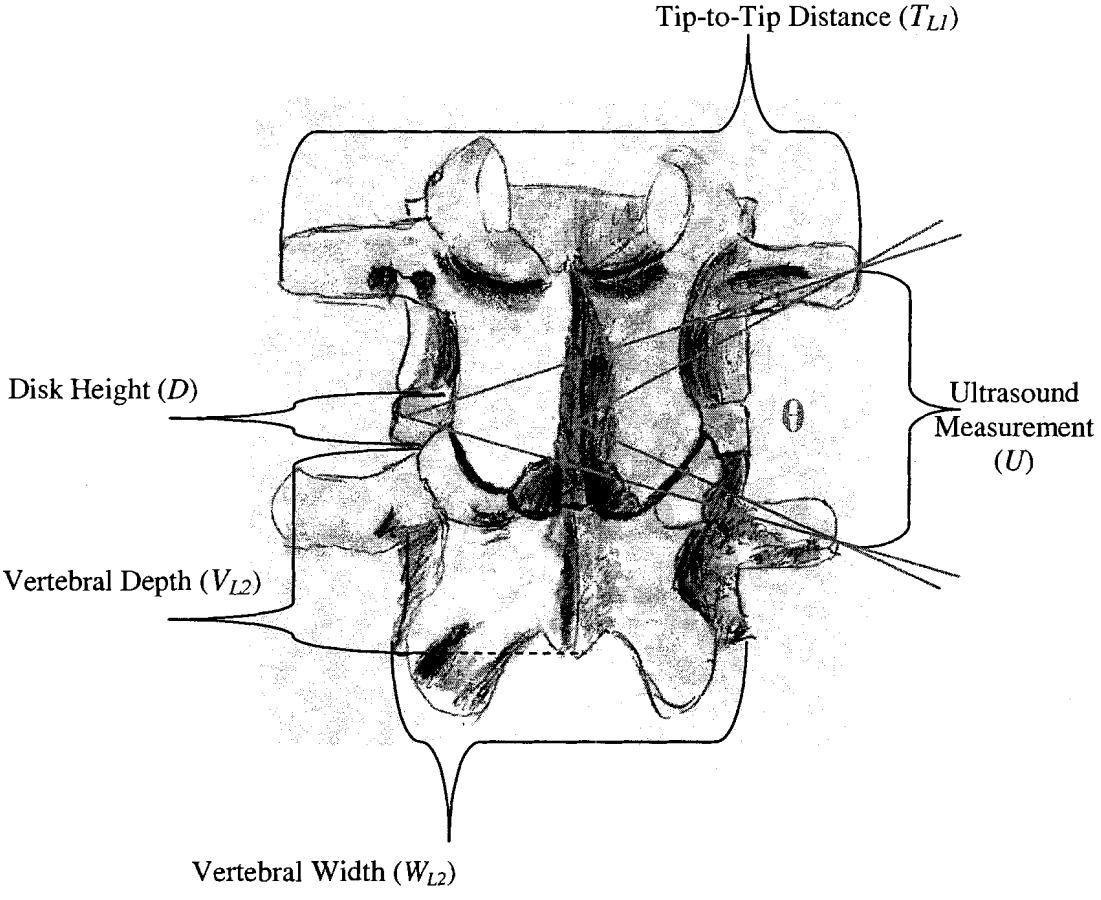

Table F.1 Geometrical measurement survey of lumbar vertebrae.

		Study					
		Tan et al., 2002	Wolf et al., 2001	Zhou et al., 2000	Panjabi et al., 1992	Davies et al., 1989	Berry et al., 1987
		Units					
		mean±1SEM	mean	mean±1SD (range)	mean±1SEM	mean (1SD)	mean
		Nationality					
Dimension (mm)	Sex	Singaporean (Asians)	Israeli (MiddleEast)	British (Caucasion)	U.S. (Caucasion)	U.S. (Caucasion)	U.S. (Caucasion)
Tip-toTip Distance (L1)	F+M	63.05±1.71	81.8	-	71.2±1.66	-	-
Tip-to-Tip Distance (L2)	F+M	75.64±1.81	80.4	-	76.1±1.48	-	-
Tip-to-Tip Distance (L3)	F+M	83.99±2.20	89.4	89.7±9.2 (69.8-114.0)	71.7±1.77	-	-
Tip-to-Tip Distance (L3)	F	-	-	84.7±6.7 (69.8-103.0)	-	-	-
Tip-to-Tip Distance (L3)	M	-	-	96.1±8.0 (79.2-114.0)	-	-	-
Vertebral Body Depth (L1)	F+M	26.37±0.49	24.9	-	23.8±1.03	-	25.8
Vertebral Body Depth (L1)	F	-	-	-	-	3.39 (0.23)	-
Vertebral Body Depth (L1)	M	-	-	-	-	-	-
Vertebral Body Depth (L2)	F+M	27.15±0.38	25.4	-	24.3±0.95	-	25.2
Vertebral Body Depth (L2)	F	-	-	-	-	3.43 (0.24)	-
Vertebral Body Depth (L2)	M	-	-	-	-	-	-
Vertebral Body Depth (L3)	F+M	25.97±0.46	25.6	29.6±2.4 (23.0-37.0)	23.8±1.10	-	26
Vertebral Body Depth (L3)	F	-	-	28.7±2.2 (7.0-13.9)	-	3.48 (0.25)	-
Vertebral Body Depth (L3)	M	-	-	30.7±2.1 (26.0-37.0)	-	-	-
Upper Vertebral Body Width (L1)	F+M	42.68±0.44	-	-	41.2±1.03	-	-
Middle Vertebral Body Width (L1)	F+M	-	40.7	-	-	-	-
Lower Vertebral Body Width (L1)	F+M	46.16±0.59	-	-	43.3±0.78	-	49.1
Upper Vertebral Body Width (L2)	F+M	44.90±0.48	-	-	42.6±0.74	-	-
Middle Vertebral Body Width (L2)	F+M	-	39.8	-	-	-	-
Lower Vertebral Body Width (L2)	F+M	48.66±0.41	-	-	45.5±1.10	-	54.8
Upper Vertebral Width (L3)	F+M	-	-	43.2±4.3 (32.3-53.3)	-	-	-
Disk Height (L3/L4)	F+M	-	-	11.6±1.8 (7.0-16.0)	-	-	-
Disk Height (L3/L4)	F	-	-	11.0±1.6 (7.0-13.9)	-	-	-
Disk Height (L3/L4)	M	-	-	12.4±1.7 (8.7-16.0)	-	-	-

APPENDIX G – TECHNICAL PROBLEMS

During initial testing of the equipment it was discovered that a 60 Hz electrical noise problem existed. Figures G.1 and G.2 illustrate the noisy data that was acquired from single channels during these initial tests.

Figure G.1 Force during isometric torso extension at 50% MVC with infiltrating 60 Hz noise.

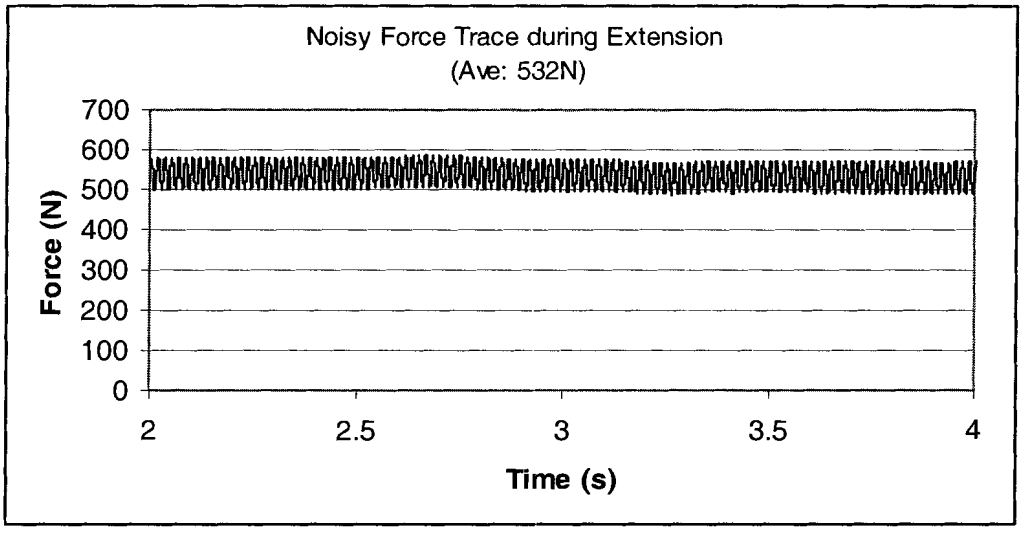

Figure G.2 Erector Spinae (longissimus thoracis) EMG during dynamic torso flexion/extension with 60 Hz noise.

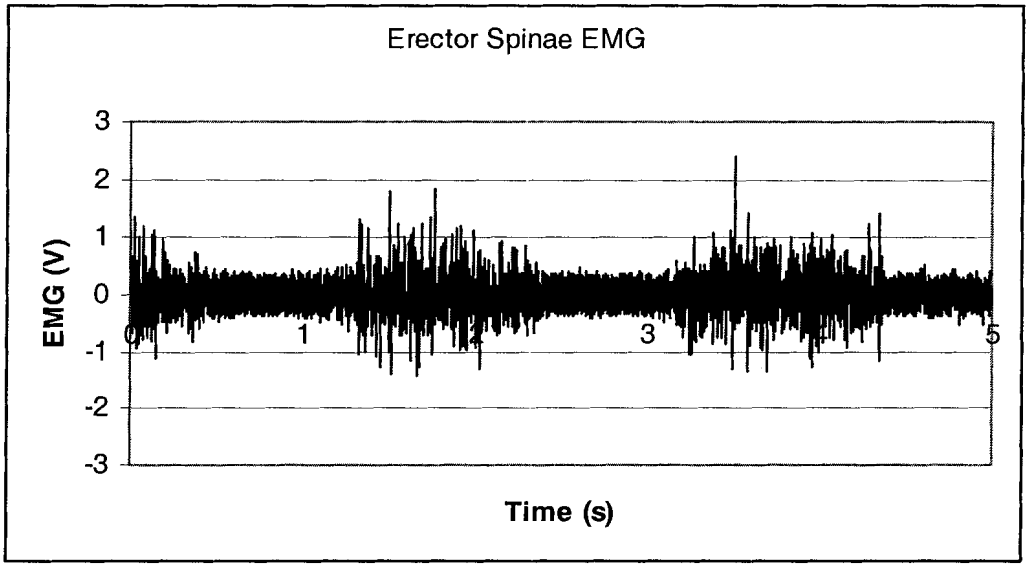

After attempting to solve the problem with conventional grounding and shielding without success it was decided for the sake of time to simply move ahead with the project. However, when sampling data on all channels simultaneously further technical problems were discovered at a later date. Although the force data was no worse than when initially tested (noise = 200 ± 20 mV), the EMG signal was further degraded by cross talk from the force channel. Figure G.3 illustrates the EMG signal that was acquired when isometric force was also being sampled.

Figure G.3 Erector Spinae (longissimus thoracis) EMG during isometric torso extension tests at 50% MVC when acquiring force simultaneously.

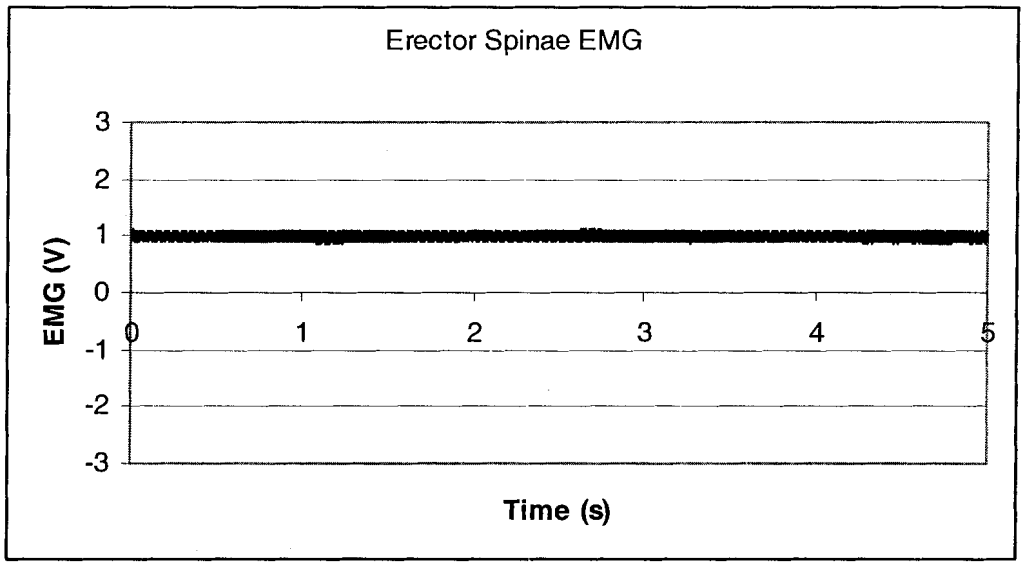

After discovering the problem depicted in Figure G.3 it was suspected that the acquisition problems (including the noise) were related to the physical data collection equipment (computer, data acquisition card and Visual C interface) as opposed to a grounding problem or some external noise source. A test was then conducted with a different data acquisition system. The result was an increase in the signal to noise ratio of every signal being acquired and all signals could now be collected simultaneously without detrimental effects or cross talk. Figures G.4 through G.7 show the improvement of the quality of the data after the data acquisition system was changed.

Figure G.4 **Force during isometric torso extension at 50% MVC after changing data acquisition system.**

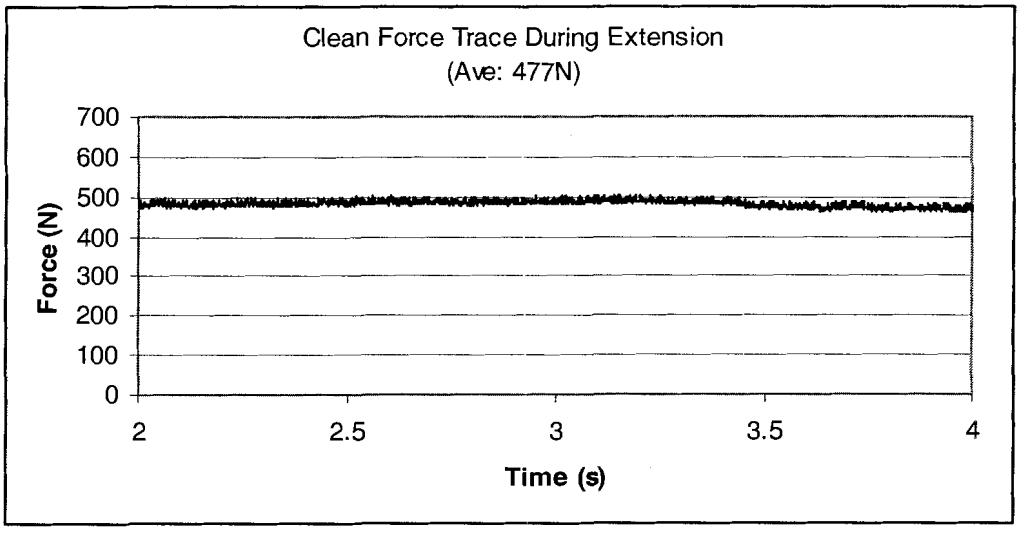

Figure G.5 **Erector Spinae (longissimus thoracis) EMG during isometric torso extension at 10% MVC after changing data acquisition system..**

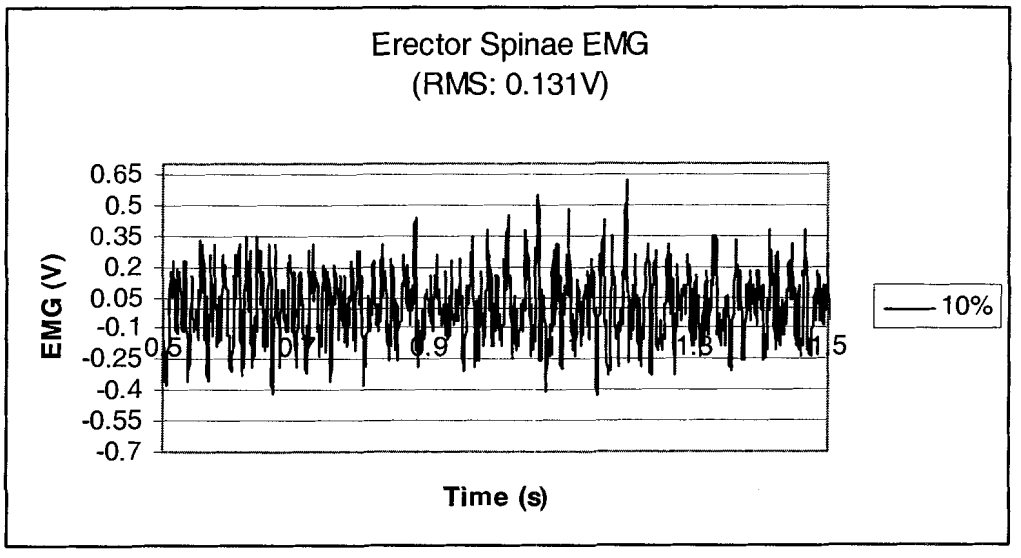

Figure G.6 Erector Spinae (longissimus thoracis) EMG during isometric torso extension at 25% MVC after changing data acquisition system.

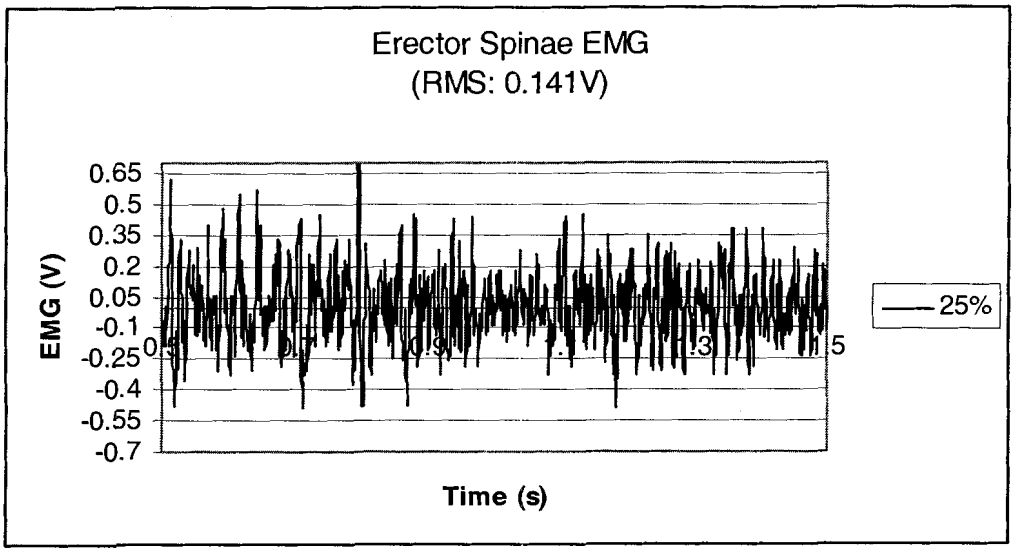

Figure G.7 Erector Spinae (longissimus thoracis) EMG during isometric torso extension at 50% MVC after changing data acquisition system.